ARMY RESEARCH LABORATORY

Standoff Variation Study III: Detonation of a Donor Munitions Stack and Responses of a Thick Rectangular Water Barricade and an Acceptor Stack

by Richard E. Lottero

ARL-TR-2035 August 1999

The findings in this report are not to be construed as an official Department of the Army position unless so designated by other authorized documents.

Citation of manufacturer's or trade names does not constitute an official endorsement or approval of the use thereof.

Destroy this report when it is no longer needed. Do not return it to the originator.

Army Research Laboratory
Aberdeen Proving Ground, MD 21005-5066

ARL-TR-2035 **August 1999**

Standoff Variation Study III: Detonation of a Donor Munitions Stack and Responses of a Thick Rectangular Water Barricade and an Acceptor Stack

Richard E. Lottero
Weapons and Materials Research Directorate, ARL

Abstract

This report documents the third stage of the continuation of the fully coupled numerical modeling of the detonation of a simplified munitions stack in a temporary storage area and the subsequent effects on the immediate surroundings of the stack. Three plausible configurations of this munitions stack, referred to as the "donor" stack, an intervening water barricade, and an "acceptor" munitions stack, are modeled in two-dimensional (2-D) Cartesian hydrocode computations using the CTH hydrodynamics computer code. The distance between each munitions stack and the barricade, referred to here as the "standoff" distance, is varied from one computation to the next, with the physical characteristics of the munitions stacks and barricade themselves remaining unchanged. The donor stack is modeled as an uncased, condensed high-explosive charge with a rectangular cross section. The water barricade has a relatively thick rectangular cross section, and the acceptor stack is modeled as a solid iron rectangle. The loadings on both the barricade and the acceptor stack are computed, as are their fully coupled responses to those loadings. Only a relatively weak inverse functional relationship with standoff distance was found in the barricade response. Weak correlations with both standoff distance and face separation were also found for all parameters that were evaluated for the acceptor stack response. The results are also compared with those of the first two parts of this study on the coupled blast loading and response computations for a massive water barricade with a trapezoidal cross section and computations for a thin rectangular water barricade.

ACKNOWLEDGMENTS

Technical consultation on the selection of munitions to be modeled and on munitions storage layouts was provided by Drs. Robert Frey and John Starkenberg of the U.S. Army Research Laboratory (ARL). Technical consultation and support in the use of the latest versions of the CTH hydrodynamics computer code were provided by Messrs. Stephen Schraml and Kent Kimsey of ARL and Dr. Eugene Hertel of Sandia National Laboratories (SNL). Technical and financial support were provided by Mr. Duane Scarborough of the U.S. Army Defense Ammunition Logistics (Ammolog) Activity. Their assistance and support are gratefully acknowledged.

INTENTIONALLY LEFT BLANK

TABLE OF CONTENTS

INTENTIONALLY LEFT BLANK

LIST OF FIGURES

LIST OF TABLES

INTENTIONALLY LEFT BLANK

1. INTRODUCTION

This report documents the continuation of a study of the detonation of a single munitions stack within a postulated munitions temporary storage area and the subsequent effects on its surroundings. The terminology for the main features that are modeled in the storage area is the same as before.[1, 2] The detonating munitions stack is referred to as the "donor" stack; the remaining munitions stacks that are in the storage area and subject to blast loading from the donor stack are the "acceptor" stacks; a postulated, field-expedient, protective wall between any two munitions stacks is the "barricade;" and the distance from the base of a munitions stack to the base of a barricade is the "standoff" distance. As stated before, the primary purpose of protective barricades is to prevent a direct, line-of-sight path from existing for either blast or fragments between munitions stacks in proximity to one another. Additionally, the impact of any part of a barricade on an acceptor stack must not itself be capable of initiating an exothermic reaction in the acceptor stack. This computational study is one part of a larger study by the U.S. Army Research Laboratory (ARL) on behalf of its customer, the U.S. Army Defense Ammunition Logistics (Ammolog) Activity, of the dynamics of a detonating munitions stack and the effectiveness of field-expedient barricades in preventing a subsequent chain reaction among acceptor stacks. The logic for considering the development of field-expedient barricades has been previously discussed in detail.[1]

The first computations in this overall study were two independent, "uncoupled" computations, the results of which have already been reported.[3] The first of those of computations modeled only the detonation of the donor stack and the subsequent blast loading on and response of a massive trapezoidal water barricade. That computation was run until the barricade had achieved a nearly steady bulk velocity toward the location of an acceptor. However, that computation failed to continue beyond 8 ms simulated time because of numerical stability problems. Therefore, it was necessary to have a second computation that modeled a reconstituted barricade, put back into its original trapezoidal cross-sectional shape, and traveling toward an acceptor stack at its late-time velocity from the first computation. It was started at the instant of impact of the barricade on the acceptor stack. Thus, these computations are termed uncoupled because of that use of two independent computations. This splitting of the computational problem was necessary because of hydrocode stability problems in the very difficult breakup phase of the barricade with an earlier version of the hydrocode. The hydrocode is discussed later in this report. That first uncoupled study showed that the massive trapezoidal water barricade was effective in keeping air blast loading on the acceptor stack low and explosive products from impinging on the acceptor stack. The peak pressures on the acceptor stack face caused by the impact on the reconstituted trapezoidal water barricade were approximately 500 MPa (5 kbar). As with any uncoupled computations, there remained open questions as to the validity of performing the computations in this way and what errors might have been introduced because of that approach. Also, the effects of variations in standoff distance were yet to be addressed.

After this initial pair of computations, three separate series of "fully coupled" computations for water barricades were performed. These computations were possible because the newer version of the CTH code, discussed later, was more stable for this class of problems. Those computations are fully coupled in the sense that the detonation of the munitions stack; the blast loading on and response of the barricade; and loading from all sources on and the response of acceptor stack are modeled in a single, continuous computation. The first study of the effects of standoff variation on the loading and response of the acceptor stack was done for a massive water barricade having a trapezoidal cross section.[1] The barricade is identical to that modeled in the uncoupled pair of computations.[3] That first study also showed that the sloping sides of the trapezoidal water barricade were effective in deflecting air blast and explosive products upward and away from the acceptor stack. The normalized blast loading on the trapezoidal barricade and its whole-body response were relatively weak functions of the inverse of the normalized standoff distance. The blast and impact loading on the acceptor stack was a three-stage process. The the first stage was from the air blast, and the next two stages came first from a water wave at the top of the barricade and second from the impact of the lower section of the barricade. The blast loading on the acceptor stack was negligible compared to that from the impact of the water. The normalized impact loading of the water barricade on the acceptor stack had a nearly one-to-one correspondence with the inverse of the normalized standoff distance. Peak pressures on the acceptor stack surface facing the barricade were below 300 MPa (3 kbar), considerably less than the 500 MPa (5 kbar) in the uncoupled computations. The five standoff distances in the first fully coupled computational study[1] were 3.048 m (10.0 ft), 2.75 m (9.02 ft), 2.50 m (8.20 ft), 2.25 m (7.38 ft), and 2.00 m (6.56 ft).

The second series of computations modeling the effects of standoff variation on the loading and response of the acceptor stack was done for a relatively thin (1.17-m width) water barricade having a rectangular cross section.[2] It showed that the thin rectangular water barricade was effective in deflecting blast upward and away from the acceptor stack, but was much less effective in keeping explosive products from impinging on the acceptor stack. The computations demonstrated a relatively weak inverse functional relationship between normalized values of the standoff distance and the loading on and whole-body response of the barricade. Similar results for both standoff and face separation were found for the loading on and whole-body response of the acceptor stack, except for a stronger functional relation of acceleration. The impact loadings on the acceptor stack by the thin rectangular water barricade are much more severe than those reported[1] for the massive trapezoidal water barricade. Peak pressures on the acceptor stack were approximately 2 GPa (20 kbar), high enough to represent a threat of initiating a chemical reaction in munitions within the acceptor stack.

This report describes a series of fully coupled computations for the same three standoff distances as were evaluated in the study involving the thin rectangular water barricade. Computation 980918 is for a 3.048-m (10.0-ft) standoff (hereinafter rounded to 3.05 m for simplicity, except when specifically used to calculate a parameter), Computation 980923 is

for a 2.50-m (8.20-ft) standoff, and Computation 980924 is for a 2.00-m (6.56-ft) standoff. The donor and acceptor stacks are modeled in a way that is identical to that used in the previous fully coupled studies[1, 2] and the first uncoupled study.[3] The 1.70-m-thick barricade is modeled as a simple rectangle having the same height as both the donor and acceptor stacks, and therefore the same height as the trapezoidal and thin rectangular barricades in the previous studies.

2. COMPUTATIONAL APPROACH AND GEOMETRY

2.1. The Hydrocode Model

The three coupled computations that are reported here were performed using the then-latest general-release version, CTH_9801, of the CTH[4] hydrocode developed at Sandia National Laboratories (SNL). It also includes the May 1998 and August 1998 "patches" (i.e., coding updates) that were released by SNL. CTH solves the inviscid Euler equations using a second-order accurate, explicit time-stepping method. A brief description of the CTH hydrocode was given in a previous report.[1] The reader is referred to McGlaun et al.[4] for a full discussion of the CTH hydrocode, and to the appropriate users' manuals for practical information about the structure and use of the CTHGEN[5] grid generation code, the CTH[6] hydrocode, and their supporting utilities.

The three computations presented here were performed using the two-dimensional (2-D) Cartesian coordinates system option in CTH, just as was done for the previous computations. The choice of 2-D Cartesian coordinates meant that the computations provided a worst-case blast loading for the simplified, uncased charge of condensed high explosives by eliminating the possibility of having any compression or expansion waves in the direction of depth of the munitions stacks and barricade. Depth is a measure parallel to both the ground and the side walls of the munitions stack, and normal to the page in the flow field plots shown later. In effect, the donor and acceptor stacks and the barricade have an infinite depth in that coordinate system. In the CTH hydrocode model, which uses the centimeter-gram-second (cgs) units system, this implies a unit depth of 1.0 cm. The same gridding was used in all computations for all of these studies. The nominal computational cell dimensions are 4.0 cm in both Δx (width) and Δy (height). These computations were performed on the Silicon Graphics, Inc., (SGI) Origin 2000 unclassified computers at the ARL Major Shared Resource Center (MSRC) at Aberdeen Proving Ground (APG), MD. This is one of four MSRCs in the United States that are administered by the High Performance Computing Modernization Office (HPCMO). Each of these 2-D Cartesian computations took about 250,000 central-processor-unit (cpu) seconds (nominally, 70 hours). Each used approximately 150,000 flow field cells, with 43 variables per cell describing the materials and their dynamic and thermodynamic attributes.

2.2. The Donor Munitions Stack

The donor stack is modeled in the same way as in the uncoupled[3] and coupled[1, 2] studies described in previous reports: as an uncased charge with no packing materials. This reduced the analysis to one of blast loading only, with no production of fragments or other debris. The explosive mass of the donor stack is modeled as a single, condensed charge rather than as a distributed set of smaller condensed charges. The choice of the munitions in the donor munitions stack was made by consulting a previous ARL report on fragment propagation probabilities by Starkenberg et al.[7] The donor munitions stack was assumed to be of the same physical dimensions as one consisting of 72 pallets of M107 155-mm projectiles, stacked three pallets high by four wide by six deep. Each pallet contains eight rounds. The dimensions of this particular stack were 2.44 m high by 2.94 m wide by 2.19 m deep (8.00 ft by 9.63 ft by 7.20 ft). A single M107 round can contain either 6.62 kg (14.6 lbm, where "lbm" denotes pounds mass, avoirdupois) of TNT or 6.98 kg (15.4 lbm) of Composition-B (hereinafter referred to as "Comp-B"). The total mass of a pallet, including packaging, is 362 kg (797 lbm).[8] Thus, a presumed stack of 72 pallets of M107 munitions would contain 576 rounds, having a total mass of Comp-B equal to 4,024 kg (8,870 lbm). For simplicity, the nominal explosive mass of Comp-B for this computational study was taken as 4,000 kg (8,818 lbm) for the donor stack, the regulatory maximum.[9] The total mass of an actual stack containing 72 pallets of M107 rounds is 26,029 kg (57,384 lbm), including all packaging materials. This equates to a mass of 118.61 kg/cm of depth for the actual stack with all materials considered. The acceptor stack was assumed to be of the same physical dimensions and total mass as those of the donor stack.

The explosive modeled was Comp-B, taken at its reference density of 1.72 g/cm^3 in its undetonated state, and modeled[10] within the Sesame[11] equation-of-state (EOS) package. The SNL Sesame EOS package includes tabular data for high explosives and separate implementations of data for the Mie-Gruneisen, Jones-Wilkins-Lee (JWL), and ideal-gas EOSs. The explosive charge was placed within the computational flow field with its center coincident with the geometric center of the M107 donor stack described before. After assigning the donor stack the nominal explosive mass of 4,000 kg and using the actual stack depth of 2.19 m, this equated to an explosive charge mass of approximately 18.227 kg/cm of depth of the stack to be modeled in the unit-depth 2-D Cartesian coordinates flow field in CTH. This mass of Comp-B was modeled as a rectangle whose width and height are in direct proportion to those for the donor stack. Specifically, the explosive charge is 93.91 cm high and 113.04 cm wide. This is the full width, and not the one-half width used because of charge symmetry about the left boundary in the 2-D computation. The charge was located with its center of mass 121.92 cm above the ground plane. The ground plane was designated as a frictionless, perfectly reflective boundary.

A small central section of the explosive charge at the left symmetry boundary served as a computational "booster" charge. It was detonated using the programmed burn[5] model using a constant detonation velocity 7.98 km/s for reference-density Comp-B.[12] This model

simulates the complete detonation of any part of an explosive charge that is passed by the expanding theoretical detonation front moving at that constant velocity. The remainder of the detonation was modeled using the "history variable reaction burn" (HVRB) model.[11] The HVRB model evaluates the thermodynamic state of a mass of undetonated explosive in a given computational flow field cell to determine if that material should be numerically "reacted" to simulate its detonation in that time step. The detonation initiation point was located at the center of the explosive charge at the (X,Y) point (0.0, 121.92 cm) on the left symmetry boundary.

2.3. The Barricade

The barricade shape chosen for the computations was a simple rectangle with a nominal height of 2.44 m (8.0 ft). This is the same height as that for the munitions stacks and for the trapezoidal and thin rectangular barricades studied previously.[1, 2] The width chosen for this thick rectangular barricade, 1.70 m, is equal to the width of the thin rectangular barricade, 1.17 m, times a factor of 1.45. The factor of 1.45 was chosen because it was numerical value of the density of the sand, 1.45 g/cm^3, in a sand-filled Concertainer barricade that was tested against a detonated pallet of M107 rounds for ARL[13, 14] by the Aberdeen Test Center (ATC). (Concertainer is marketed by Hesco Bastion Limited.[15]) This produced a water barricade with the same total mass as one made out of sand with a density of 1.45 g/cm^3 and a 1.17-m width. This was done because earlier attempts to model a rectangular sand barricade matching the Concertainer barricade failed because of numerical stability problems soon after the initial interaction of the blast wave with the barricade. These computations with the thick rectangular water barricade were performed as a compromise to at least simulate the same mass and inertial effects as a sand-filled Concertainer barricade with a height of 2.44 m. Other than using this nominal value of 1.70 m for the width of the rectangular water barricade, the rectangular water barricade simulated in the computations reported here has no relation, direct or indirect, to Concertainer or any other product by Hesco Bastion. Any data related to or evaluation of the rectangular water barricade simulated here also should not be construed as having any relation to any commercial product by Hesco Bastion. An idealized cross section that has no internal air spaces and consists only of water is assumed. No construction or supporting materials are considered. The mass of water for the barricade is 41.49 kg/cm of depth. The water in the barricade was modeled using the CTH Sesame EOS for water.[16] The face of the barricade closest to the donor stack was placed at the defined standoff distance, which was varied from 3.05 m (10 ft) to 2.00 m (6.56 ft), from the nearest side of the donor stack. The standoff distance in the computations here is measured from the face of what would have been the actual side of the donor munitions stack, not the condensed explosive charge representing the stack.

2.4. The Acceptor Munitions Stack

The acceptor munitions stack was modeled in all computations as a simple, relatively inert mass of iron[17] with the same height (2.44 m) and width (2.94 m) as the reference M107 munitions stack. This is identical to the way the acceptor stack was modeled in all previous uncoupled[3] and coupled[1, 2] computations. The acceptor stack in each computation was located at a standoff distance equal to that between the donor stack and the barricade. The purpose in modeling the acceptor stack as a full-sized mass of iron was for the convenience of having a massive, relatively non-responding object with the correct physical dimensions in order to observe wave interactions on the surface and to provide surface blast loading data through the use of CTH's "tracer" particles placed in the air near the surfaces. Tracer particles are massless points that are specified at desired locations by the user at grid generation time. They may be fixed in computational space or be free to move along one or more of the principal axes in the grid. A relatively full complement of data describing the thermodynamic state and other physical parameters at the location of each tracer is recorded for later processing by the user. When analyzing the whole-body response of the acceptor stack later in this report, the correct acceptor stack mass (118.61 kg/cm of depth) was used to compute the motion of the acceptor stack from the X-direction momentum of the massive iron stack. Some of the details of the blast development in this computational series and subsequent interactions between the blast and the barricade and then the barricade and the acceptor stack are surely artifices of the simplified geometries, but the overall dynamics appear to be quite reasonable.

3. THE HYDROCODE COMPUTATIONS

3.1. Flow Field Development

Computation 980918 simulated a fully coupled blast and impact loading sequence at a standoff of 3.05 m (10.0 ft). Even though the standoff is the same at that in Computation 980505[1] and Computation 980825,[2] there are significant differences in the barricades and their relative positions beyond the obvious differences in the cross sections and slopes of the left and right faces. The trapezoidal water barricade mass is 58.71 kg/cm of depth with an X-direction distance of its center of mass equal to 4.96 m from the right face of the donor stack. The thin rectangular water barricade has a mass of 28.61 kg/cm of depth with an X-direction distance of its center of mass equal to 3.63 m from the right face of the donor stack. The thick rectangular water barricade has a mass of 41.49 kg/cm of depth with an X-direction distance of its center of mass equal to 3.90 m from the right face of the donor stack. These parameters are summarized in Table 1 in dimensional form and also normalized by dividing by the particular value for the massive trapezoidal water barricade for the 3.05-m standoff as well as the other standoff distances.

Table 1. Barricade Geometries and Comparisons for Three Standoffs.

Geometry	Massive Trapezoidal	Thick Rectangular	Thin Rectangular
Mass (kg/cm of depth)	58.71	41.49	28.61
Normalized Mass (-)	1.000	0.7067	0.4873
Inside Angle of Side to the Vertical (Degrees)	30.0	0.0	0.0
3.048-m Standoff, Donor Right Face to Barricade Center of Mass (m)	4.9558	3.8988	3.6347
Normalized by Massive Trapezoidal Value (-)	1.0000	0.7867	0.7334
2.50-m Standoff, Donor Right Face to Barricade Center of Mass (m)	4.4078	3.3508	3.0867
Normalized by Massive Trapezoidal Value (-)	1.0000	0.7602	0.7003
2.00-m Standoff, Donor Right Face to Barricade Center of Mass (m)	3.9078	2.8508	2.5867
Normalized by Massive Trapezoidal Value (-)	1.0000	0.7295	0.6619

Figure 1 shows the computational flow field at the start of Computation 980918. This is the instant of the initiation of the detonation (hereinafter referred to as "initiation"), with time defined to be equal to zero. The "Y" axis at the left of the figure represents the height measured from the ground plane. In this simple 2-D Cartesian coordinate system, the left boundary at the Y axis is designated as a frictionless, perfectly reflective plane of symmetry. The "X" axis represents the measure of width in the system and coincides with the frictionless, perfectly reflective ground plane. The X direction therefore represents the measure of thickness of the barricade. The Y axis at the X = 0.0 location is also a vertical bisector of the donor stack. The air in the flow field, modeled with data from Graboske[18] within the Sesame[11] EOS, is shown with the color yellow. The top and right transmissive boundaries are marked by the top and right edges of that yellow region. These transmissive boundaries were designated as zero-gradient, outflow-only boundaries to minimize the possibilities of generating spurious, mathematically generated reflected waves or inflows when those boundaries are struck by large-gradient outflows. The explosive charge representing the donor stack is shown as the red (one-half) rectangle on the left symmetry boundary, the water barricade is shown as the blue rectangle, and the acceptor stack is shown as the black rectangle (the object closest to the right transmissive boundary). These settings and general descriptions, except for the shape of the barricade, are the same as those for the previous series[1, 2] of computations. In order to facilitate direct comparison of the flow fields for the 3.05-m standoff for the thick rectangular versus the thin rectangular and trapezoidal barricades, representative flow fields from Computations 980505[1] and 980825[2] are also presented. Figure 2 shows the flow field at the instant of initiation for Computation 980505 for the trapezoidal barricade. Figure 3 shows the flow field at the same initial time for Computation 980825. A comparison between Figures 1, 2, and 3 provides a good visual indication of the differences in spacing and mass of the different barricades for the same standoff distance. The spatial extent of the flow field in each direction is the same for all three computations, as is the fineness of the computational gridding. The donor stack, its initiation point, and its location are also identical. The acceptor stack itself is the same in all three computations, but its X location varies because of the differences in the width of the barricades at their bases.

Figure 4 shows the computational flow field for 980918 at 5.0 ms after the initiation of the donor stack. The detonation process had already been completed by this time (theoretically at 0.092 ms). The expanding explosive products and leading shock have deformed and accelerated the barricade. A section of the expanding explosive products has already passed over the acceptor stack. The lower section of the barricade is translating laterally toward the acceptor stack as a relatively unified block with the lower section of the barricade leading the rest of the barricade. The bottom-most part of the barricade is approximately 1.4 m away from the acceptor stack left face. There is some shearing off of the top of the barricade. As yet, no part of the barricade has arrived at the left face of the acceptor stack. No significant amounts of explosive products appear to have reached the acceptor stack. For comparison, Figure 5 shows the computational flow field for 980505 at 5.0 ms after the initiation of the donor stack. The more massive trapezoidal water barricade in that computation is also

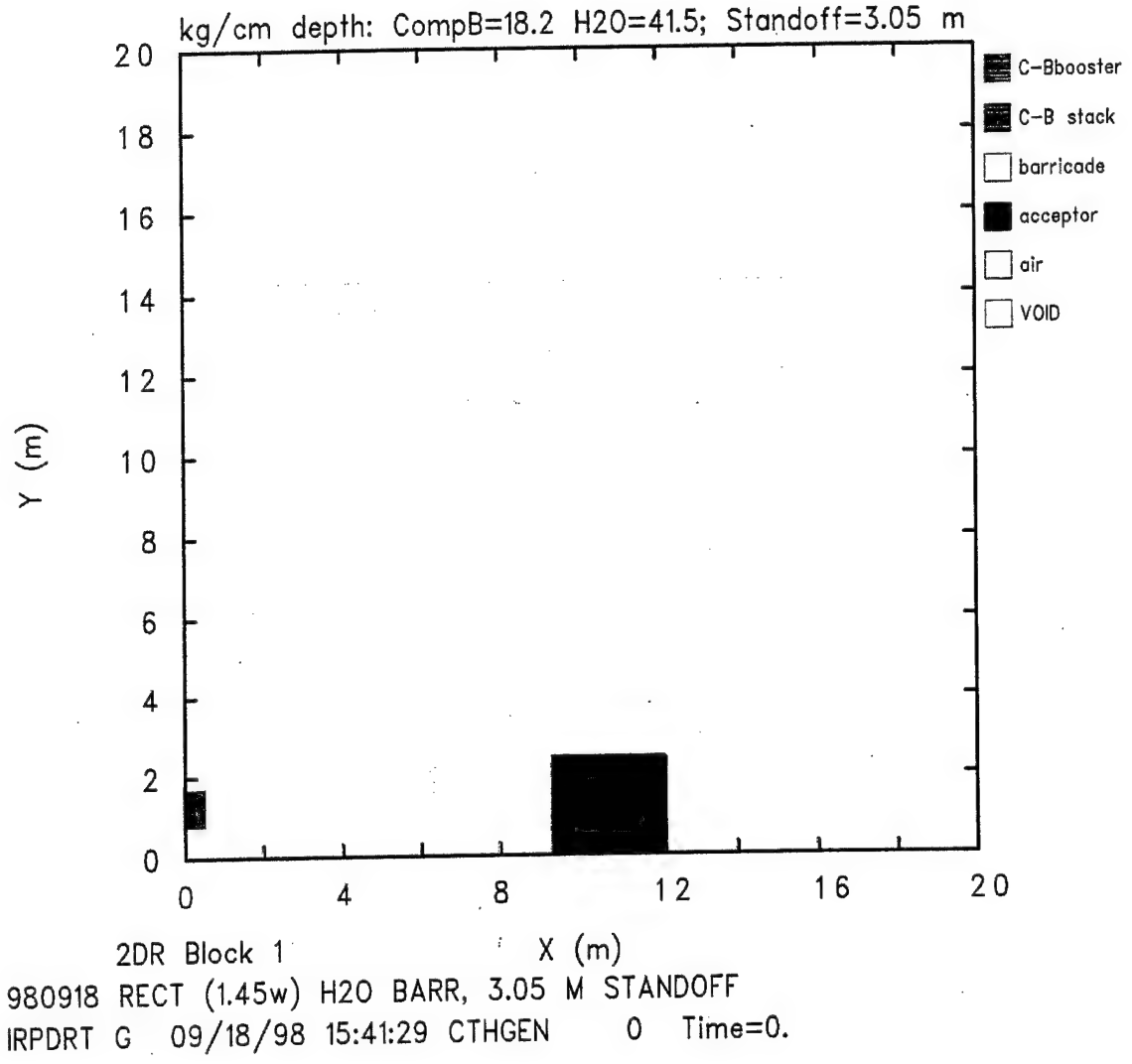

Figure 1. Flow Field at Time = 0.0 for Computation 980918, 3.05-m Standoff, Thick Rectangular Barricade.

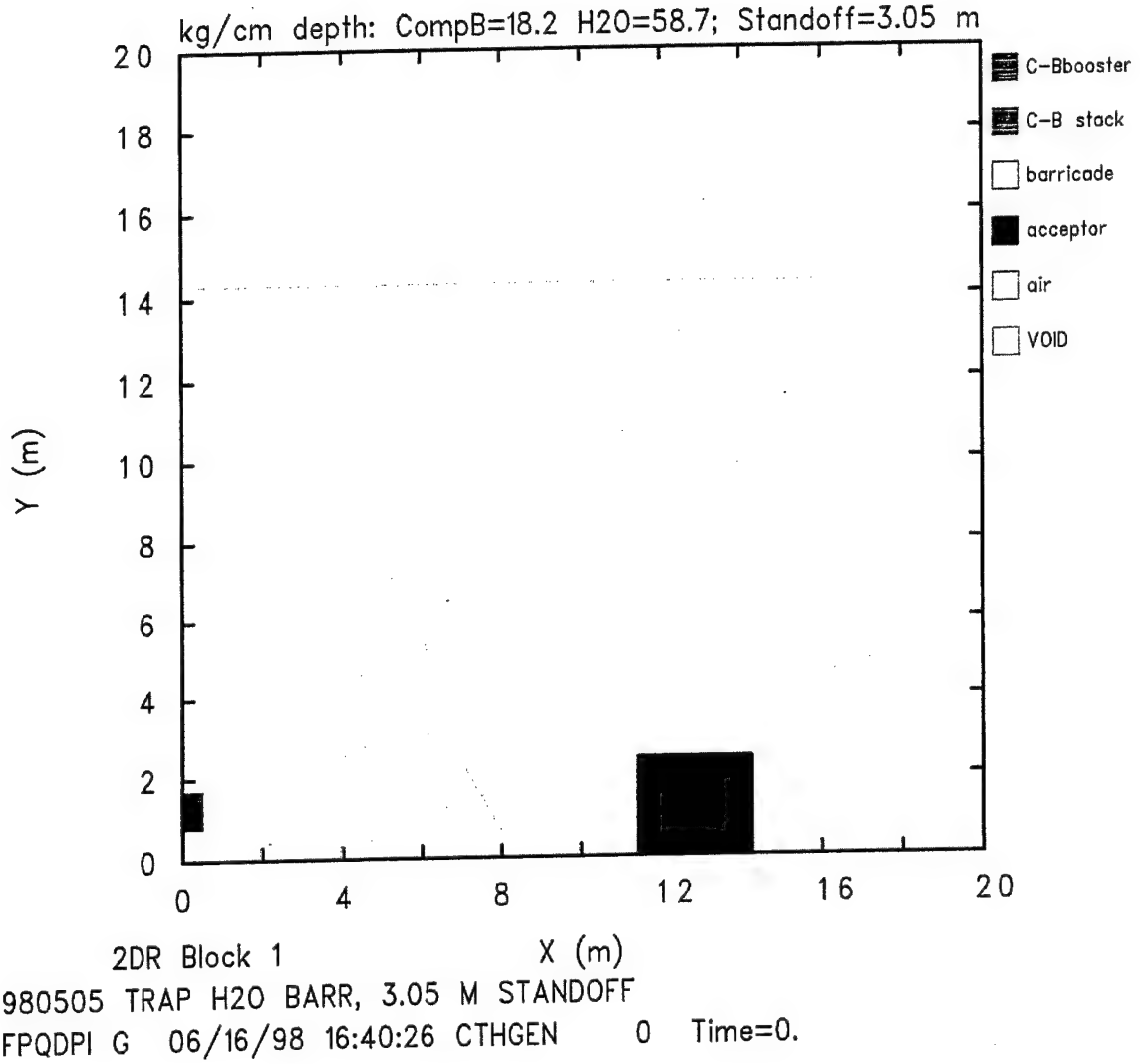

Figure 2. Flow Field at Time = 0.0 for Computation 980505, 3.05-m Standoff, Massive Trapezoidal Barricade.

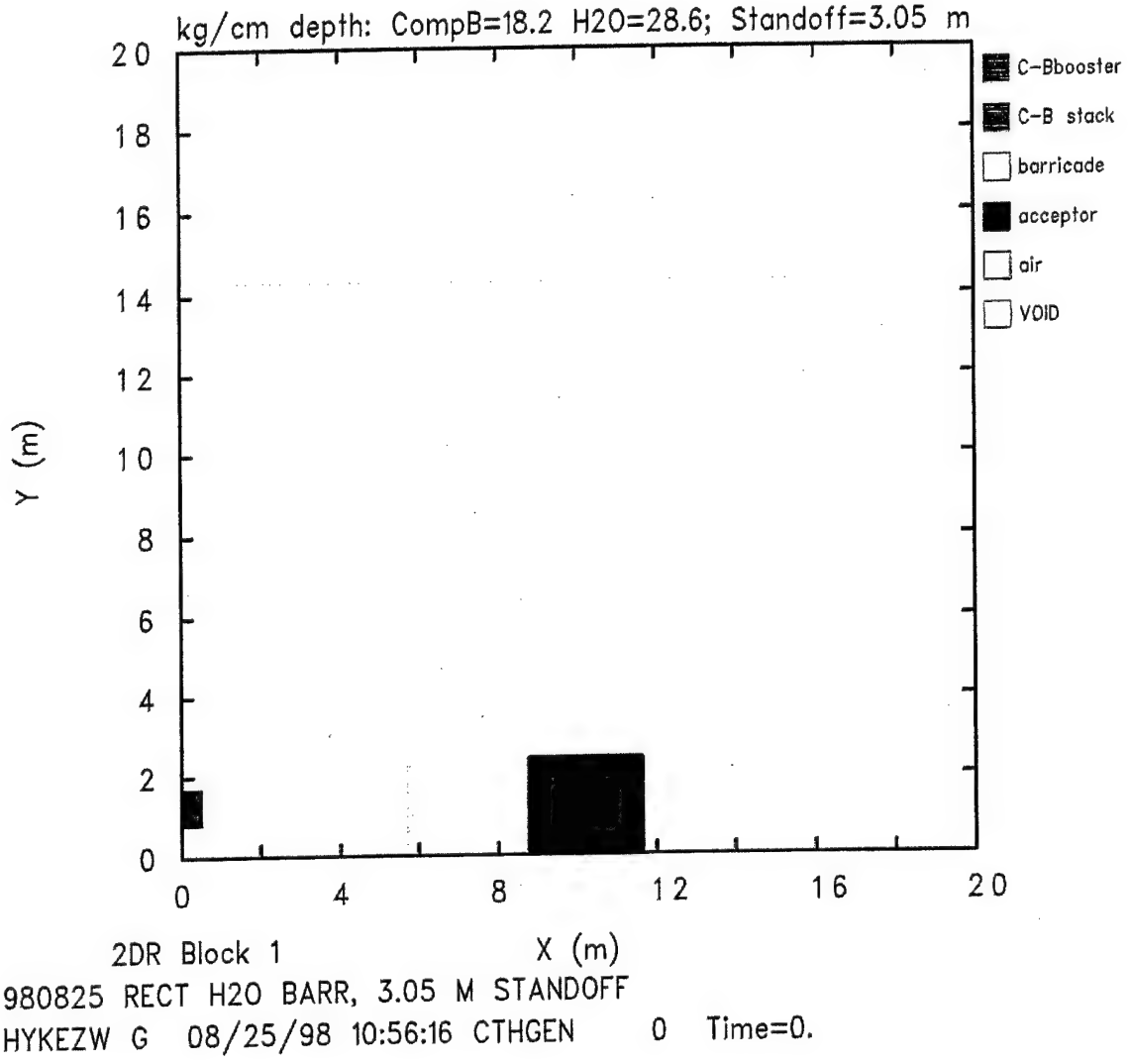

Figure 3. Flow Field at Time = 0.0 for Computation 980825, 3.05-m Standoff, Thin Rectangular Barricade.

showing the leading action of the lower section of the barricade, but with significantly less motion. This leading action is occurring in a two-fold manner. First, the base of the barricade is simply translating laterally toward the acceptor stack in response to the blast loading. Second, there is a single wave developing on the lower-right surface of the barricade that is already beginning to lead the rest of the lower section of the barricade and travel up the right surface of the barricade. At this time, the tip of that wave is approximately 2.5 m from the left surface of the acceptor stack and 0.4 m above the ground plane. This wave development was discussed in detail previously.[1] Conversely, Figure 6 shows the computational flow field for 980825 for the thin rectangular barricade at 5.0 ms. It shows the greatest distortion and movement toward the acceptor stack. The base of the barricade is approximately 1.1 m from the left surface of the acceptor stack. It is leading the rest of the barricade, except for the shearing and dispersion at its top.

Figure 7 shows the computational flow field for the thick rectangular barricade at 10.0 ms after initiation. The impact of the barricade on the left surface of the acceptor stack is nearly at the end of its full-interaction phase, covering the entire left surface of the acceptor stack. The lower part of the barricade is still in the form of a relatively thick wedge of water on the acceptor stack left surface. The upper part of the barricade has distorted an additional amount and is extending farther upward. Explosive products are approaching the top-rear corner of the acceptor stack. The interactions for the other two computations at the same time are in very different phases from this and from one another. Figure 8 for 980505 shows that the upward-moving wave on the right surface of the barricade is continuing to develop. The base of the barricade is approximately 2.0 m away from the left surface of the acceptor stack. The tip of the wave is now 1.2 m above the ground plane and 1.2 m away from the acceptor stack left surface. Figure 9 for the thin rectangular barricade in 980825 has already completed its impact on the acceptor stack, has rebounded from it, and is moving in the negative X direction. Although it still has appearance of a continuous structure in front of the acceptor stack left surface, it is quite ragged. The remainder of the barricade has been dispersed upward and away from the acceptor stack. Some explosive products are relatively close to the top-rear corner of the acceptor stack.

Figure 10 shows the flow field for the thick rectangular barricade at 15.0 ms. By this time, the barricade has rebounded from the acceptor stack left face, but still shows a moderate amount of coherent structure in front of the acceptor stack. Much of the barricade has been dispersed upward to two or more multiples of its original height as well as being spread downstream. Explosive products are approaching the top face of the acceptor stack. Figure 11 shows the flow field at 15.0 ms for the trapezoidal barricade in Computation 980505. It shows a distorted but still-intact barricade with the tip of the wave on its right-rear face almost at the point of its first contact with the left face of the acceptor stack. The base of the barricade is 1.4 m away from the left surface of the acceptor stack. Most of the air blast and virtually all of the explosive products have been deflected upward and away from the acceptor stack by the trapezoidal barricade. Figure 12 shows that by 15.0 ms after initiation, the thin rectangular barricade no longer has any useful structural integrity and no readily

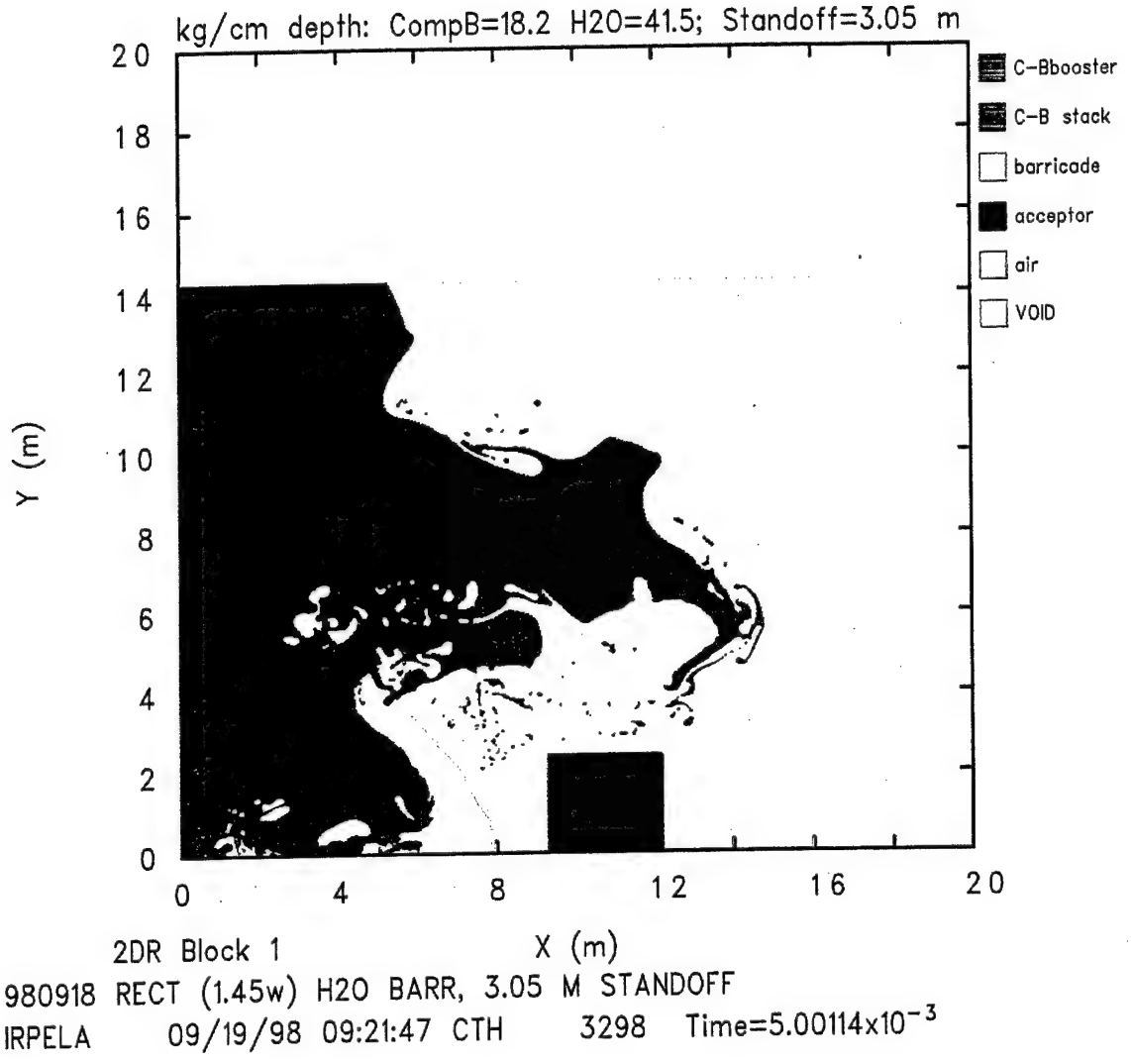

Figure 4. Flow Field at Time = 5.0 ms for Computation 980918, 3.05-m Standoff, Thick Rectangular Barricade.

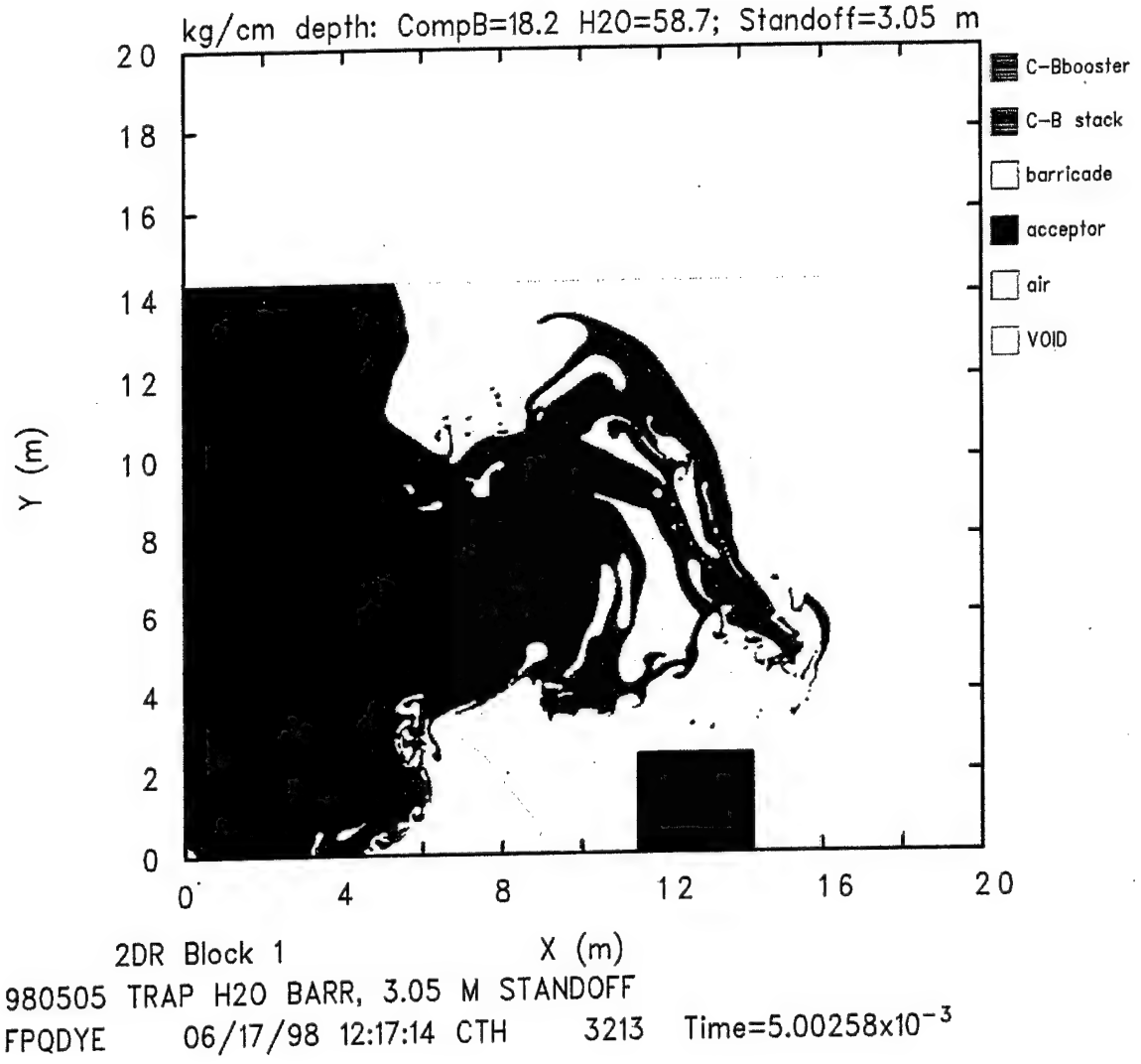

Figure 5. Flow Field at Time = 5.0 ms for Computation 980505, 3.05-m Standoff, Massive Trapezoidal Barricade.

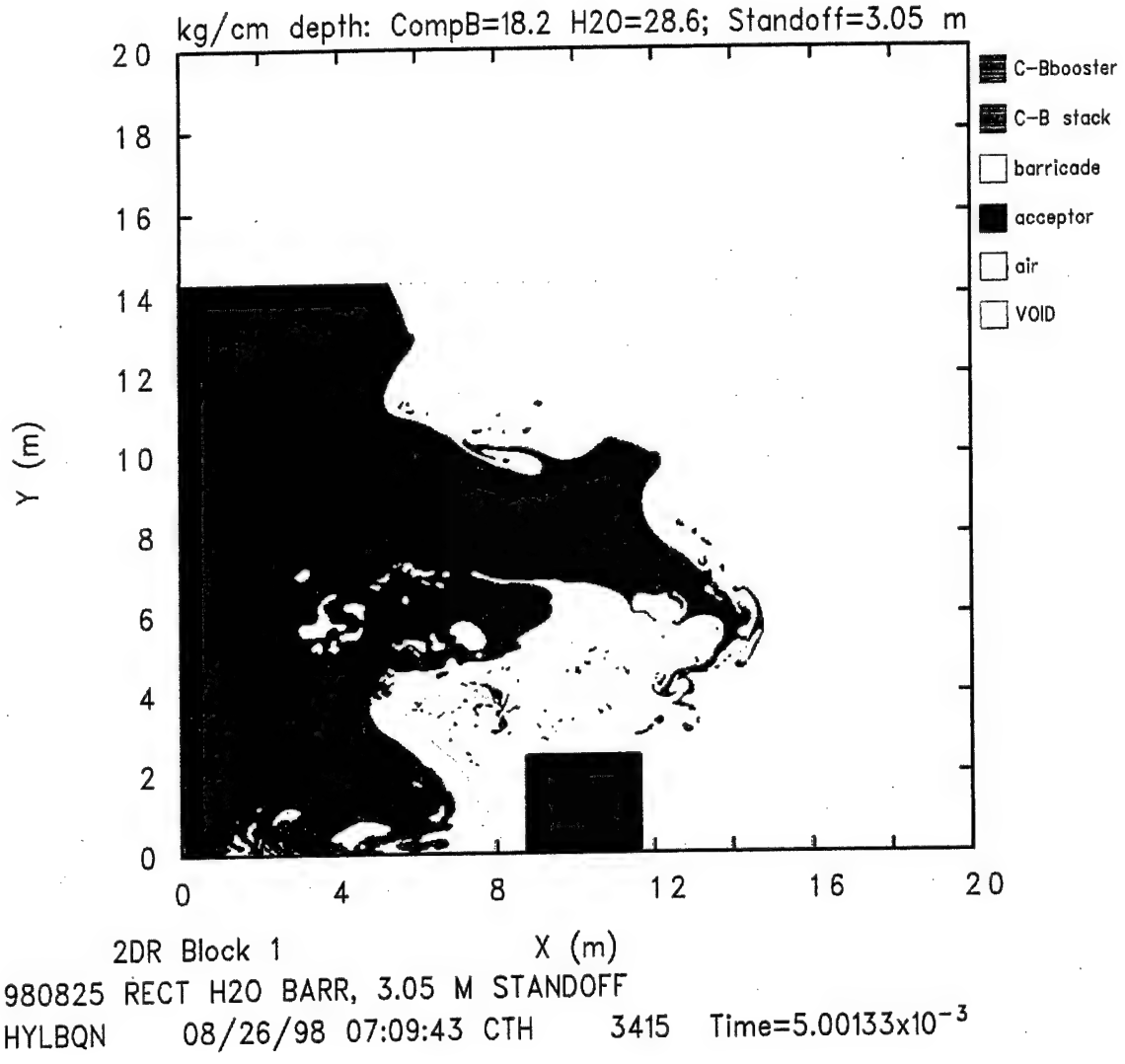

Figure 6. Flow Field at Time = 5.0 ms for Computation 980825, 3.05-m Standoff, Thin Rectangular Barricade.

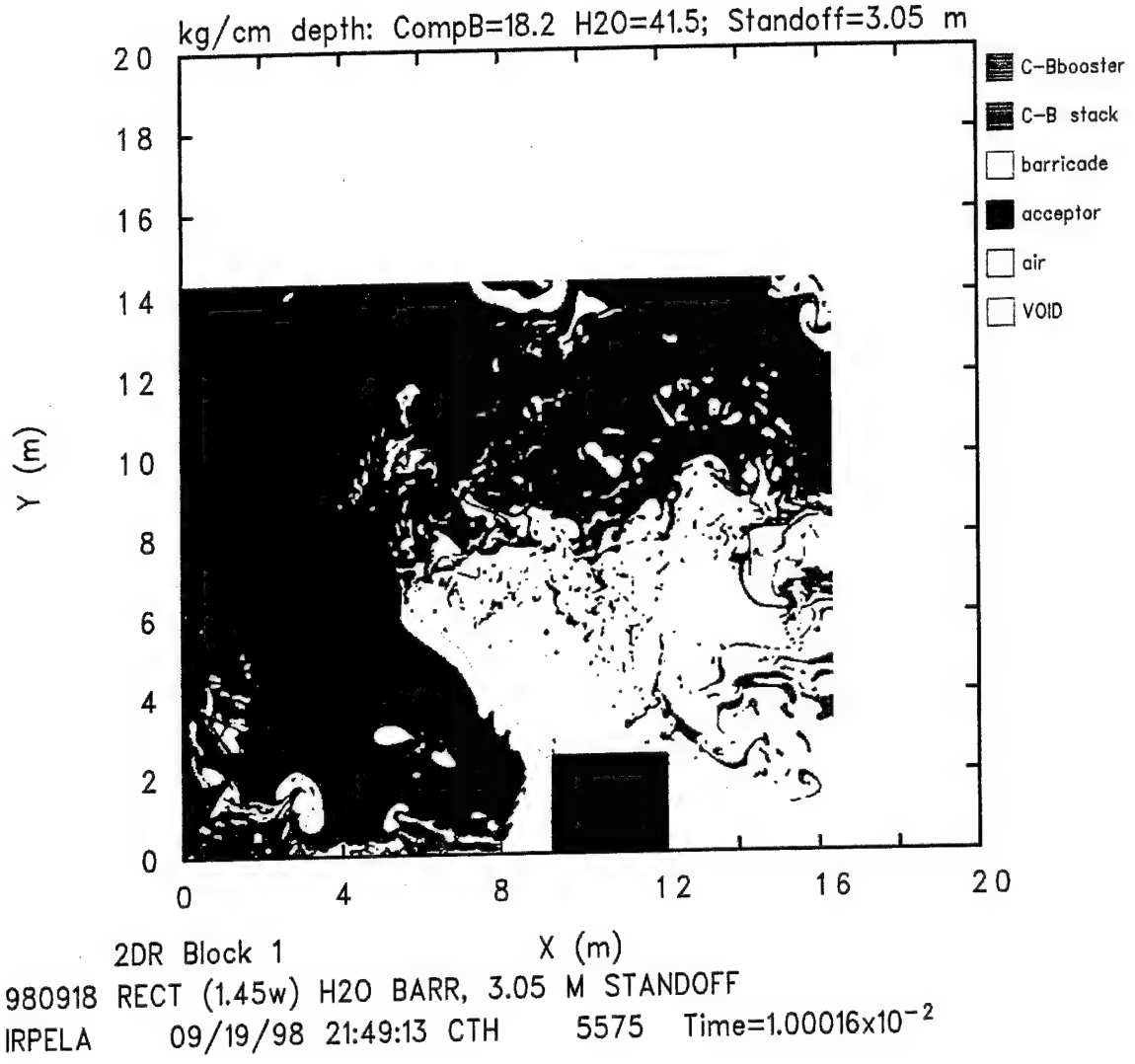

Figure 7. Flow Field at Time = 10.0 ms for Computation 980918, 3.05-m Standoff, Thick Rectangular Barricade.

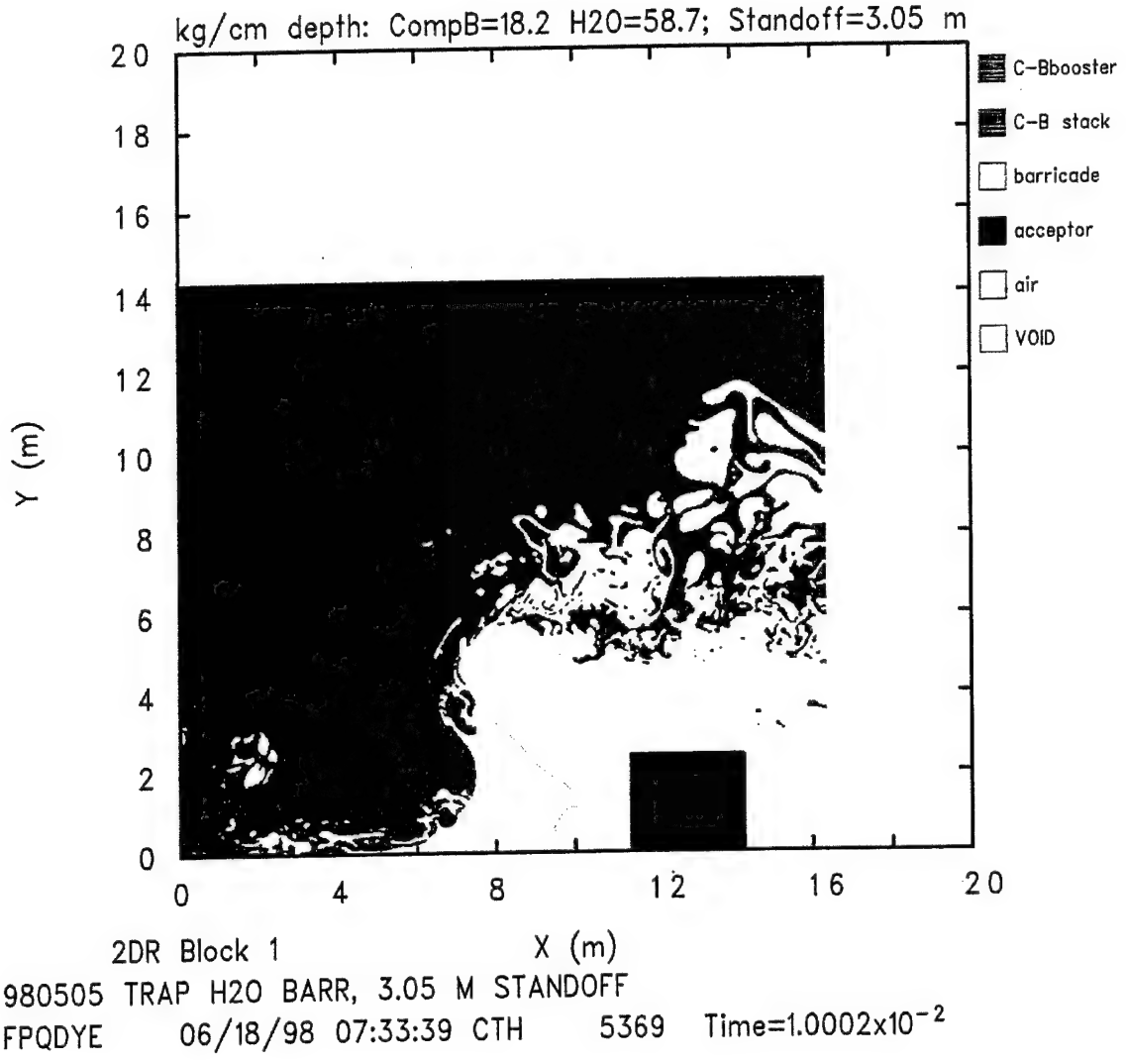

Figure 8. Flow Field at Time = 10.0 ms for Computation 980505, 3.05-m Standoff, Massive Trapezoidal Barricade.

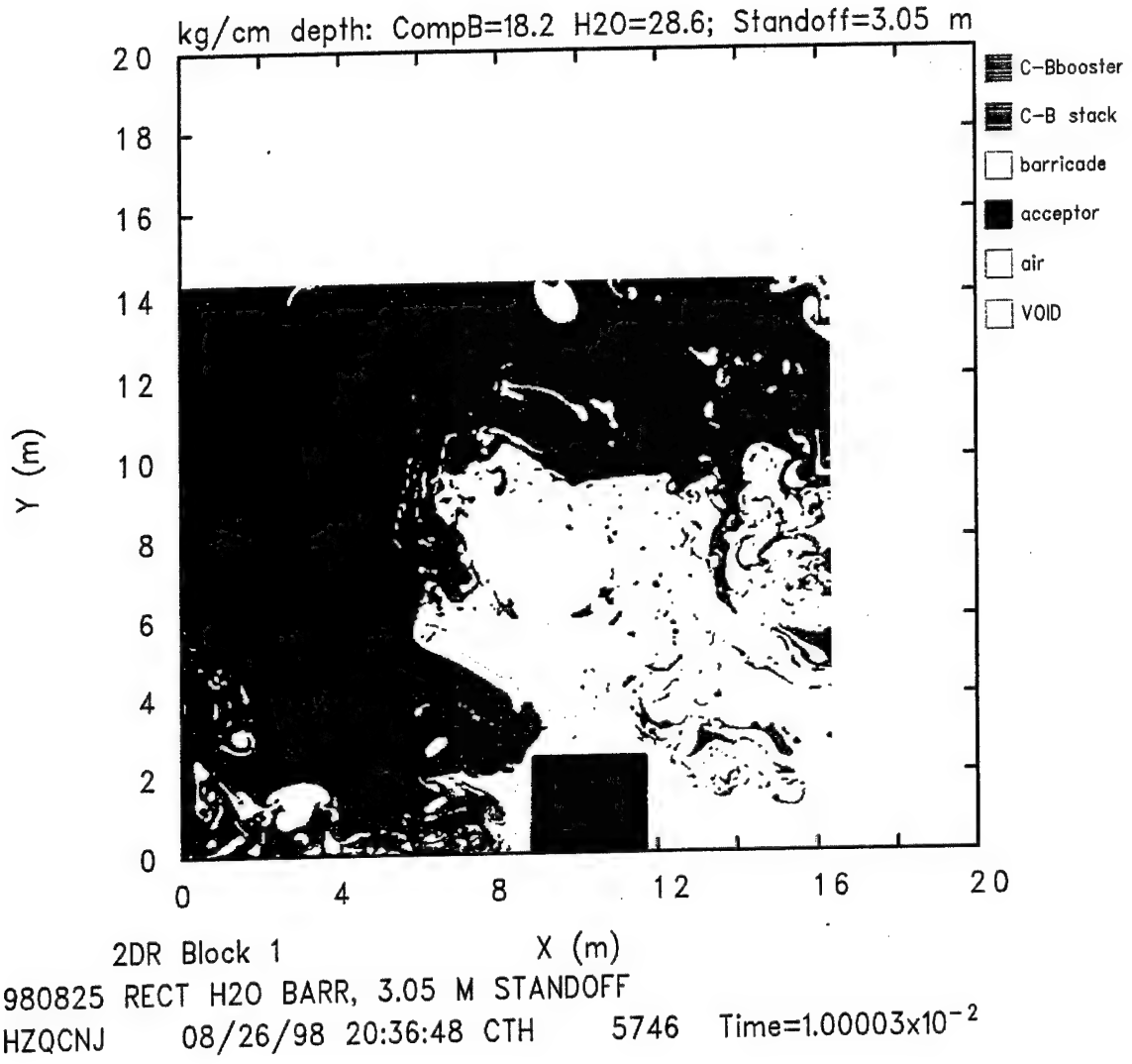

Figure 9. Flow Field at Time = 10.0 ms for Computation 980825, 3.05-m Standoff, Thin Rectangular Barricade.

recognized shape. A small amount of explosive products appears to be making contact with the lower-left corner of the acceptor stack, and a large region of explosive products seems to be moving very close to the top-left corner of the stack.

Figure 13 shows the computational flow field for the thick rectangular barricade at 20.0 ms after initiation. The rebound of the barricade from the left surface of the acceptor stack is continuing, and the barricade is in the process of being dispersed into the rest of the flow field. Explosive products seem to now be contacting at least part of the top surface of the acceptor stack and are close to the bottom-left corner. Figure 14 for 980505 shows the first interaction of water from the wave on the right face of the trapezoidal barricade with the top section of the acceptor stack. The bottom of the barricade is approximately 0.9 m from the acceptor stack left surface. The barricade is still largely intact, providing good protection for the acceptor stack, and no explosive products are near the surfaces of the acceptor stack. Figure 15 shows the computational flow field at 20.0 ms after initiation. Much of the top face of the barricade has contact or near contact with explosive products, as does its lower-left corner. Some explosive products are nearing the back face. There is no longer any structurally meaningful section of barricade in front of the left surface of the acceptor stack or anywhere else in the flow field.

Progressing further in time, Figures 16 and 17 show the computational flow field for the thick rectangular barricade at 30.0 ms and 40.0 ms, respectively, after initiation. They show remnants of the barricade being pressed once again against the left surface of the acceptor stack and then dispersed into the flow field. By 40.0 ms, there is general contact of explosive products with the acceptor stack surfaces. There are no recognizable, contiguous sections of the barricade left in the computational flow field. A significant portion of the original barricade mass has exited the flow field. In contrast, the interaction of the massive trapezoidal barricade with the left surface of the acceptor stack had not yet reached its peak by 30 ms. The base was still about 0.5 m from the left surface of the acceptor stack. By 40 ms, the interaction had passed its peak and the lower section of the barricade was in a rebound phase and showing a relatively good continuous, though highly distorted, structure in front of the acceptor stack. Those flow fields are not shown here, but may be seen in the report on the trapezoidal barricade computations.[1] The flow fields for the thin rectangular barricade at 30 and 40 ms show that the barricade has been effectively removed from the flow field and that explosive products are in general contact with the acceptor stack. A more complete description along with plots of those flow fields may be seen in the report on the thin rectangular barricade computations.[2]

From a qualitative point of view from comparing the flow fields for the 3.05-m standoff, there is a clear hierarchy in the effectiveness of these three different water barricades. The thick rectangular barricade was more effective for a longer period of time than was the thin rectangular barricade. However, both of the rectangular barricades were considerably less effective in protecting the acceptor stack than was the more massive trapezoidal barricade. This statement is quantified in the following sections of this report. First, sets of similar sequences of the flow fields for the thick rectangular water barricade for a 2.50-m and a

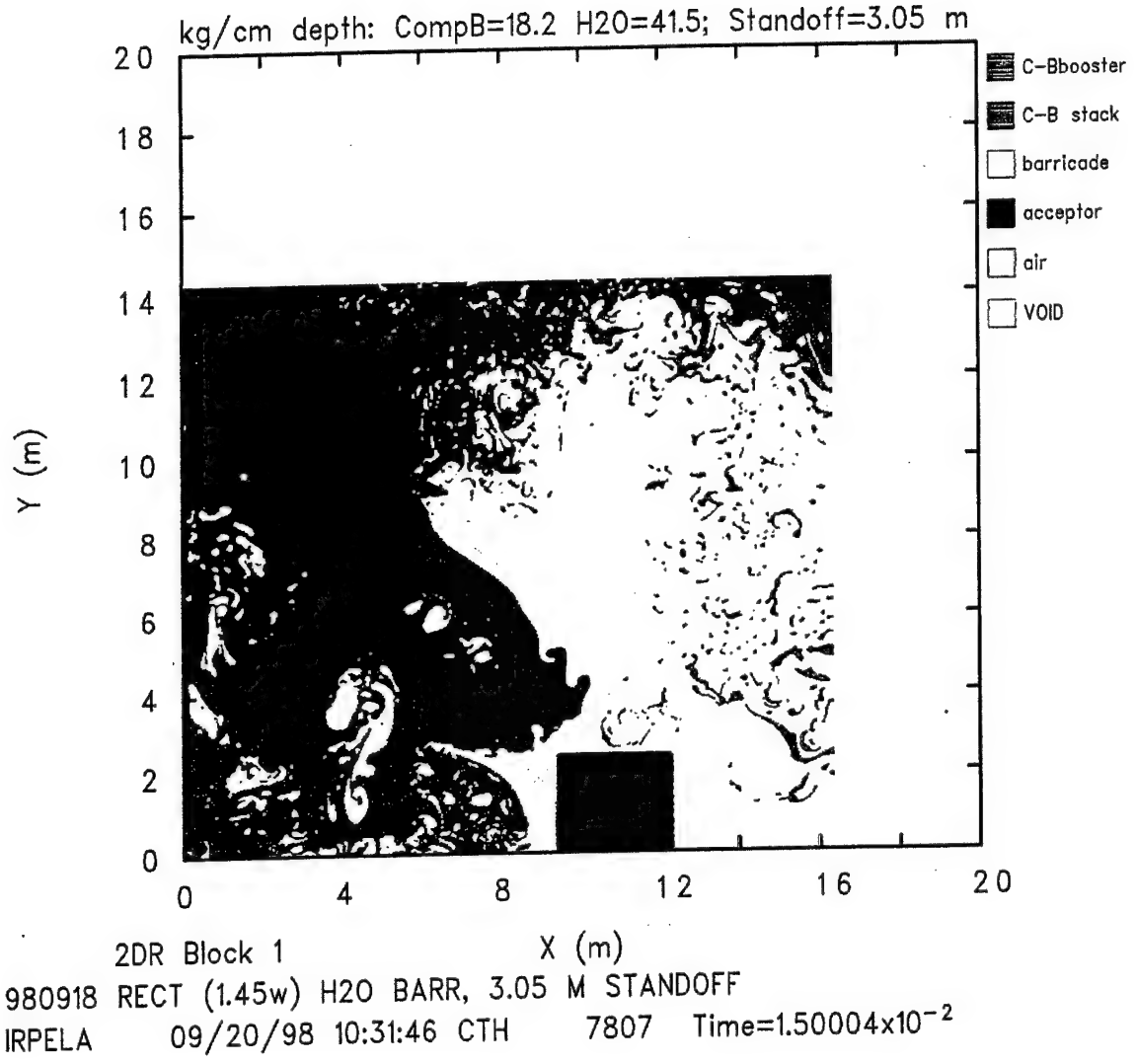

Figure 10. Flow Field at Time = 15.0 ms for Computation 980918, 3.05-m Standoff, Thick Rectangular Barricade.

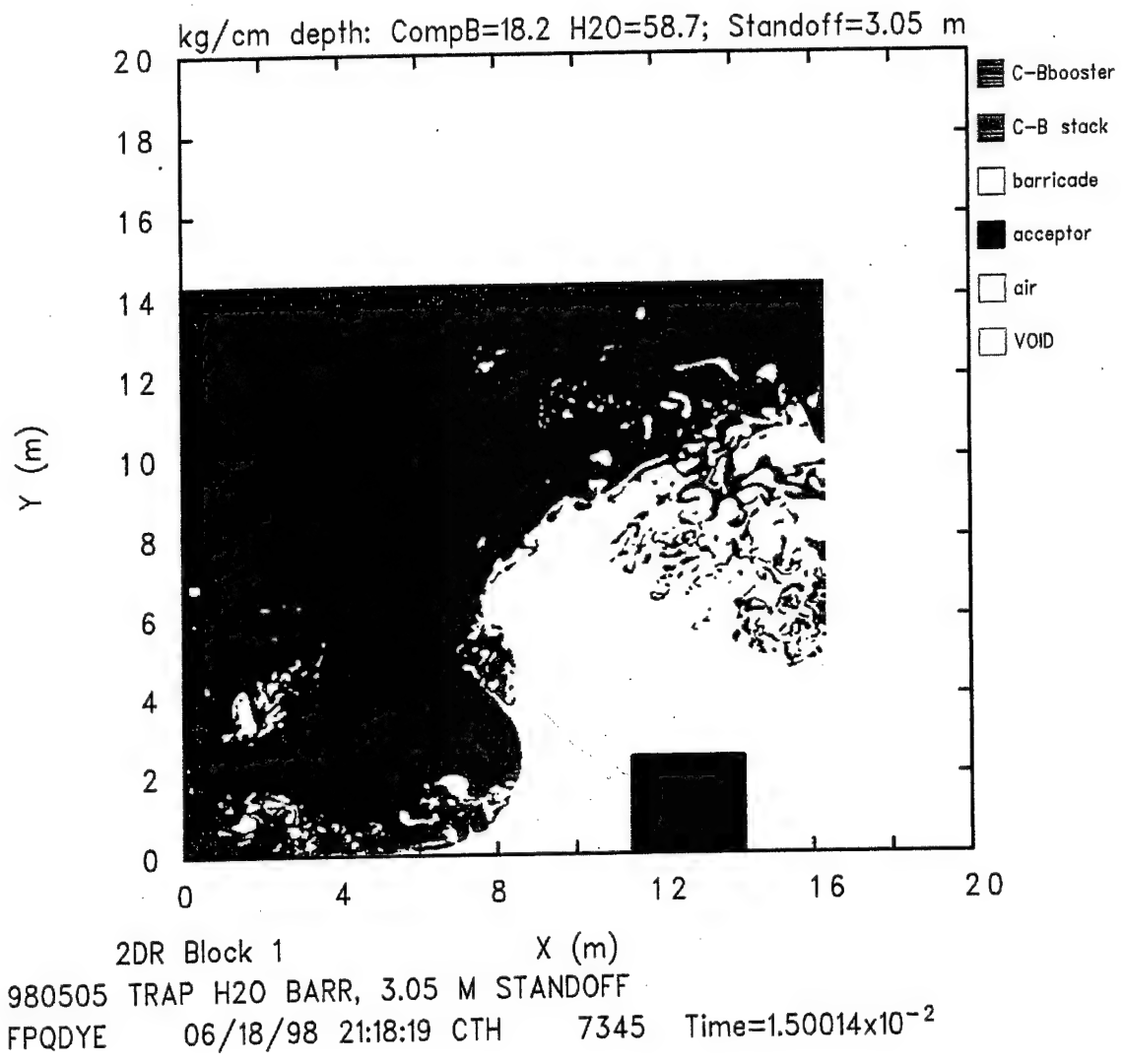

Figure 11. Flow Field at Time = 15.0 ms for Computation 980505, 3.05-m Standoff, Massive Trapezoidal Barricade.

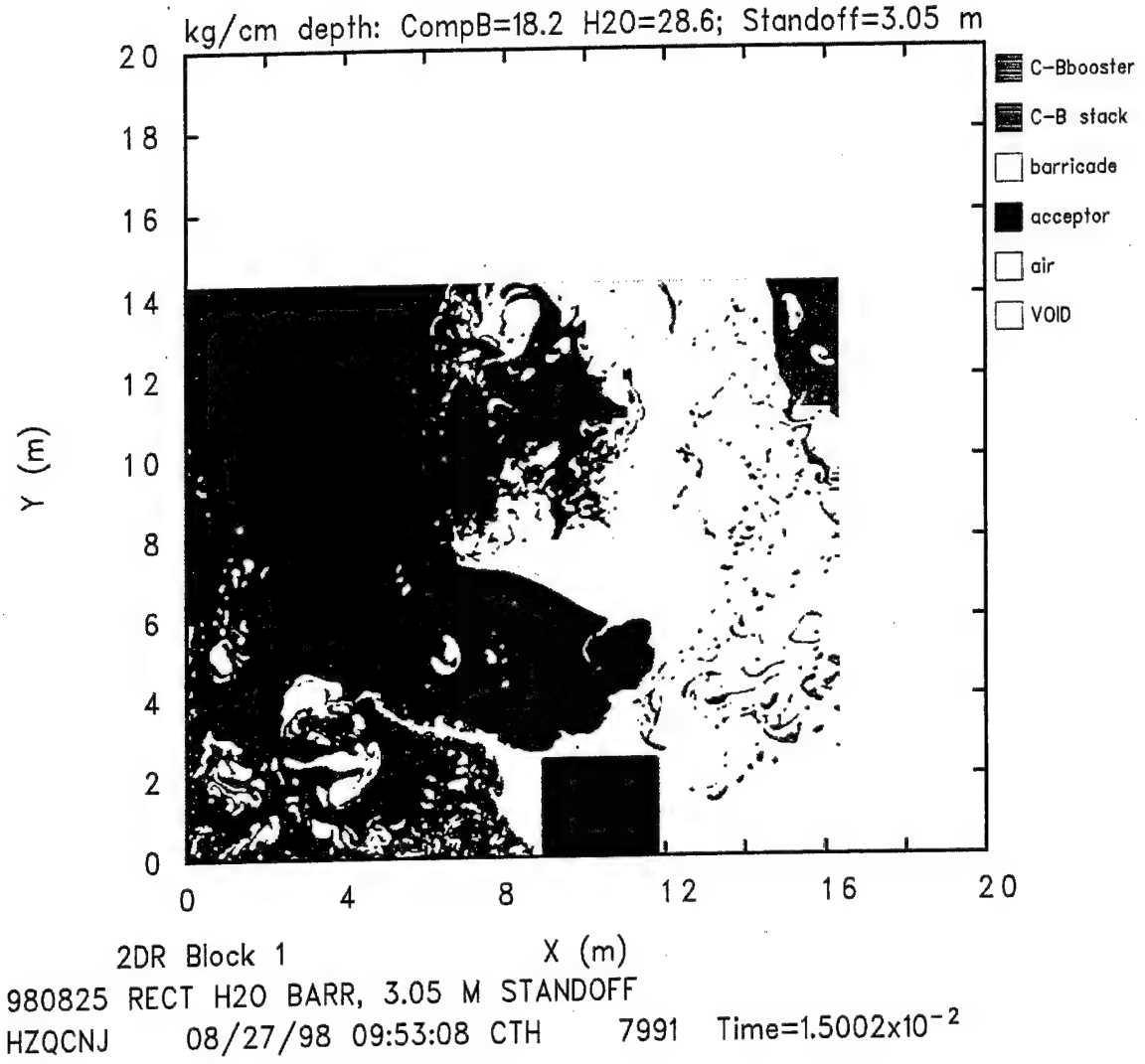

Figure 12. Flow Field at Time = 15.0 ms for Computation 980825, 3.05-m Standoff, Thin Rectangular Barricade.

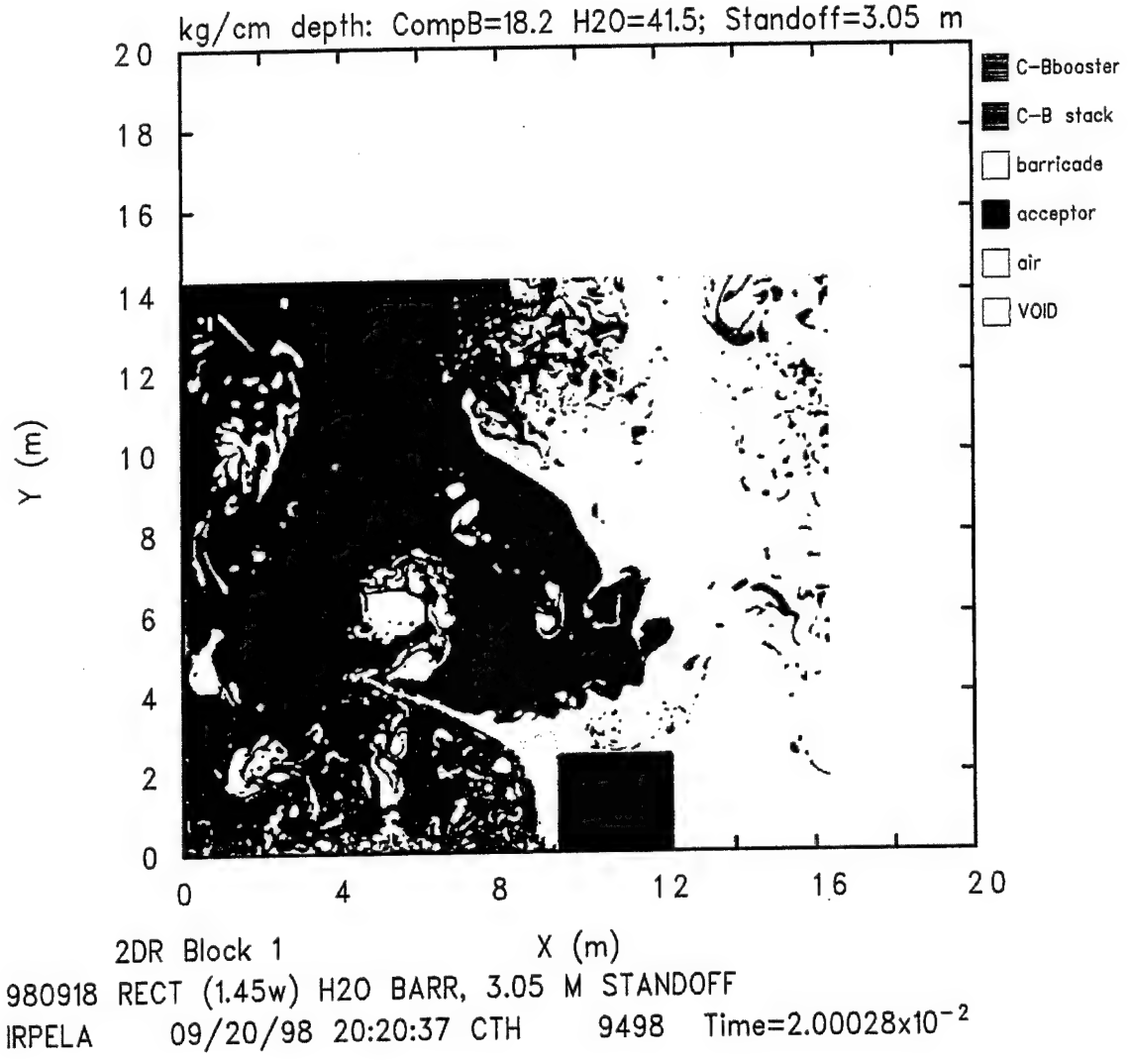

Figure 13. Flow Field at Time = 20.0 ms for Computation 980918, 3.05-m Standoff, Thick Rectangular Barricade.

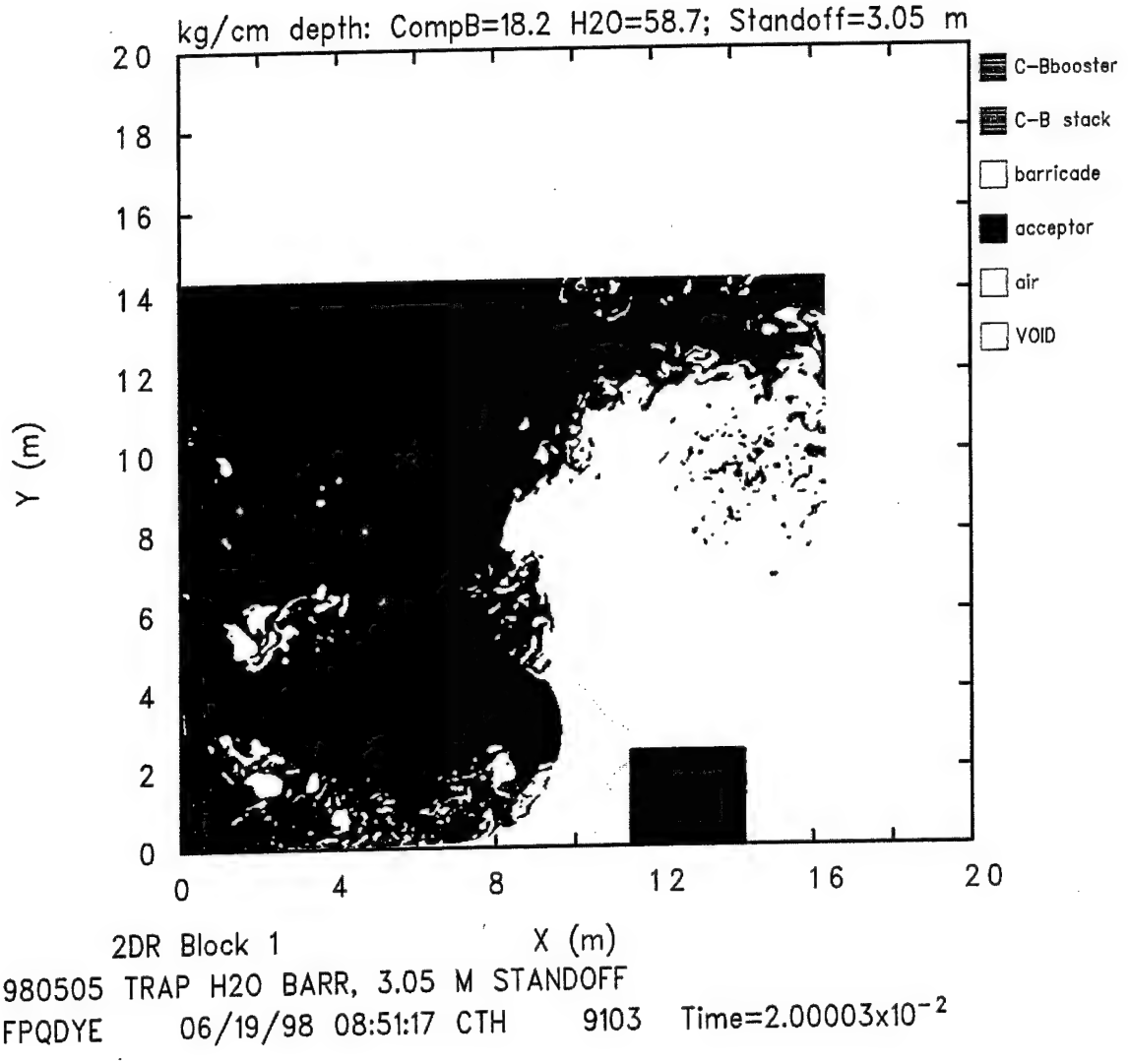

Figure 14. Flow Field at Time = 20.0 ms for Computation 980505, 3.05-m Standoff, Massive Trapezoidal Barricade.

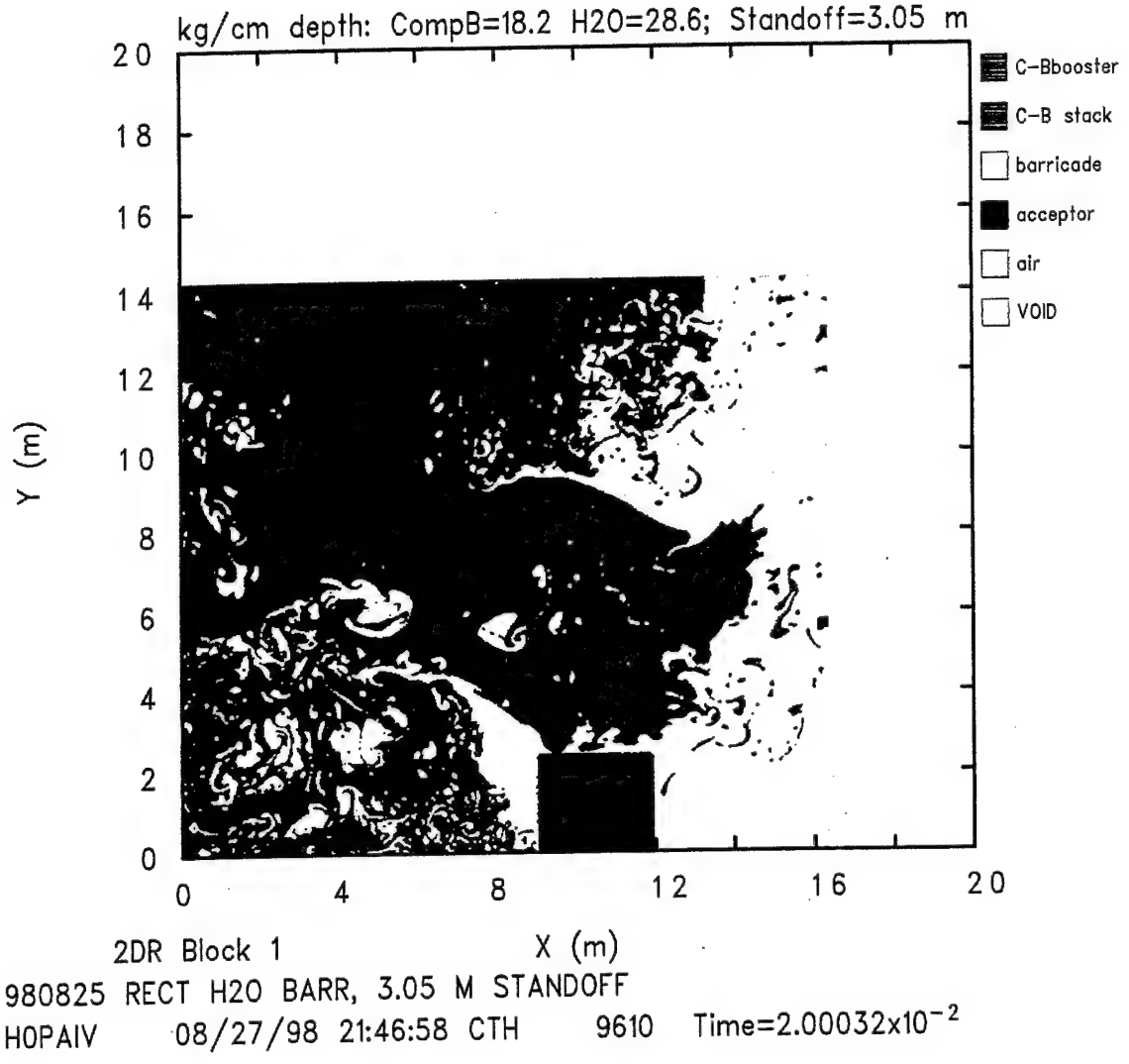

Figure 15. Flow Field at Time = 20.0 ms for Computation 980825, 3.05-m Standoff, Thin Rectangular Barricade.

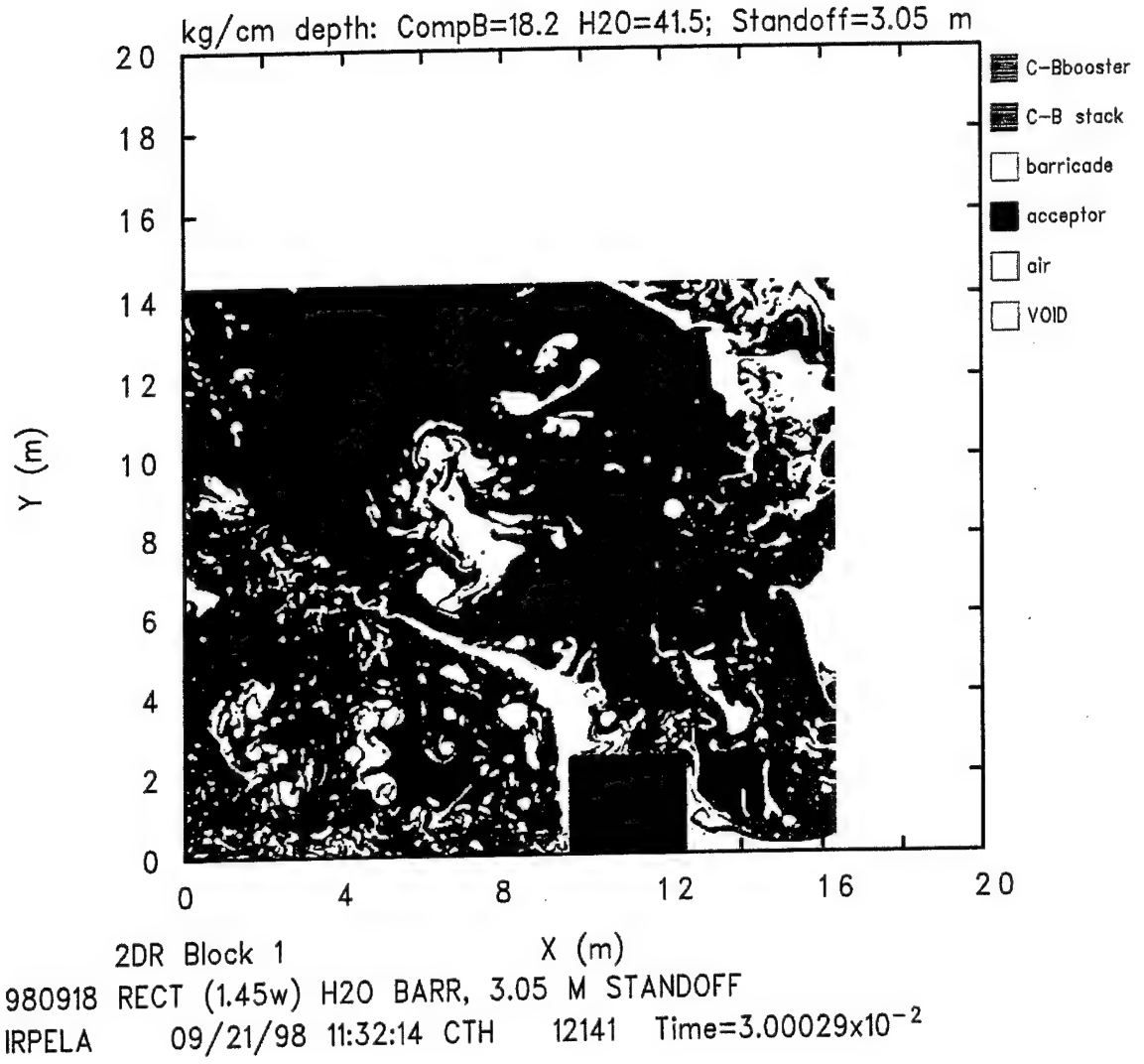

Figure 16. Flow Field at Time = 30.0 ms for Computation 980918, 3.05-m Standoff, Thick Rectangular Barricade.

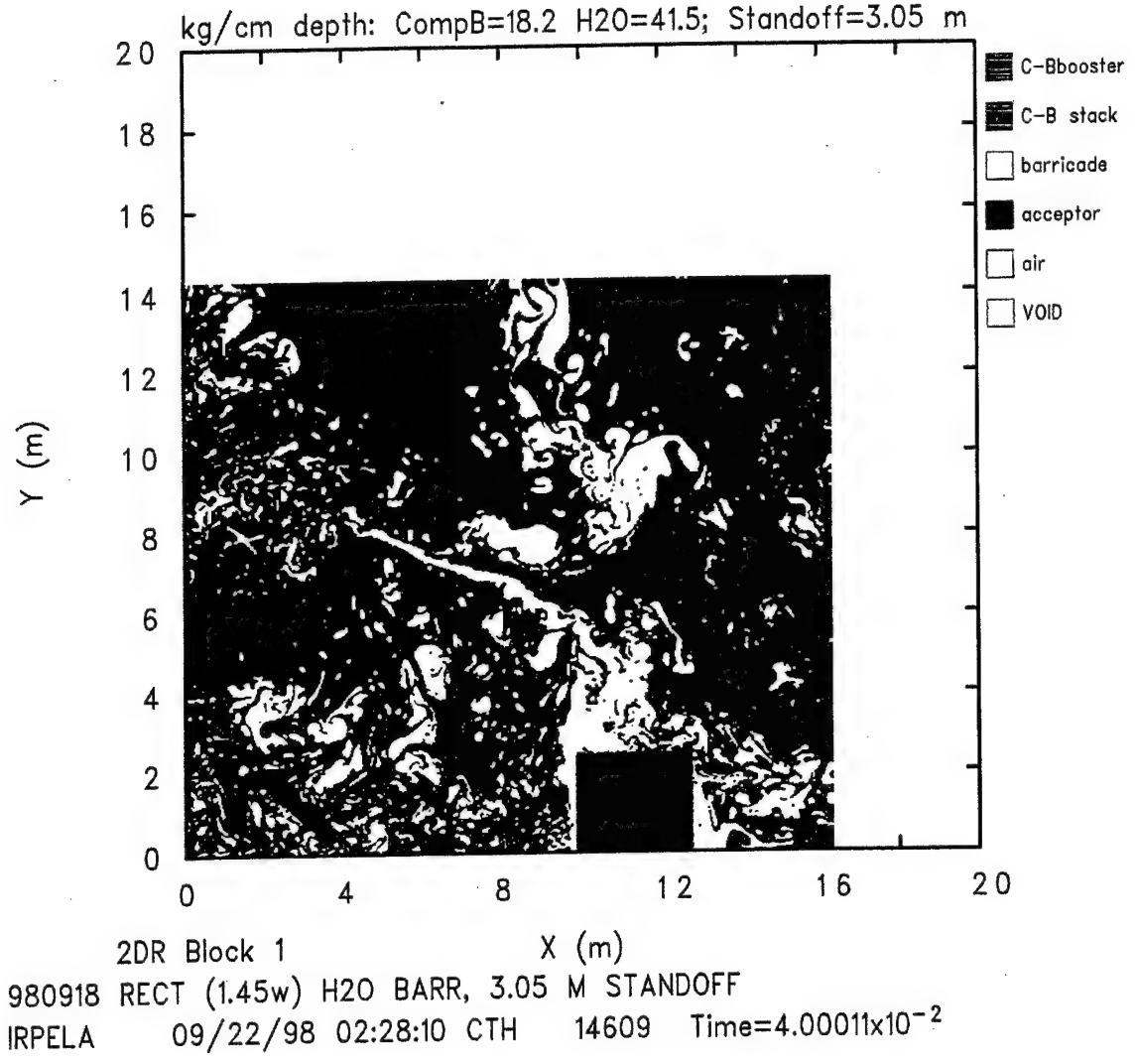

Figure 17. Flow Field at Time = 40.0 ms for Computation 980918, 3.05-m Standoff, Thick Rectangular Barricade.

2.00-m standoff are shown. They both show similar behavior to that for 980918, so fewer snapshots in time are presented, and no direct comparison to corresponding flow fields for the previous two series of computations[1, 2] for the massive trapezoidal and thin rectangular barricades, respectively, are shown.

Computation 980923 simulated a standoff distance of 2.50 m for the same thick rectangular water barricade as in 980918. Figure 18 shows the computational flow field at time = 0.0. Only the standoff distance has been changed from that for 980918, thereby moving the barricade leftward in the flow field toward the donor stack by 0.55 m and the acceptor stack leftward by 1.1 m. The gridding for the computational flow field, the spatial dimensions of the flow field, the munitions stacks, and the barricade are all identical to those for 980918 (see Figure 1). Figure 19 shows the computational flow field at time = 5.0 ms for Computation 980923. This shows similar behavior to that shown in Figure 4 for 980918, except that the barricade is closer in space and time to its initial contact with the acceptor stack left face. The base of the barricade is 0.7 m from the left surface of the acceptor stack and leading the main body of the translating barricade. Explosive products are approaching the top-left corner of the acceptor stack, possibly being drawn in by the low-pressure center of a vortex originating from that corner. Figure 20 shows the flow field at 10.0 ms after initiation. This is approximately 2.0 ms after the peak pressures have been incurred on the acceptor stack left face. This is documented and quantified in a later section of this report. The rebound from the acceptor stack left surface of the water from the barricade is now under way. The section of the barricade in front of the acceptor stack still has a reasonable structural integrity. Explosive products are near the top-left corner of the acceptor stack. Figure 21 shows the flow field for 980923 at 15.0 ms. The rebound from the left surface of the acceptor stack of the water is continuing, and the structural integrity of that section of water is showing rapid degradation. Figure 22 shows that by 20.0 ms, any protection of the acceptor stack by the barricade has essentially ended. Figures 23 and 24 for 30 ms and 40 ms, respectively, show the remnants of the barricade being swept out of the flow field and explosive products in general contact with the acceptor stack.

The last computation in this series for thick rectangular water barricades, Computation 980924, simulated a standoff distance of 2.00 m. As was the case for Computation 980923, the initial flow field and layout of objects are the same as for Computation 980918 except for the standoff distance and the subsequent leftward shifting of the barricade and acceptor stack. Figure 25 shows the computational flow field at time = 0.0. Figure 26 shows the flow field for Computation 980924 at 5.0 ms. At this time the lower, leading section of the barricade is just about to strike the left face of the acceptor stack. Explosive products are approaching the top-left corner of the acceptor stack. They will soon be pushed upward and away from it by the air being forced upward along the left surface of the stack by the water impact moving up the stack. Figure 27 shows the flow field for 980924 at 10.0 ms. The rebound from the acceptor stack left surface of the water is well under way. There are trace amounts of explosive products near the top surface of the acceptor stack, just downstream from the top-left corner. Figures 28, 29, 30, and 31 show subsequent images of

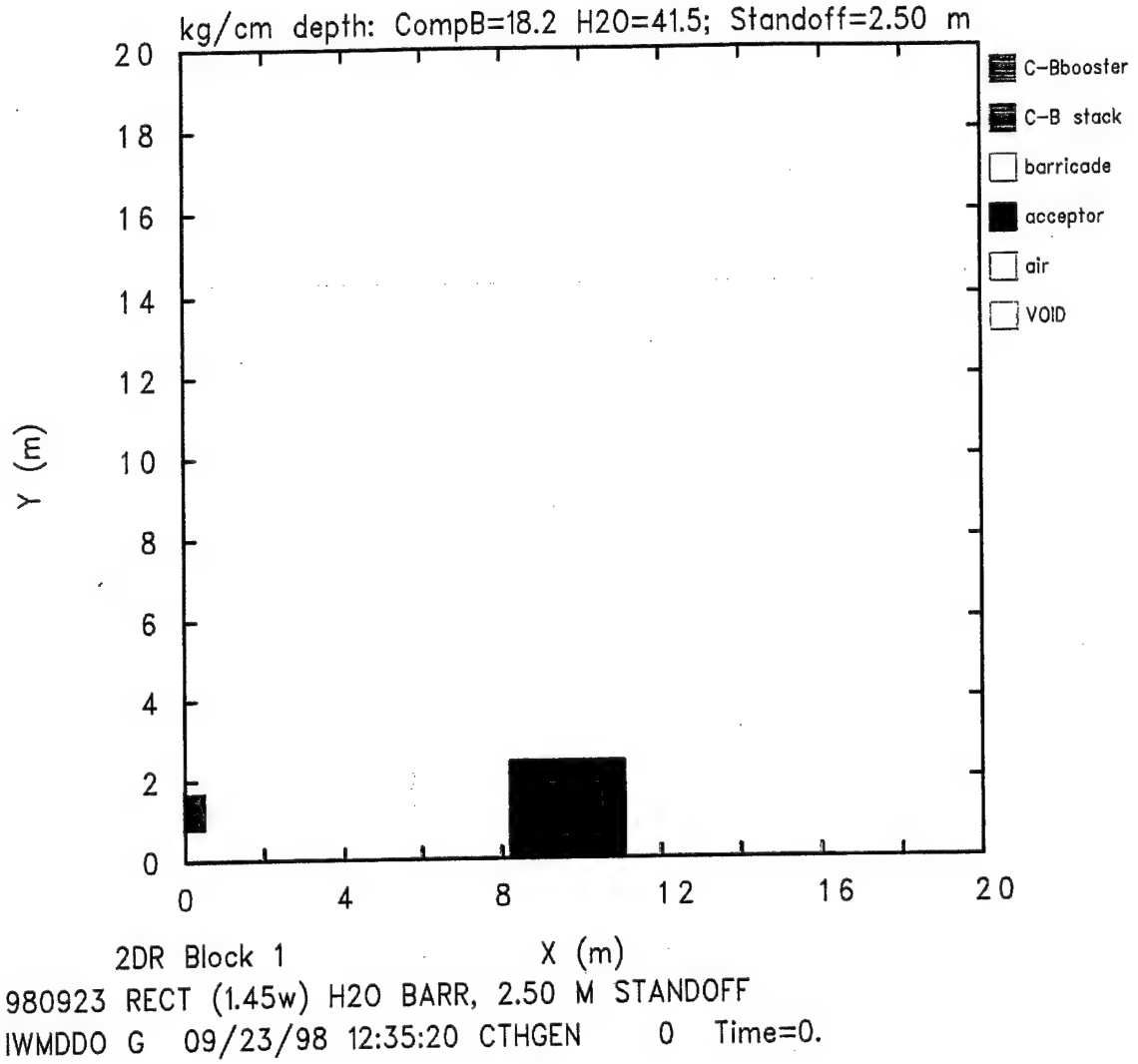

Figure 18. Flow Field at Time = 0.0 for Computation 980923, 2.50-m Standoff, Thick Rectangular Barricade.

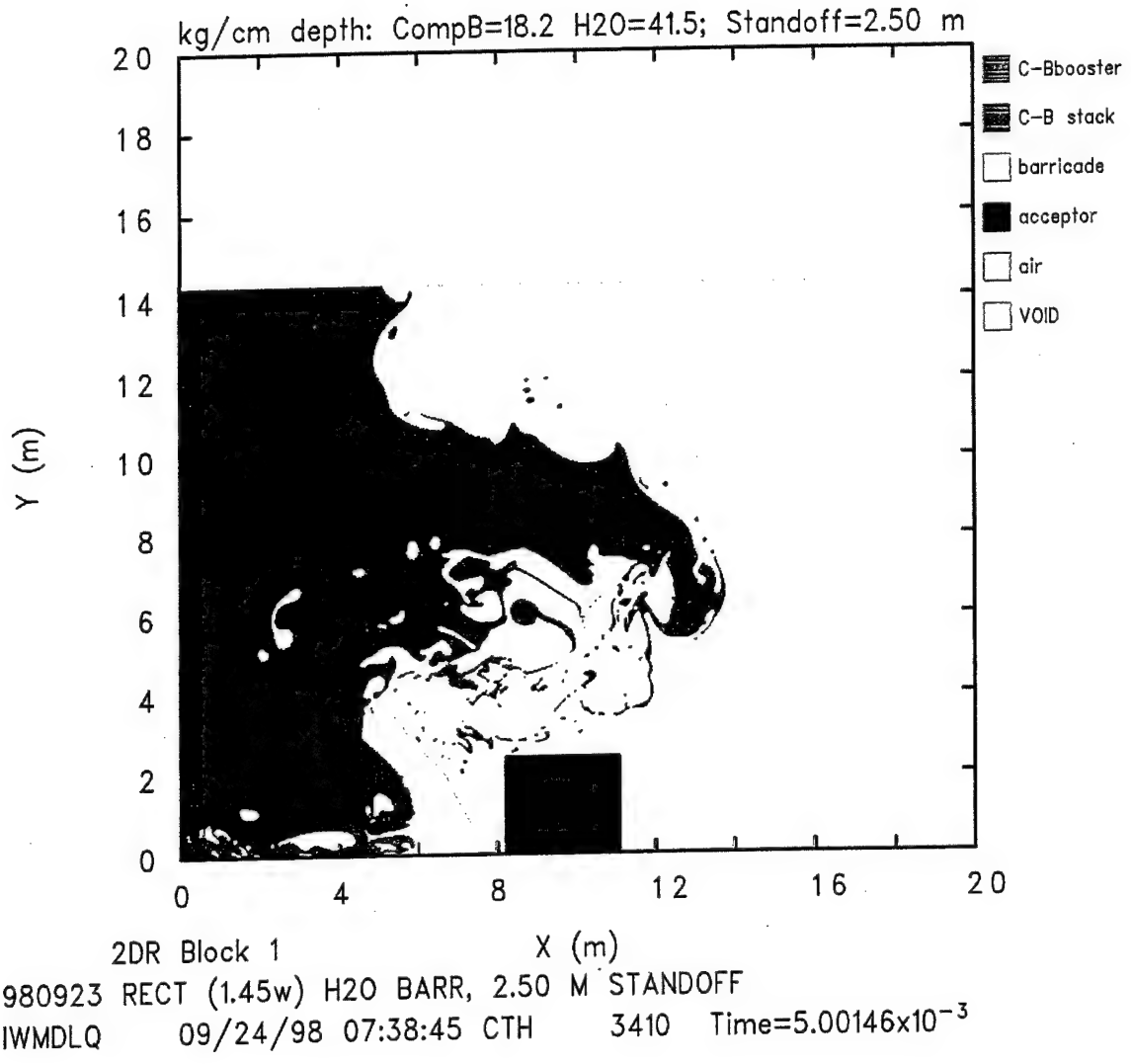

Figure 19. Flow Field at Time = 5.0 ms for Computation 980923, 2.50-m Standoff, Thick Rectangular Barricade.

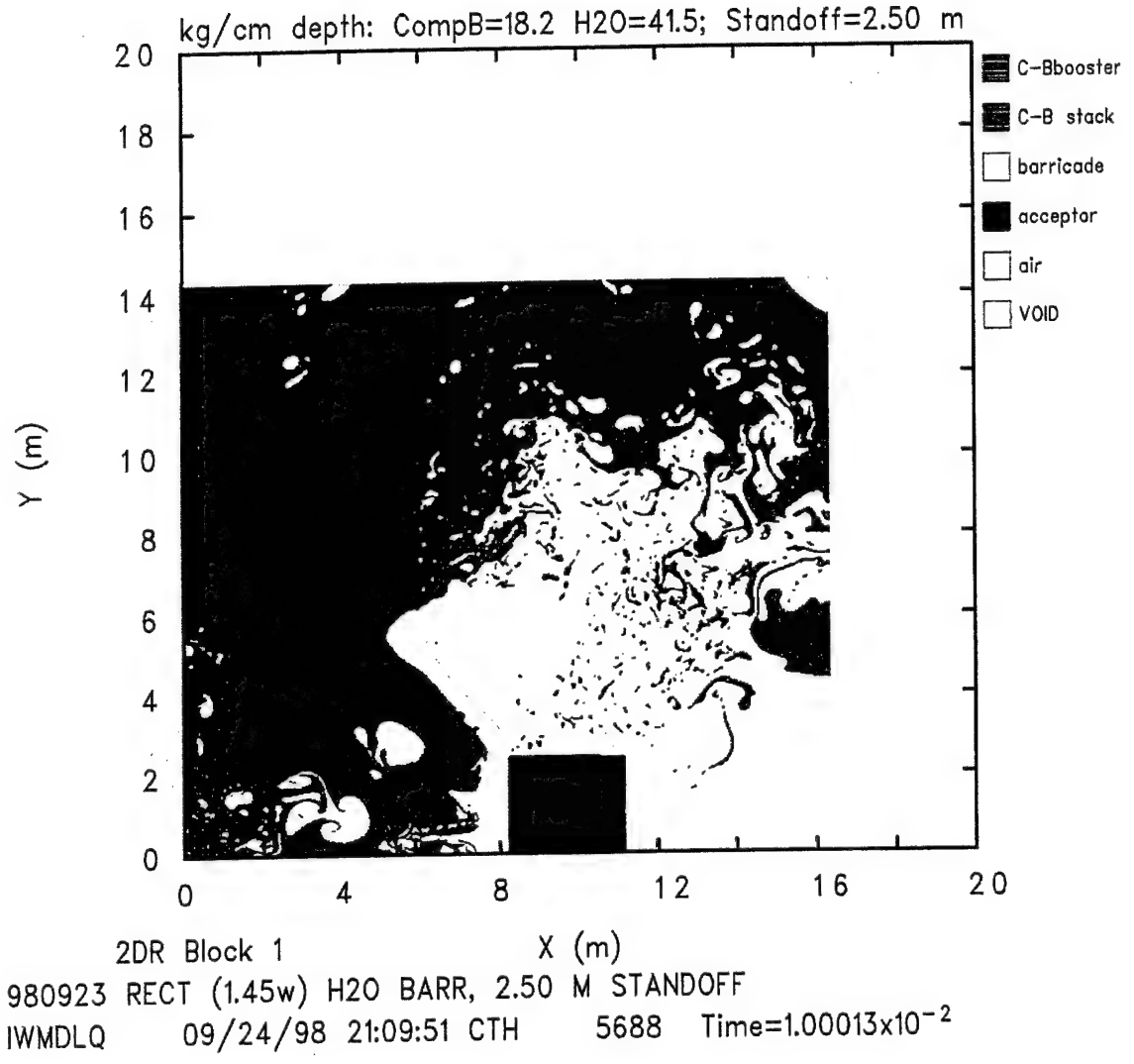

Figure 20. Flow Field at Time = 10.0 ms for Computation 980923, 2.50-m Standoff, Thick Rectangular Barricade.

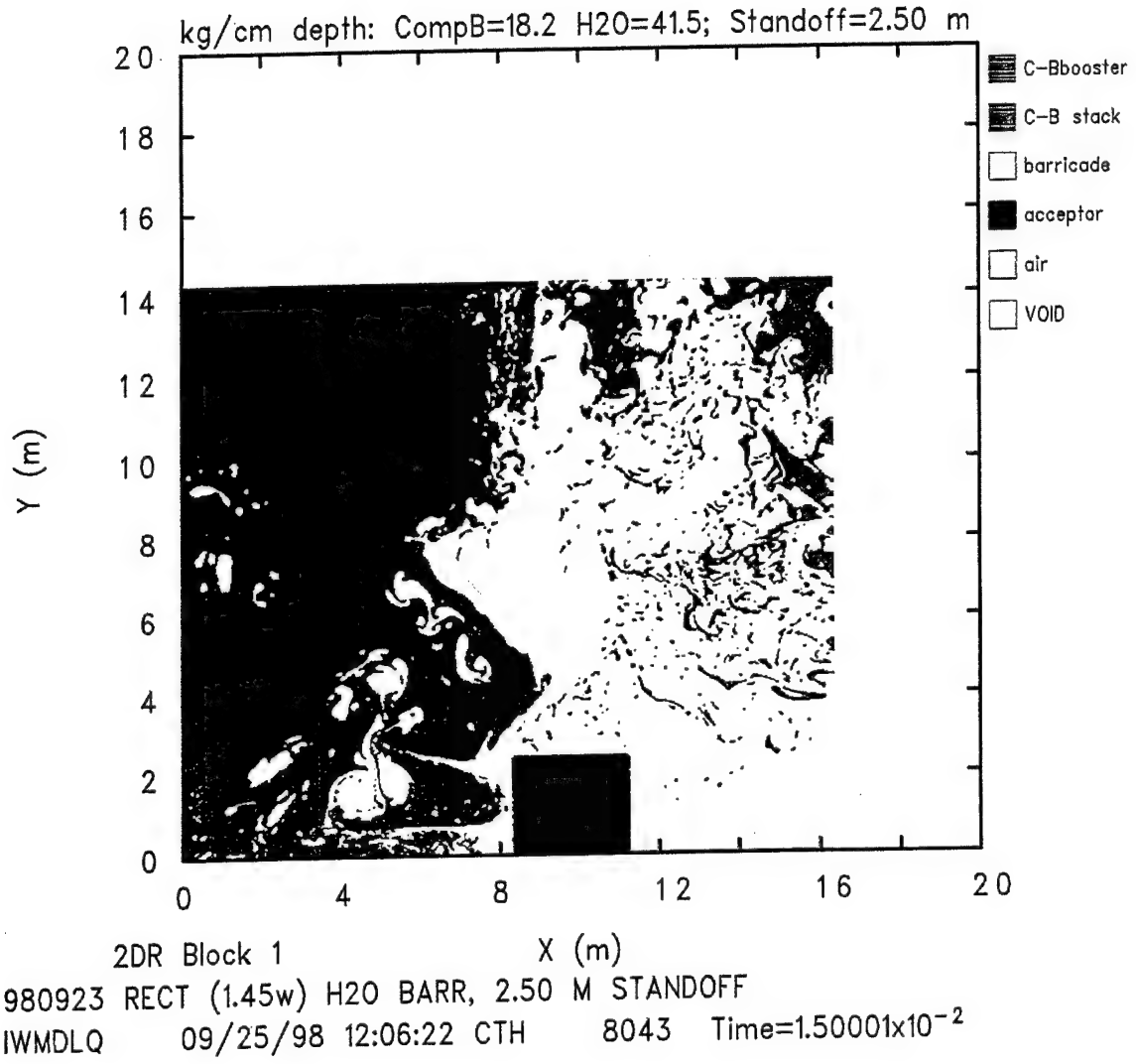

Figure 21. Flow Field at Time = 15.0 ms for Computation 980923, 2.50-m Standoff, Thick Rectangular Barricade.

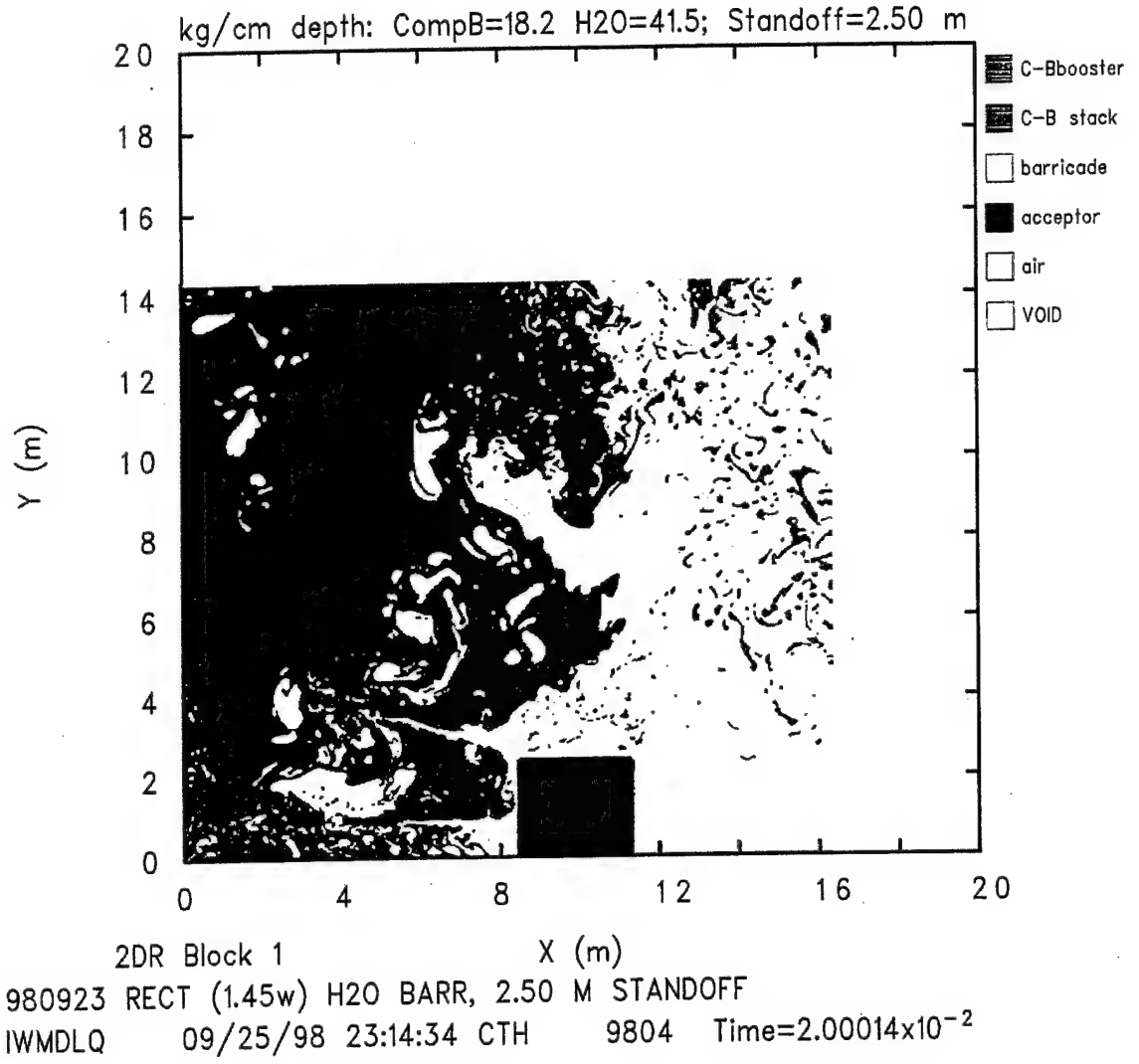

Figure 22. Flow Field at Time = 20.0 ms for Computation 980923, 2.50-m Standoff, Thick Rectangular Barricade.

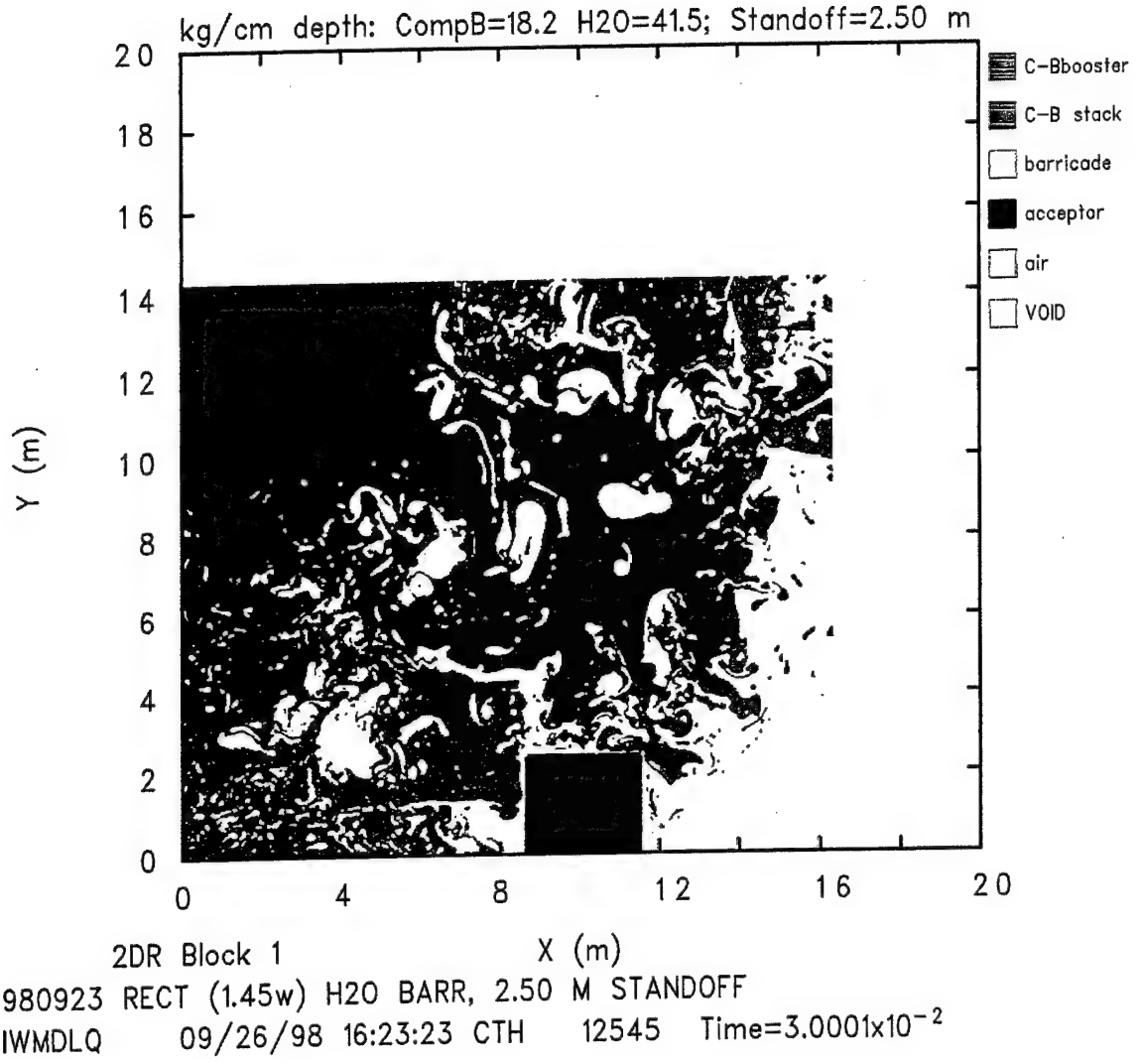

Figure 23. Flow Field at Time = 30.0 ms for Computation 980923, 2.50-m Standoff, Thick Rectangular Barricade.

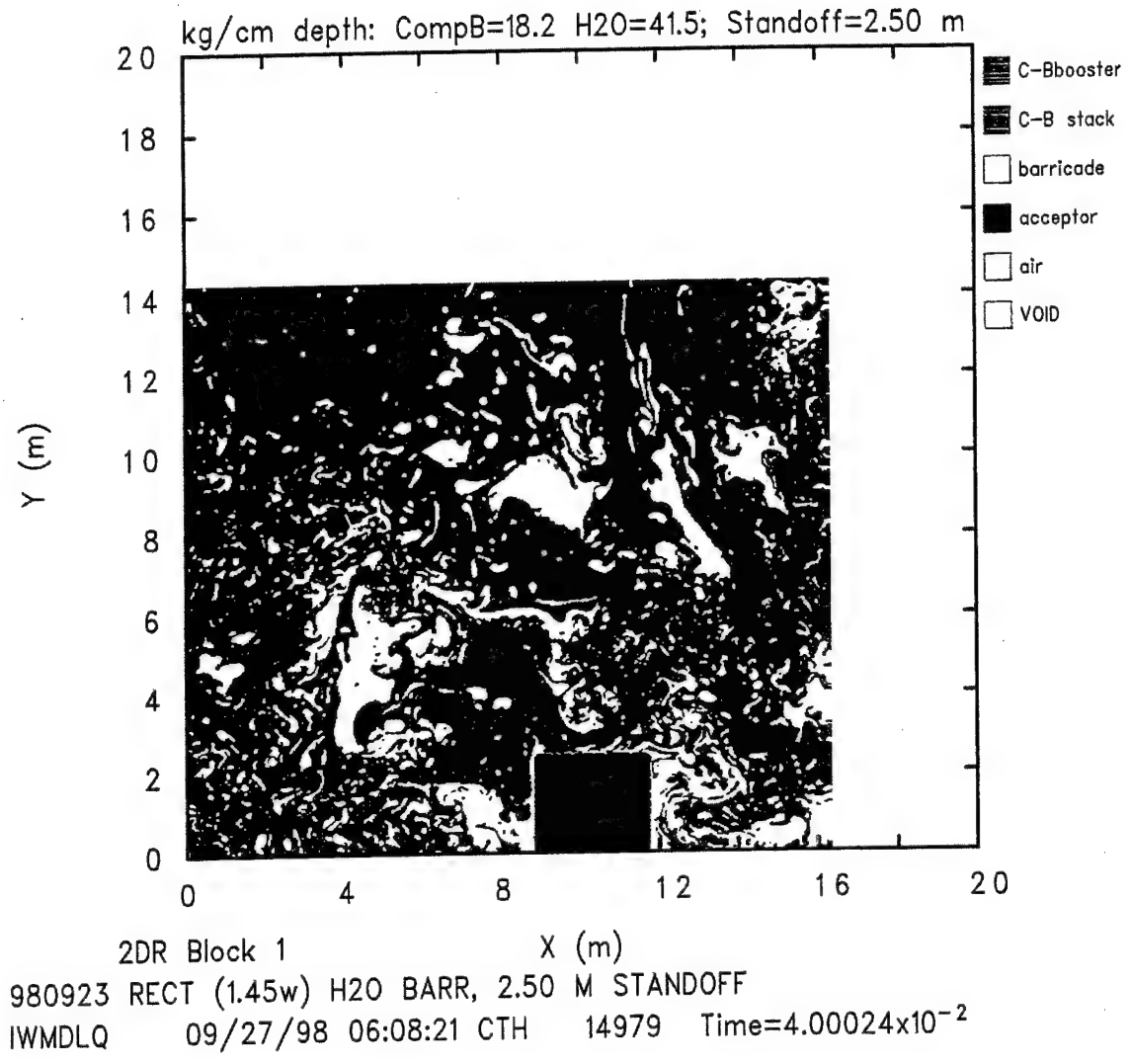

Figure 24. Flow Field at Time = 40.0 ms for Computation 980923, 2.50-m Standoff, Thick Rectangular Barricade.

the computational flow field at time = 15.0 ms, 20.0 ms, 30.0 ms, and 40.0 ms, respectively, for Computation 980924. Collectively, the figures show the same qualitative behavior as those for Computations 980918 and 980923, with events happening at a faster rate with respect to time simply because of the closer initial standoff.

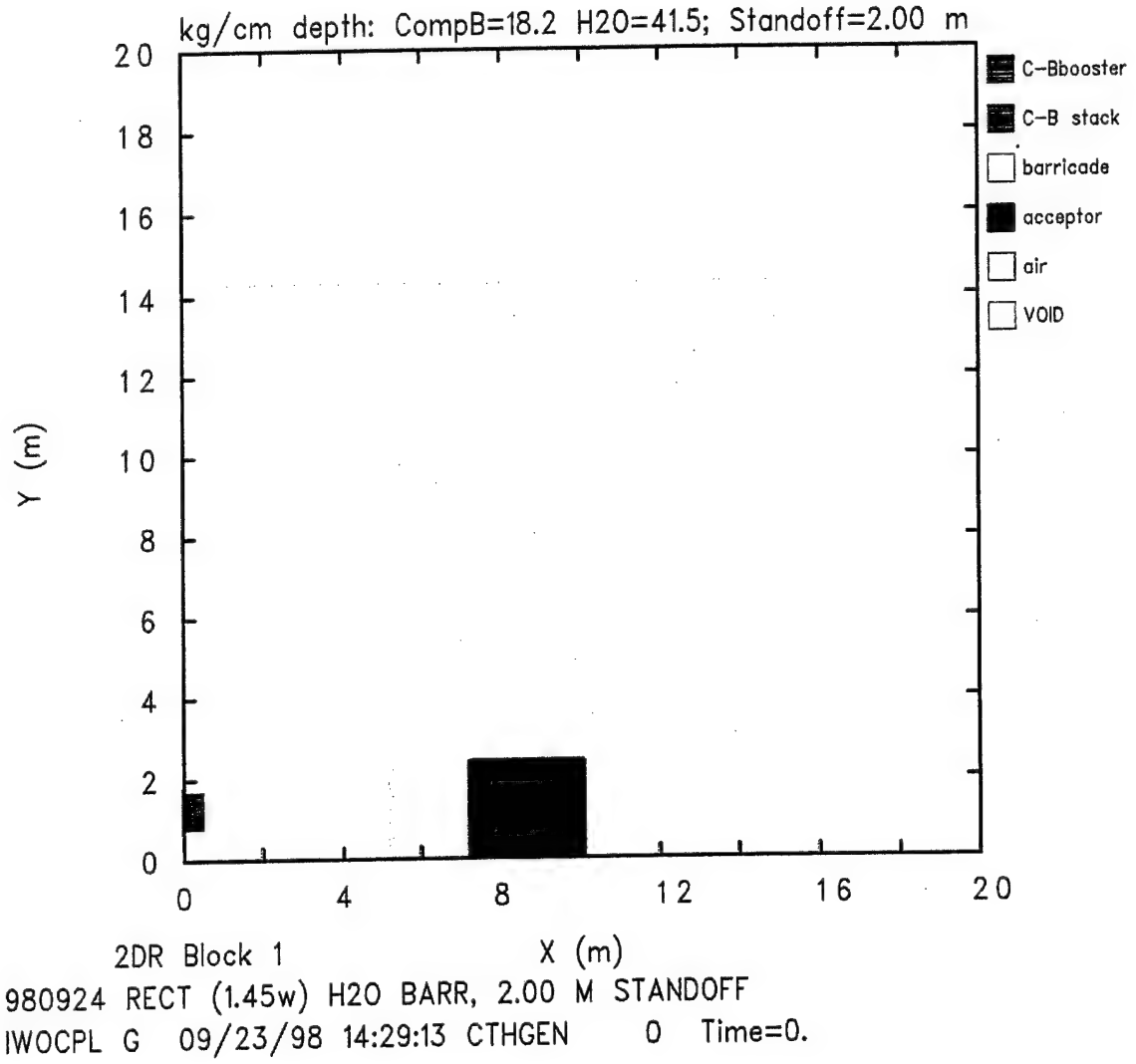

Figure 25. Flow Field at Time = 0.0 for Computation 980924, 2.00-m Standoff, Thick Rectangular Barricade.

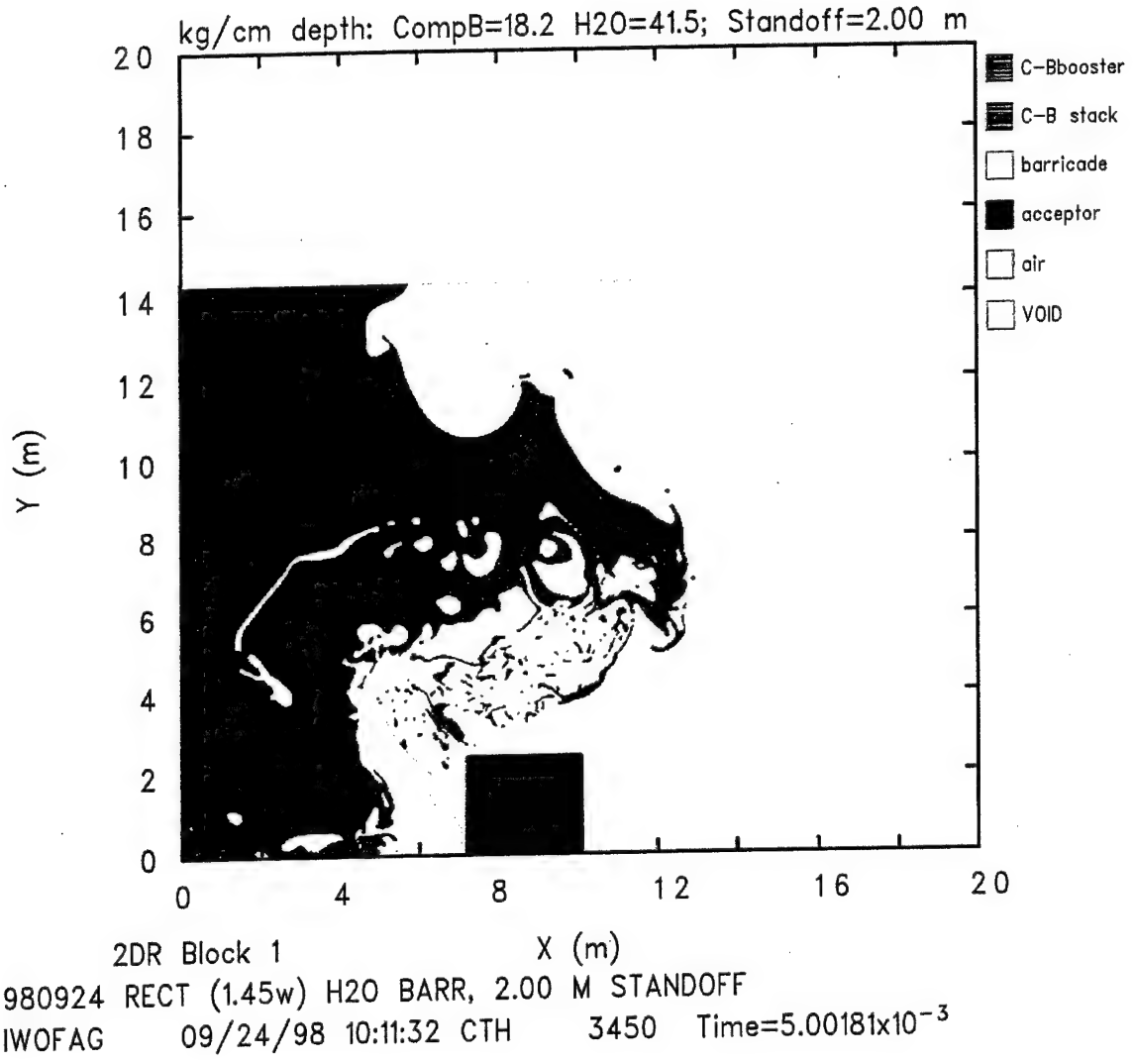

Figure 26. Flow Field at Time = 5.0 ms for Computation 980924, 2.00-m Standoff, Thick Rectangular Barricade.

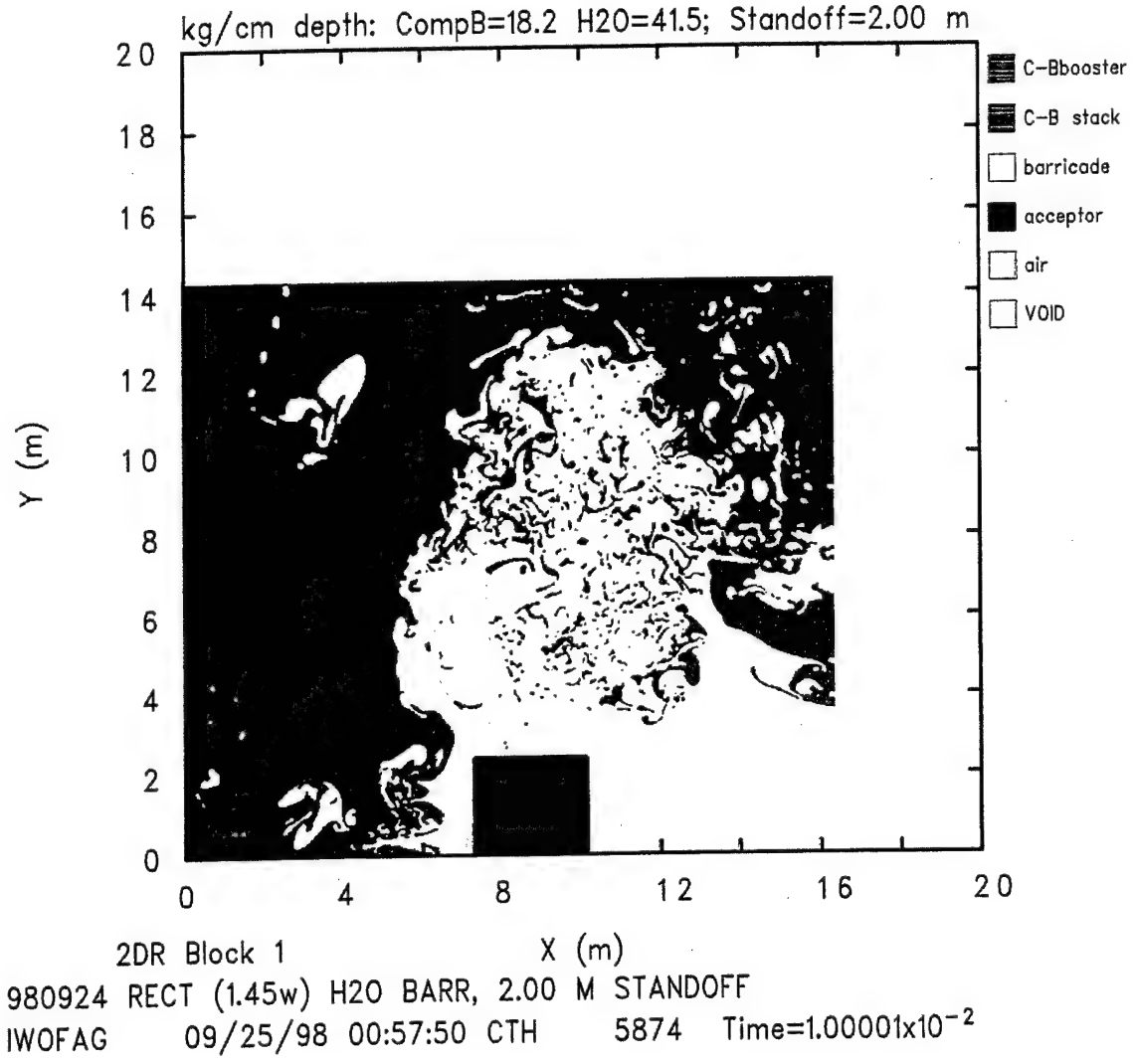

Figure 27. Flow Field at Time = 10.0 ms for Computation 980924, 2.00-m Standoff, Thick Rectangular Barricade.

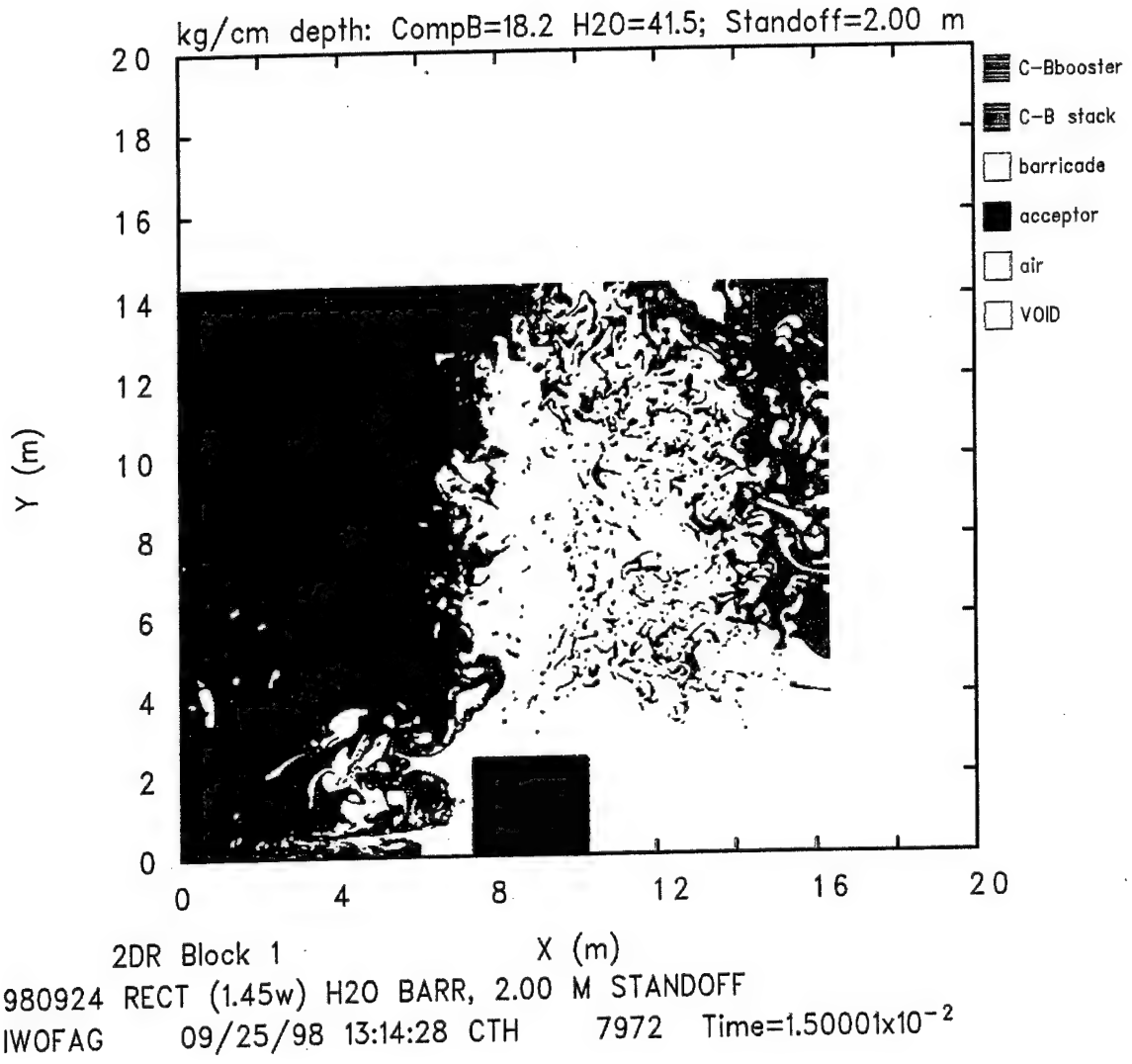

Figure 28. Flow Field at Time = 15.0 ms for Computation 980924, 2.00-m Standoff, Thick Rectangular Barricade.

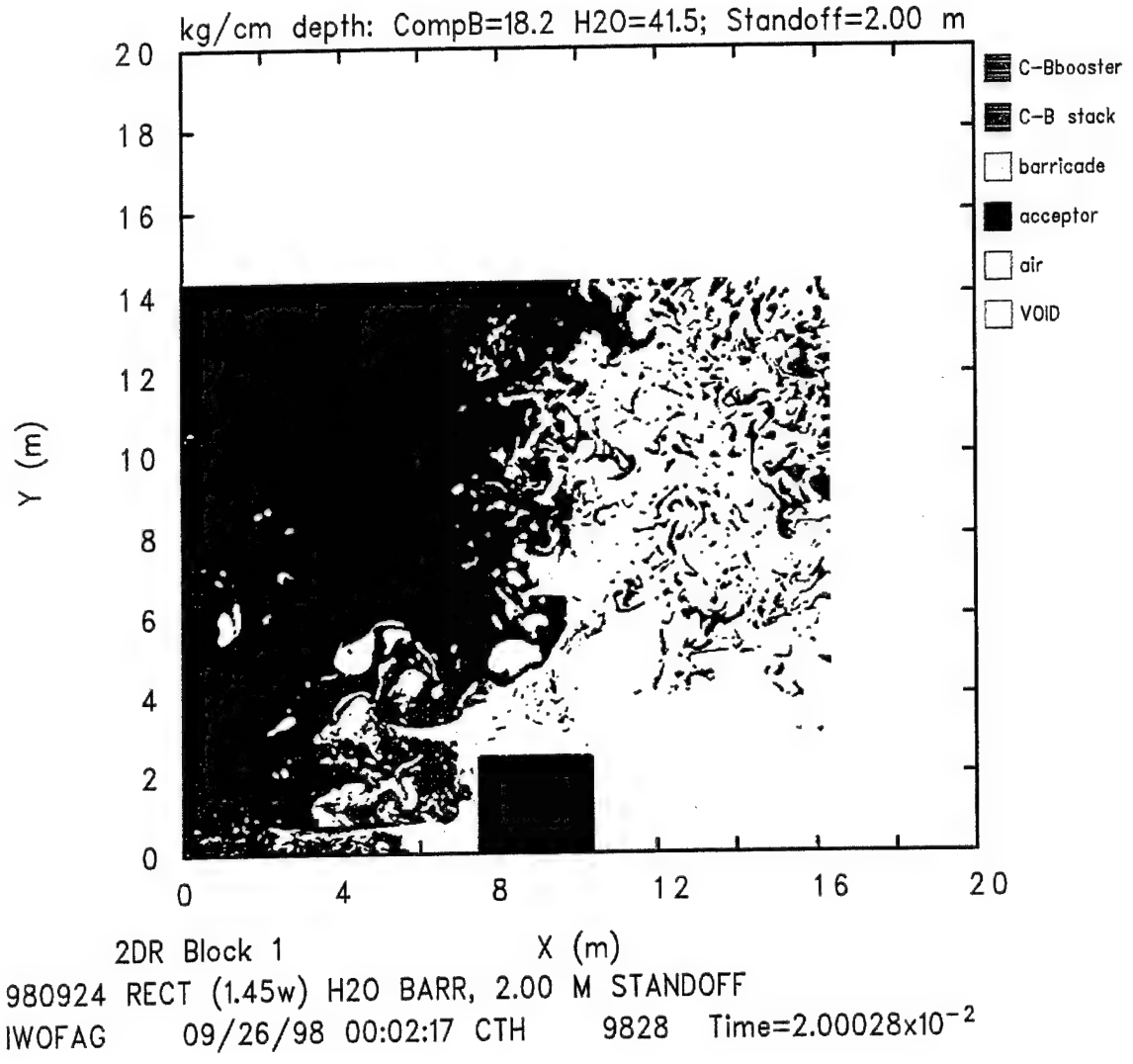

Figure 29. Flow Field at Time = 20.0 ms for Computation 980924, 2.00-m Standoff, Thick Rectangular Barricade.

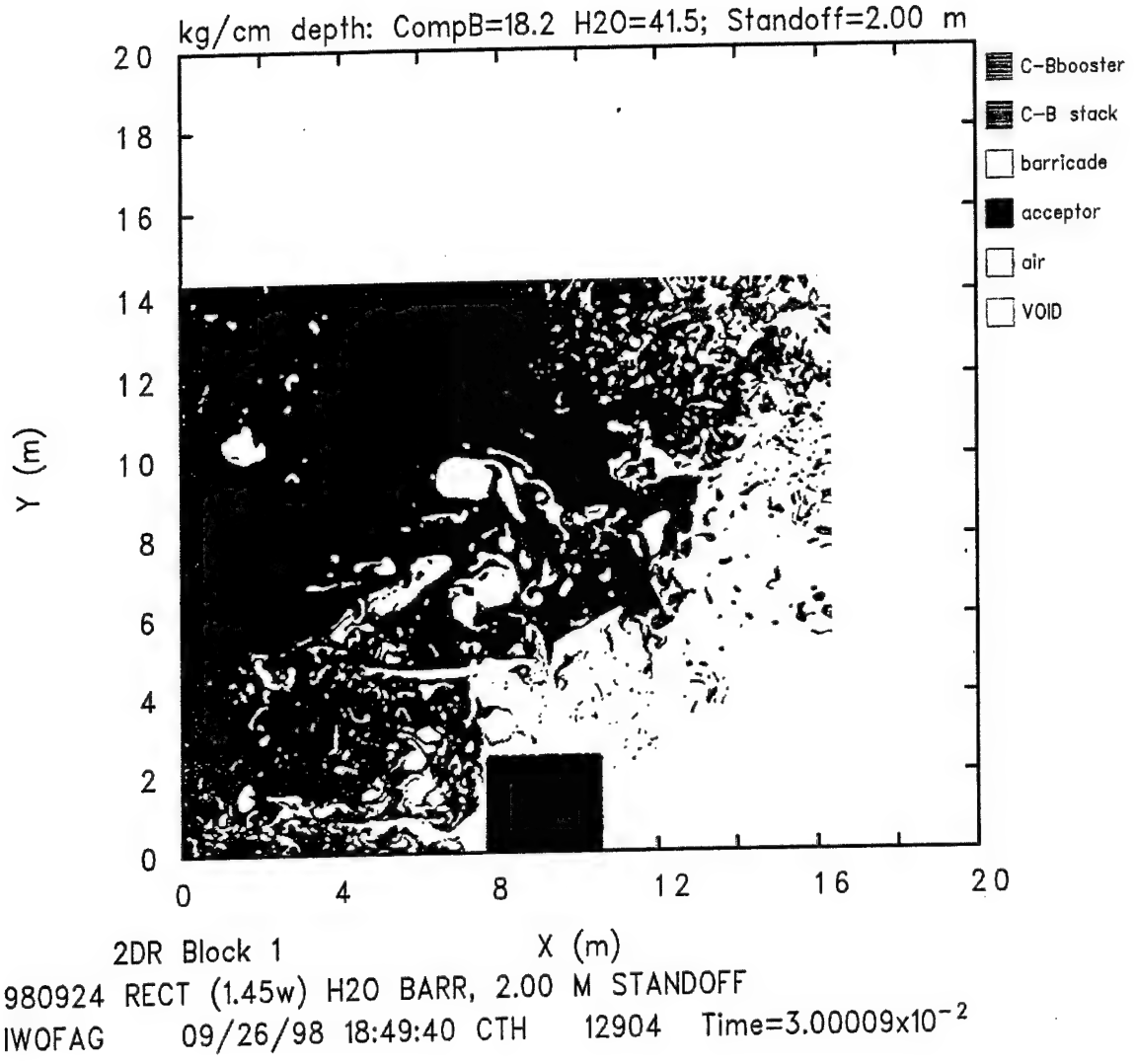

Figure 30. Flow Field at Time = 30.0 ms for Computation 980924, 2.00-m Standoff, Thick Rectangular Barricade.

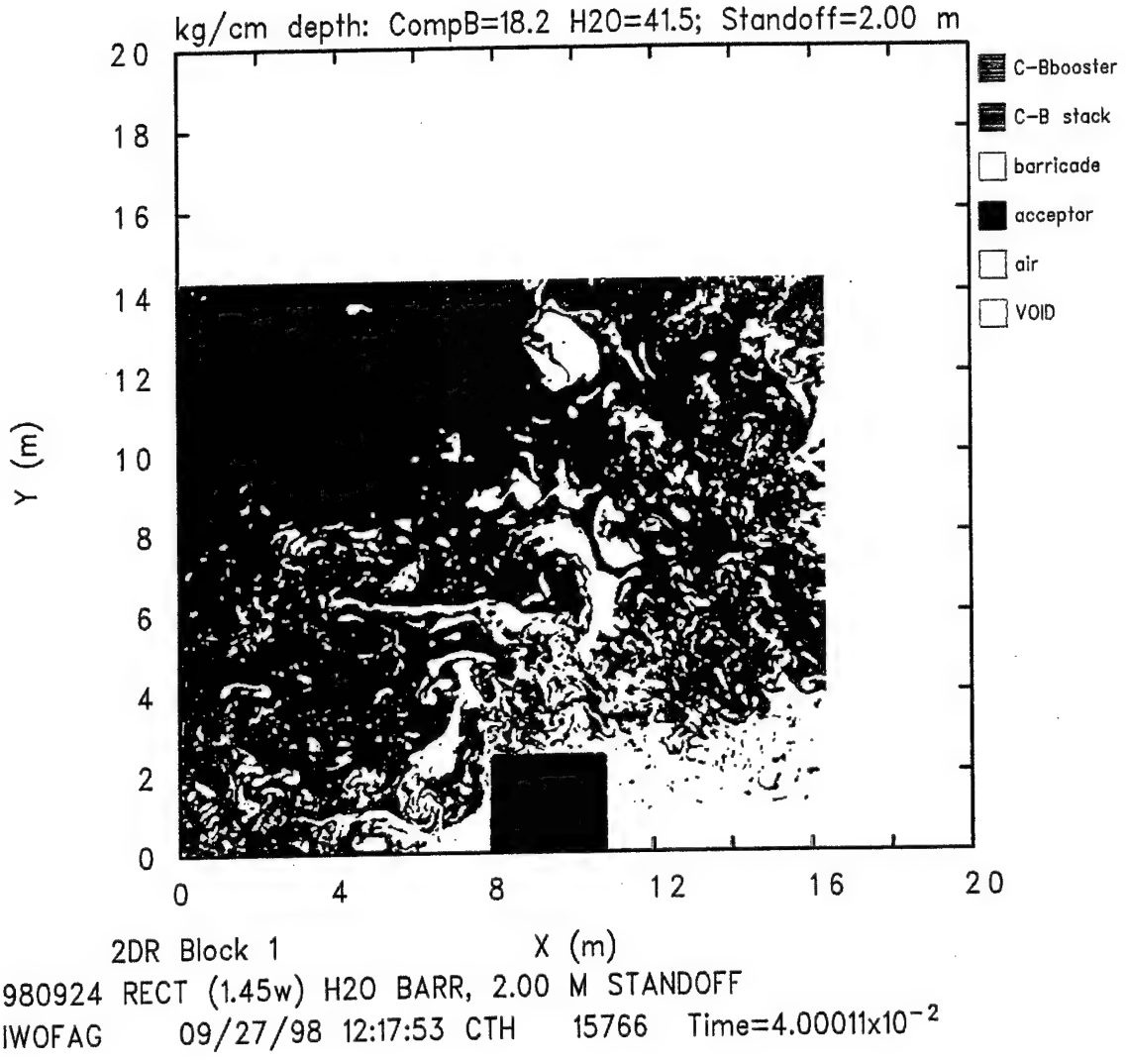

Figure 31. Flow Field at Time = 40.0 ms for Computation 980924, 2.00-m Standoff, Thick Rectangular Barricade.

3.2. Barricade Dynamics

Figure 32 shows the bulk momentum per centimeter depth of the water barricade in the X direction. Positive momentum is in the direction of increasing values of X. Figure 32 includes the X-direction momentum for each of the three fully coupled computations in this series for the thick rectangular barricade, plus that for Computation 980825 for the thin rectangular water barricade[2] and Computation 980505 for the massive trapezoidal water barricade[1] at a 3.05-m standoff. Hereinafter, any use of the term "momentum" or the other variables (e.g., velocity, acceleration, and displacement) derived from it should be construed as referring to the bulk value in the X direction per centimeter of depth, unless specifically stated otherwise. The term "bulk" is implied but used only sparingly in order to avoid repetition. The momentum shown here is the combined momentum for all of the water in the flow field at each computational time step. Values for the mass and momentum for the water (and all other materials) are saved after each time step. During any given time step later in the computations, some water flows out of the flow field through either or both of the top and right transmissive boundaries. Each of the three curves for the thick rectangular barricade shows a very rapid, monotonic initial increase in momentum with decreasing standoff. The curve for Computation 980924 (2.00-m standoff) shows the first, very abrupt decrease in momentum after its peak at 5.1 ms, followed by 980923 (for the 2.50-m standoff) after its peak at 6.6 ms, and then by 980918 (3.05-m standoff) after its peak at 8.3 ms. This very rapid drop in each curve for the thick rectangular barricade is because of the nearly simultaneous bottom-to-top strike of the barricade on the left face of the acceptor stack. As may be seen in Figure 32, the thick rectangular barricade delivers most of its momentum to the acceptor stack over a very short period of time, as does the representative plot for the thin rectangular barricade[2] at a 3.05-m standoff, labeled "Thin Rect, Standoff 3.05 m." The fifth curve shown in Figure 32, labeled "Trap Standoff 3.05 m," is for the momentum of the massive trapezoidal water barricade at a 3.05-m standoff.[1] It shows a more gradual increase to a considerably lower peak momentum with a two-stage, much smaller total decrease in momentum.

It is interesting to point out here that, while there is not much difference in both the peak momenta and the values to which the momenta for the both the thick and thin rectangular barricades decrease by 10 ms as a function of standoff distance, there is a great difference in both peak momentum and change in momentum that can be seen when comparing both rectangular barricades with the massive trapezoidal barricade at the same 3.05-m standoff distance. Table 2 contains a summary of several X-direction parameters that describe some of the bulk motion of the barricade for the various computations. First among those parameters, after the computation numbers, standoff distances, and then barricade masses, are the peak X-direction bulk momentum values for the barricade, along with their respective times of occurrence, listed with more significant figures than were typically used in the text for completeness. In order to facilitate comparisons, the first column of numbers is for the massive trapezoidal barricade at a 3.05-m standoff, followed by data for the thin rectangular

barricade at a 3.05-m standoff, and then the three standoffs for the thick rectangular barricade. The rest of the parameters in the table are discussed in the following paragraphs.

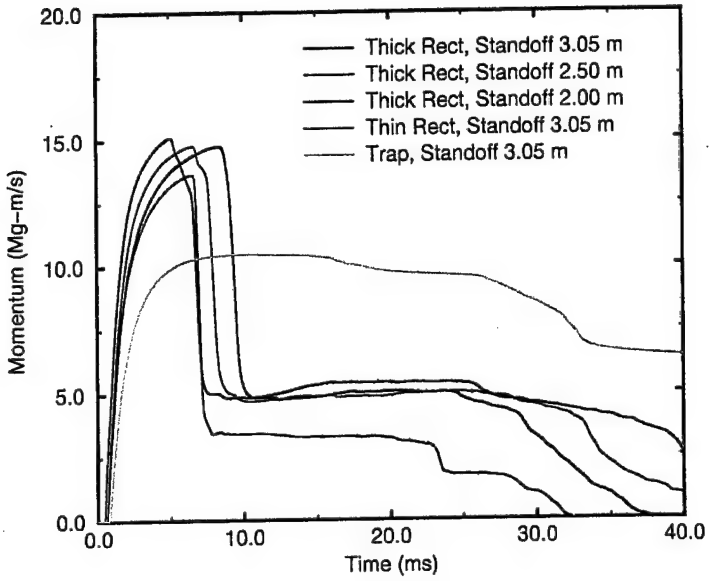

Figure 32. Water Barricade X-Direction Momentum Toward the Acceptor Stack, Computations 980918 Through 980924 (Thick Rectangular), Plus 980825 (Thin Rectangular) and 980505 (Trapezoidal).

After each computational time step, both the total momentum and mass of the water in the flow field are known. The X-direction bulk velocity (hereinafter referred to as "X-direction velocity") of the barricade may be computed for each time step by dividing the instantaneous momentum by the corresponding mass. The X-direction velocity of the water barricade toward the acceptor stack for each standoff for the thick rectangular barricade, plus the velocity for the trapezoidal barricade and the thin rectangular barricade at a 3.05-m standoff, is shown in Figure 33. These curves are essentially scaled variants of the momentum curves shown in Figure 32 and therefore show the same relative behavior described for the momenta. The peak X-direction velocity for the thick rectangular barricade at each standoff distance is 355.3 m/s at 8.33 ms (3.05-m standoff), 355.9 m/s at 6.56 ms (2.50-m standoff), and 364.0 m/s at 5.09 ms (2.00-m standoff). For comparison, the curves for the thin rectangular and trapezoidal barricades for a 3.05-m standoff are included in Figure 33 with the same legend labels as were used for their momentum plots in Figure 32. For the 3.05-m standoff, the thin rectangular barricade has a peak velocity of 476.6 m/s and the trapezoidal barricade has a peak velocity of 178.2 m/s. The X-direction barricade velocities become less meaningful at late time as far as the acceptor stack is concerned because of

Table 2. Barricade Peak X-Direction Bulk Motion Parameters.

Computation Number	Massive Trape-zoidal 980505	Thin Rectan-gular 980825	Thick Rectan-gular 980918	Thick Rectan-gular 980923	Thick Rectan-gular 980924
Standoff (m)	3.048	3.048	3.048	2.50	2.00
Barricade Mass (kg/cm of depth)	58.71	28.61	41.49	41.49	41.49
Peak Momentum (Mg-m/s)	10.46	13.64	14.74	14.77	15.10
Time (ms)	10.07	6.560	8.334	6.559	5.089
Peak Velocity (m/s)	178.2	476.6	355.3	355.9	364.0
Time (ms)	10.93	6.560	8.334	6.559	5.089
Peak Positive Acceleration (km/s/s)	143.4	631.5	434.7	453.3	468.9
Time (ms)	10.04	0.8141	0.8141	0.6947	0.5948
Peak Negative Acceleration (km/s/s)	-19.22	-808.7	-310.0	-317.8	-347.9
Time (ms)	32.80	7.093	9.494	8.023	6.883
Peak Left-Surface Impulse (MN-s/m)	0.9016	1.185	1.241	1.308	1.396
Time (ms)	34.48	38.29	39.99	39.88	39.37

the increasing proportion of water that is in the air above the plane of the top face of the acceptor stack.

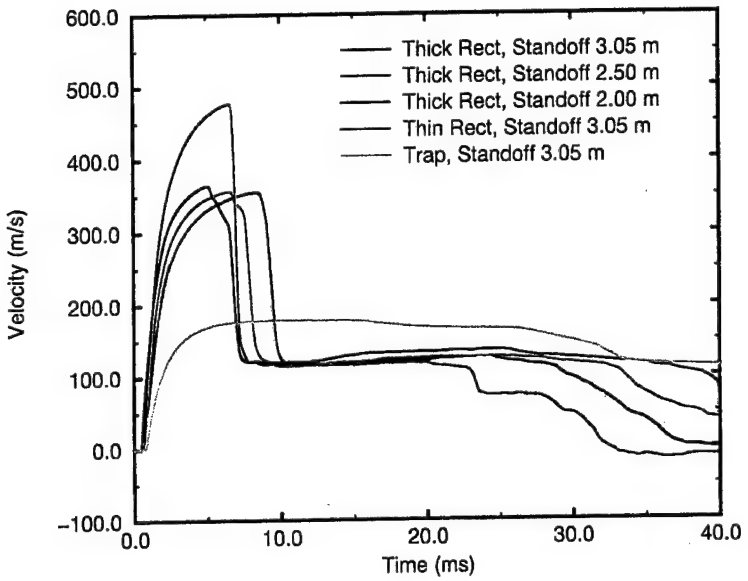

Figure 33. Water Barricade X-Direction Velocity Toward the Acceptor Stack, Computations 980918 Through 980924 (Thick Rectangular), Plus 980825 (Thin Rectangular) and 980505 (Trapezoidal).

The momentum curves in Figure 32, and hence the velocity curves in Figure 33, are relatively smooth functions with respect to time. The velocities were piecewise differentiated with respect to time, using the difference values of velocity and time in the data file, to produce the curves of bulk X-direction acceleration for each standoff as shown in Figure 34. The peak positive accelerations for the thick rectangular barricade are 434.7 km/s^2 at 0.81 ms (3.05-m standoff), 453.3 km/s^2 at 0.69 ms (2.50-m standoff), and 468.9 km/s^2 at 0.59 ms (2.00-m standoff). For comparison, the peak positive acceleration of the thin rectangular barricade is 631.5 km/s^2 at 0.814 ms. For the trapezoidal barricade it is 143.4 km/s^2 at 10.0 ms. These plots are also shown in Figure 34. The peak negative accelerations (i.e., decelerations) caused by the barricade striking the acceptor stack are particularly informative, especially when viewed in conjunction with the acceptor stack loading that is presented in a following section of this report. The negative accelerations for the thick rectangular barricade are minus 310.0 km/s^2 at 9.49 ms (3.05-m standoff), minus 317.8 km/s^2 at 8.02 ms (2.50-m standoff), and minus 347.9 km/s^2 at 6.88 ms (2.00-m standoff). For a 3.05-m standoff, the thin rectangular barricade has a peak negative acceleration of minus 808.7 km/s^2 at 7.09 ms. The trapezoidal barricade has a peak negative acceleration of minus 19.2 km/s^2 at 32.8 ms. Because the full simulation time is displayed on the abscissa, the initial accelerations of the

barricade for each standoff for the thick rectangular barricade appear to nearly overlay one another. Figure 35 shows a temporally expanded plot of the first 12.0 ms of the X-direction acceleration of the barricade for each computation. The initial accelerations for the thick rectangular barricade occur in a direct sequence based on standoff distance, with the initial accelerations for the thin rectangular and the trapezoidal barricades at a 3.05-m standoff beginning at about the same time as that for the thick rectangular barricade at that same standoff. The deceleration sequence for the thick rectangular barricade also occurs in direct correspondence to the standoff distance. No meaningful deceleration of the trapezoidal barricade occurs during the first 12.0 ms, but the thin rectangular barricade clearly shows a great deceleration at 7.09 ms.

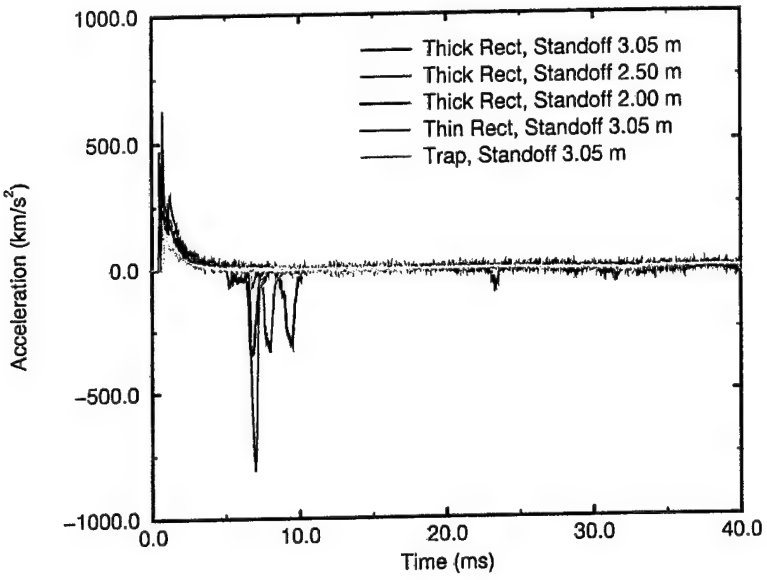

Figure 34. Water Barricade X-Direction Acceleration Toward the Acceptor Stack, Computations 980918 Through 980924 (Thick Rectangular), Plus 980825 (Thin Rectangular) and 980505 (Trapezoidal).

Figure 36 shows the total X-direction impulse per meter depth on the left surface of the barricade. This was computed by integrating the overpressure over space and time using 30 tracer particles that were placed along the left surface of the barricade at time zero, the grid generation time. The overpressure is the absolute pressure minus the ambient atmospheric pressure. The tracer particles were allowed to move freely with the flow in the grid. As the simulated time in the computations progressed, the left surface of the barricade became increasingly distorted to the point that it was no longer clearly definable as a simple surface. Correspondingly, the impulse integral itself probably lost meaning after about 10 ms. Essentially all of the impulse from the detonation of the donor stack is delivered

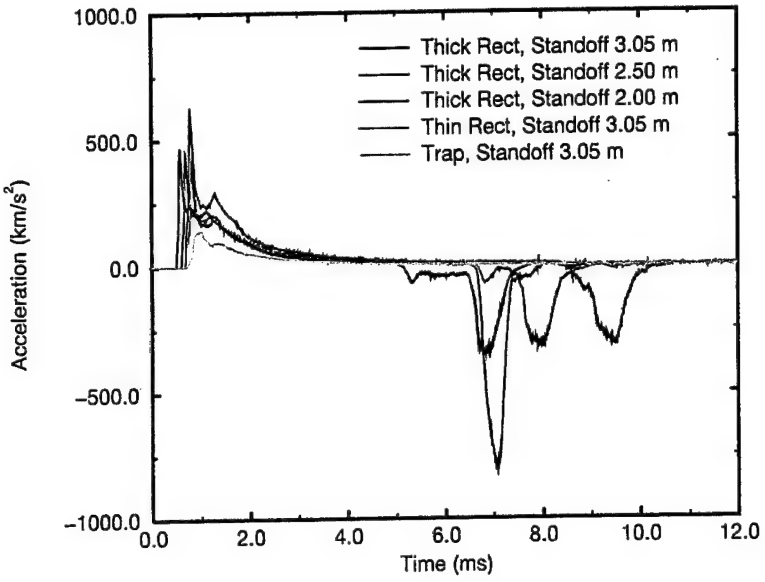

Figure 35. Water Barricade Initial X-Direction Acceleration Toward the Acceptor Stack, Computations 980918 Through 980924 (Thick Rectangular), Plus 980825 (Thin Rectangular) and 980505 (Trapezoidal).

to the barricade in the first few milliseconds. There is a moderate inverse functional relation in impulse delivered to the thick rectangular barricade with respect to standoff distance. There is less impulse delivered to the thin rectangular barricade than to the thick rectangular barricade at a 3.05-m standoff distance. Even less impulse is delivered to the trapezoidal barricade than to the thick rectangular barricade at a 3.05-m standoff distance. The peak values for the thick rectangular barricade are 1.241 MN-s/m at 40.0 ms (3.05-m standoff), 1.308 MN-s/m at 39.9 ms (2.50-m standoff), and 1.396 MN-s/m at 39.4 ms (2.00-m standoff). Because of the surface distortion just discussed, the times of these peaks are not particularly important and are included only for completeness. This equates to a direct ratio of peak impulse for the thick rectangular barricade of 1.125 for an inverse ratio in relative standoff distance of 1.524 for the standoff range of 3.05 m to 2.00 m. For comparison, the peak impulse for the thin rectangular barricade is 1.185 MN-s/m at 38.3 ms (3.05-m standoff), and 0.9016 MN-s/m at 34.5 ms for the trapezoidal barricade at that same standoff.

The velocity data are used to compute the bulk translation of the barricade versus time, which is shown in Figure 37. The curves for the thick rectangular barricade are most meaningful through about 6 to 7 ms. At about this time the barricade impacts the acceptor stack. The peak distances for the thin and thick rectangular barricades are reduced because of the net rebound of parts of the barricades from the acceptor stack left surface. The curve for the displacement of the trapezoidal barricade in Computation 980505 shows less

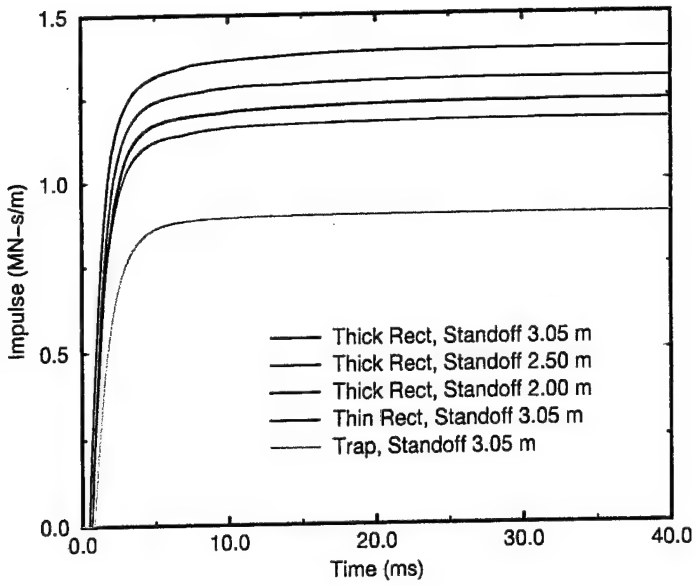

Figure 36. Water Barricade Left Surface Total X-Direction Impulse per Meter Depth, Computations 980918 Through 980924 (Thick Rectangular), Plus 980825 (Thin Rectangular) and 980505 (Trapezoidal).

displacement through about 30 ms and the greatest displacement at 40 ms because there is very little rebound.

Figure 38 shows the functional relations of the peak (at different times) values of the several parameters just described for the thick rectangular barricade in the preceding figures. The abscissa shows the dimensional standoff distance. The ordinate shows the normalized direct ratio of parameters, the value of a given parameter at a given standoff divided by the corresponding value for the 3.048-m standoff. Figure 39 shows the same ordinate data as in Figure 38, but with the abscissa showing the normalized inverse standoff ratio, computed as 3.048 m divided by each successive standoff. Thus, the value for the 3.048-m standoff itself is 1.0, and the value for the 2.00-m standoff is 1.524. The ordinate is the same as for Figure 38 except for its scaling. The abscissa and ordinate scales are forced to be equal so that any $\Delta X/\Delta Y = \pm 1.0$ relationship would show as a ± 45-degree straight line. The figures show a weak functional relation of all of these normalized parameters with both dimensional and normalized standoff. This shows that, as far as these parameters for this simplified barricade are concerned, there is only a minor penalty in barricade whole-body dynamics incurred by moving the barricade closer to the donor stack to a nominal 2-m from a nominal 3-m standoff. The apparent lack of a visible black curve for the peak momentum in both figures is caused by the precise overlay by the red curve for peak velocity because of their direct scaling by mass.

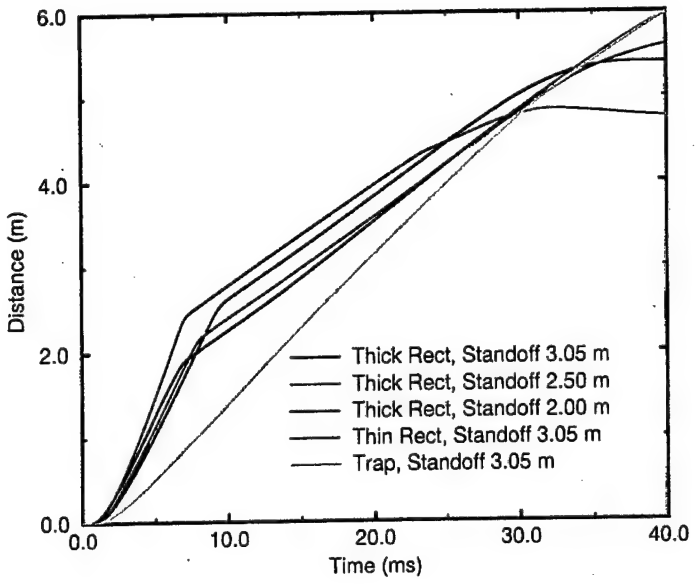

Figure 37. Water Barricade X-Direction Distance Moved Toward the Acceptor Stack, Computations 980918 Through 980924 (Thick Rectangular), Plus 980825 (Thin Rectangular) and 980505 (Trapezoidal).

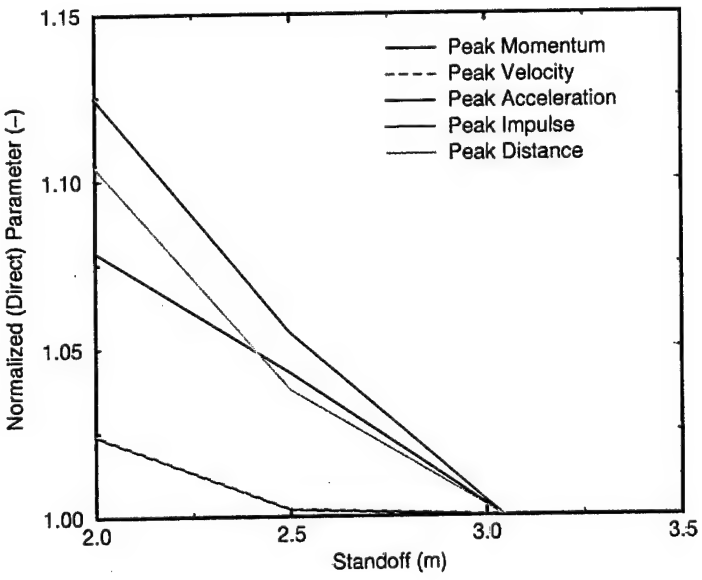

Figure 38. Normalized (Direct Ratio) Thick Rectangular Barricade Parameters Versus Standoff Distance, Computations 980918 Through 980924.

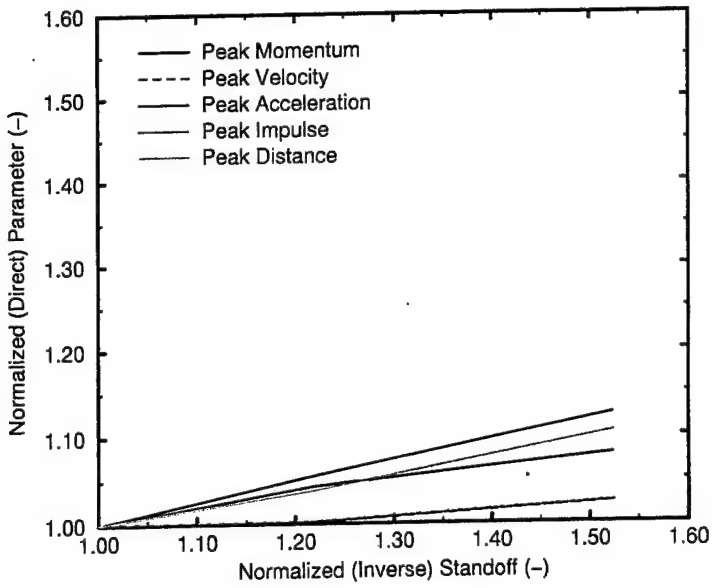

Figure 39. Normalized (Direct Ratio) Thick Rectangular Barricade Parameters Versus Normalized (Indirect Ratio) Standoff Distance, Computations 980918 Through 980924.

3.3. Acceptor Stack Dynamics

Figure 40 shows the bulk momentum per centimeter depth of the acceptor stack in the X direction for the three computations for the thick rectangular barricade, plus Computations 980825 for the thin rectangular barricade[2] and 980505 for the massive trapezoidal barricade,[1] both of which were for a 3.05-m standoff. Positive momentum is defined in the positive X direction as before. There is only a minimal increase in the momentum of the acceptor stack caused by the air shock for the three thick rectangular barricade computations. After about 5 ms, all three computations show a very rapid increase in momentum caused by the impact of the water barricade. The acceptor stack momentum for the thin rectangular barricade from the 3.05-m standoff computation begins a rapid increase about 2 ms sooner than the corresponding curve for the thick rectangular barricade at the same standoff and reaches the greatest value of 11.90 Mg-m/s for all curves by 40 ms. The acceptor stack momentum from the 3.05-m standoff computation for the massive trapezoidal water barricade shows the three-stage sequence increase in momentum described previously[1] that is caused by the air shock, the impact of the water wave on the top-left surface of the acceptor stack, and then the impact of the lower sections of the barricade on the acceptor stack. The momentum of the acceptor stack at a nominal time of 40 ms for Computation 980918 (thick rectangular barricade, 3.05-m standoff, 28.61 kg/cm of depth) is 11.11 Mg-m/s, which is 2.80 times greater than the corresponding value of 3.962 Mg-m/s for Computation 980505 (trapezoidal barricade, 3.05-m standoff, 58.71 kg/cm of depth). The final values of the momentum of the

acceptor stack for the thick rectangular barricade computations at a nominal time of 40 ms are 11.35 Mg-m/s for the 2.50-m standoff and 11.73 Mg-m/s for the 2.00-m standoff. Table 3 contains a summary of several X-direction parameters that describe some of the bulk motion of the acceptor stack for the various computations. First among those parameters, after the computation numbers and standoff distances, are the peak X-direction bulk momentum values for the acceptor stack, along with their respective times of occurrence, listed with more significant figures than were typically used in the text for completeness. In order to facilitate comparisons, the first column of numbers is for the acceptor stack in Computation 980505 for the massive trapezoidal barricade at a 3.05-m standoff, followed by data for Computation 980825 for the thin rectangular barricade at a 3.05-m standoff, and then followed by columns of data for the three thick rectangular barricade computations. The rest of the parameters in the table are discussed in the following paragraphs.

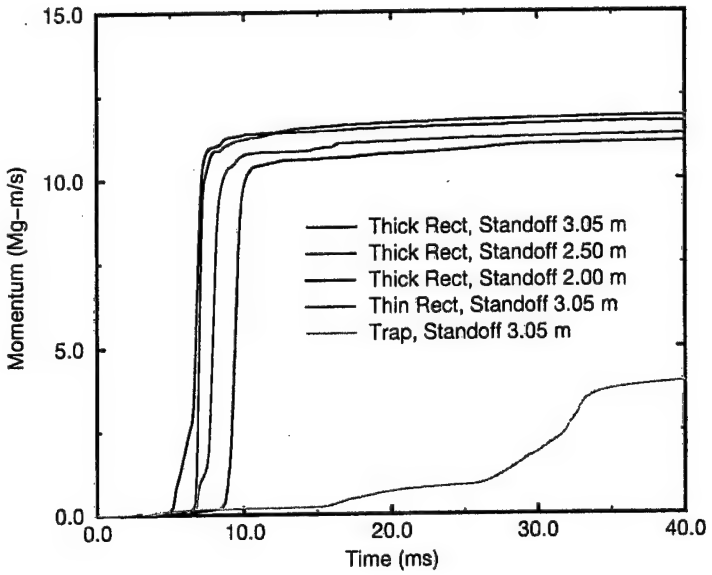

Figure 40. Acceptor Stack X-Direction Momentum, Computations 980918 Through 980924 (Thick Rectangular), Plus 980825 (Thin Rectangular) and 980505 (Trapezoidal).

The corrected mass of the acceptor stack was used to compute the bulk X-direction velocity from the momentum of the acceptor stack. The results are shown in Figure 41. The curves show the same timing and differentiation as those for the acceptor stack momentum. The velocities at 40 ms for the thick rectangular barricade are 93.66 m/s (3.05-m standoff), 95.68 m/s (2.50-m standoff), and 98.93 m/s (2.00 m standoff). The velocities at 40 ms at a 3.05-m standoff for the thin rectangular water barricade and the massive trapezoidal water barricade, also shown in Figure 41, are 100.3 m/s and 33.4 m/s, respectively.

Table 3. Acceptor Stack Peak X-Direction Bulk Motion Parameters.

Computation Number	Massive Trapezoidal 980505	Thin Rectangular 980825	Thick Rectangular 980918	Thick Rectangular 980923	Thick Rectangular 980924
Standoff (m)	3.048	3.048	3.048	2.50	2.00
Peak Momentum (Mg-m/s)	3.962	11.90	11.11	11.35	11.73
Time (ms)	40.00	39.87	39.62	39.71	39.69
Peak Velocity (m/s)	33.40	100.3	93.66	95.68	98.93
Time (ms)	40.00	39.87	39.62	39.71	39.69
Peak Acceleration (km/s/s)	9.277	197.5	109.8	112.8	123.6
Time (ms)	32.80	7.093	9.494	8.023	6.883
Peak Left-Surface Impulse (MN-s/m)	0.3725	1.138	1.063	1.098	1.144
Time (ms)	39.99	39.99	39.99	39.99	39.99
Distance Traveled (m)	0.4065	3.237	2.805	3.014	3.246
Time (ms)	39.99	39.99	39.99	39.99	39.99

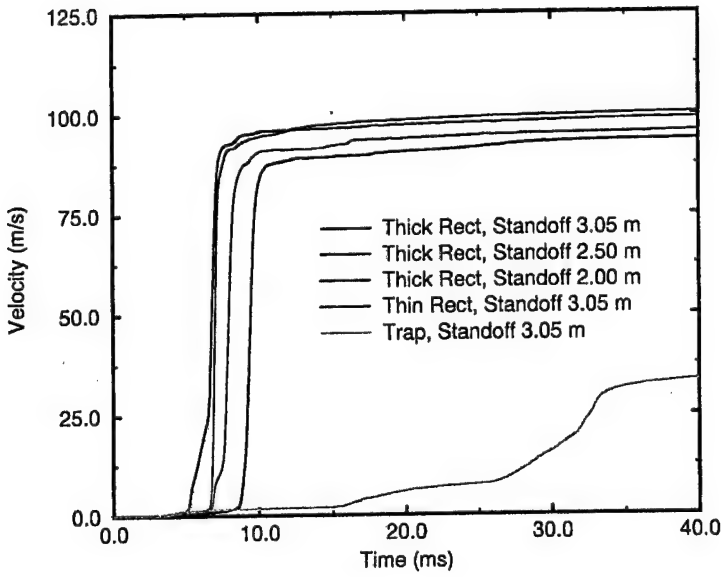

Figure 41. Acceptor Stack X-Direction Velocity, Computations 980918 Through 980924 (Thick Rectangular), Plus 980825 (Thin Rectangular) and 980505 (Trapezoidal).

As was done for the barricade, the acceptor stack velocity for each standoff was piecewise differentiated with respect to time to compute the bulk X-direction acceleration of the acceptor stack. The acceleration curves for the three thick rectangular barricade computations and Computations 980505 and 980825 are shown in Figure 42. Each individual curve for the thick rectangular barricade shows a large spike in acceleration in the order of increasing standoff distance. All occur before 10 ms. The curves for the 2.50-m and 2.00-m standoffs show some leading structure in the acceleration curves prior to the main acceleration spike, most likely because of the leading impact of the bottom section of the barricade against the bottom of the left face of the acceptor stack, followed by a progressive impact of the rest of the barricade moving up the acceptor stack left face. The curve for the thin rectangular barricade at a 3.05-m standoff shows a single, large spike in acceleration at an early time, as does the curve for the thick rectangular barricade at that same standoff. The peak accelerations for the two different rectangular barricades are far greater than the 9.28 km/s^2 for the trapezoidal barricade at a 3.05-m standoff that occurs at 32.8 ms.

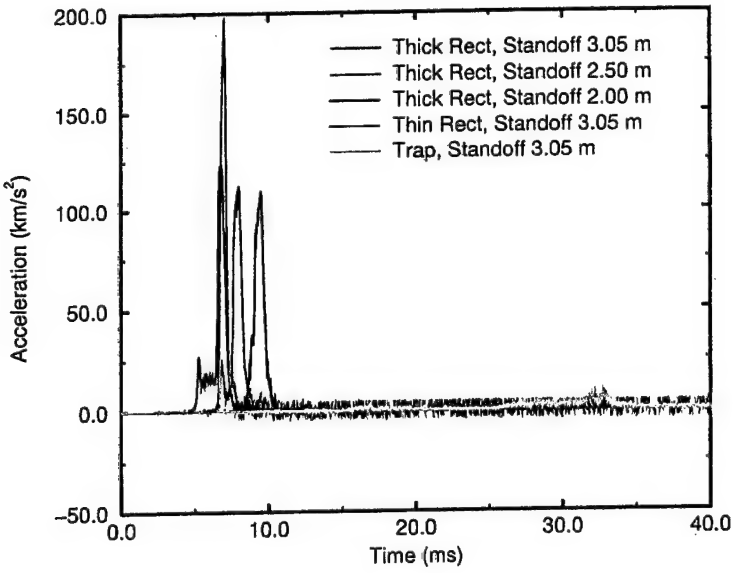

Figure 42. Acceptor Stack X-Direction Acceleration, Computations 980918 Through 980924 (Thick Rectangular), Plus 980825 (Thin Rectangular) and 980505 (Trapezoidal).

The acceptor stack was modeled as a solid iron rectangle so that the most reliable loading possible could be computed for its left face. Thirty tracer particles were uniformly spaced along the left face, top to bottom, of the acceptor stack. They were constrained from moving in either the X or Y direction so that the ensuing hydrodynamic flows would not sweep them off the face of the acceptor stack or reposition them horizontally or vertically. The overpressure histories were integrated over space and time to compute the total X-

direction impulse per meter depth versus time for each standoff. These curves are shown in Figure 43. The acceptor stack shows that the thick rectangular water barricade provided a very efficient delivery of its left-face impulse from the blast loading caused by the detonation of the donor stack (see Figure 36) to the acceptor stack at its right face. The acceptor stack left-face values are nearly equal to the respective barricade left-face values. The final impulse values per meter depth on the acceptor stack left face are 1.063 MN-s/m (3.05-m standoff), 1.098 MN-s/m (2.50-m standoff), and 1.144 MN-s/m (2.00-m standoff). For comparison, the final impulse values on the left face of the thick rectangular water barricade (see Table 2) are 1.241 MN-s/m (3.05-m standoff), 1.308 MN-s/m (2.50-m standoff), and 1.396 MN-s/m (2.00-m standoff). The term "impulse-transfer efficiency" is herein defined as the impulse delivered to the left face of the acceptor stack divided by the impulse delivered to the left face of the barricade. The impulse-transfer characteristics of all of the water barricades studied to date are summarized in Table 4. Although impulse and impulse-transfer efficiency as defined and used herein are not the only valid indicators of the efficacy of a given barricade design, they are important. The data listed in Table 4 are grouped by barricade design in ascending order of impulse-transfer efficiency, moving from top to bottom in the table. A low value of impulse on the acceptor stack is desirable, as is a low value of impulse-transfer efficiency. The thin rectangular barricade showed the worst performance by this measure, having the highest values of impulse-transfer efficiency. The rate of delivery of impulse is also very important because of its direct relation to peak loads and accelerations. Two simple but relatively effective methods for showing the peak impulse on the left face of the acceptor stack versus a geometrically scaled barricade mass were found, which help to tie the results of all of the water barricade computations together. The first method, Scaling Method 1, is shown in Figure 44. The water barricade mass, in units of kg/cm of depth, was multiplied by the square of the secant of the angle, Θ, to the vertical of the front and back faces, once for the slope of the front face and again for the slope of the back face for a compounded factor equal to the fourth power of the secant of Θ. This produced a scaled barricade mass, M_1, from the mass in kg per cm of depth, M, and the face angle in degrees, Θ, shown in equation 1.

$$M_1 = M\,(sec(\Theta))^4 \tag{1}$$

For the trapezoidal water barricade, Θ is equal to 30 degrees for both faces. This resulted in the three-tiered set of lines shown in Figure 44, one line for each standoff distance. A second method, Scaling Method 2, is shown in Figure 45, in which the scaled barricade mass in Figure 44 is further multiplied by the cube root of the standoff distance, S, in meters to form a new scaled barricade mass, M_2. This is shown in equation 2.

$$M_2 = M\,(sec(\Theta))^4\,S^{1/3} \tag{2}$$

The data are shown with symbols to make it easier to discuss the two differentiated sets that are indicated in this figure. The first set, represented by those symbols for which the scaled abscissa value is less than 75, is comprised of points only for the rectangular water barricade. The second set, represented by those symbols for which the scaled abscissa value is greater than 125, is comprised of points only for the trapezoidal water barricade. These

two sets fall almost on the same line. These relatively simple and reasonably successful attempts at scaling the impulse data were not pursued any further because they are based only on a limited set of data for water. No further scaling is proposed at this time until additional computations can be made for sand barricades, at which time factors for density and perhaps other shapes should be considered.

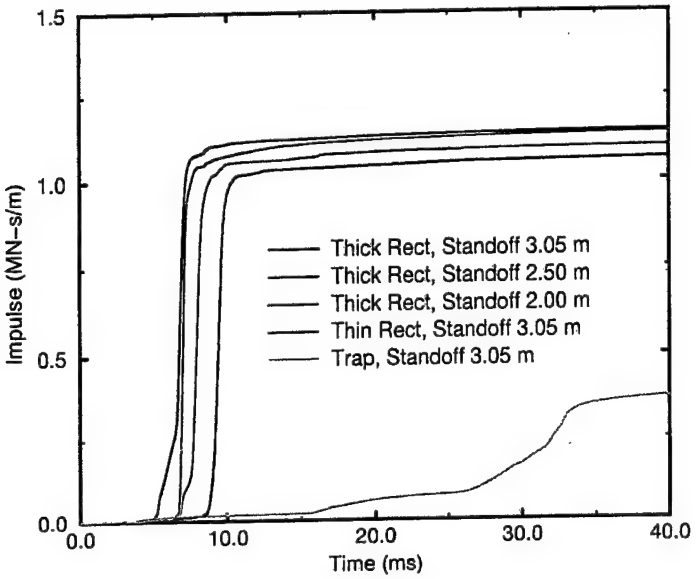

Figure 43. Acceptor Stack X-Direction Total Impulse per Meter Depth, Computations 980918 Through 980924 (Thick Rectangular), Plus 980825 (Thin Rectangular) and 980505 (Trapezoidal).

Figure 46 shows the distance that the acceptor stack moves as a result of the blast and impact loading by 40.0 ms. The range for Computations 980918 through 980924 for the thick rectangular barricade is from 2.80 m (3.05-m standoff) to 3.25 m (2.00-m standoff). Computation 980825 for the thin rectangular barricade shows a movement of the acceptor stack of 3.24 m at the 3.05-m standoff. In Computation 980505 for the trapezoidal barricade, the acceptor stack moves 0.41 m in 40.0 ms, 12.6 percent of that for the acceptor stack in Computation 980825, and 14.5 percent of that for Computation 980918.

Figure 47 shows the functional relations of the peak (at different times) and final (at 40.0 ms) values of the several parameters versus standoff distance that were just described for the acceptor stack with the thick rectangular barricade in the preceding figures. The ordinate parameters are normalized in the same way as was done in Figure 38: the direct ratio of the respective parameters relative to the values for the 3.05-m standoff. The black momentum curve does not show because it is overlaid by the red velocity curve. This is because of the simple scaling of the two curves by mass. Figure 48 shows the same ordinate

Table 4. Impulse-Transfer Efficiency of All Water Barricades.

Barricade and Standoff	Peak Barricade Left-Surface Impulse (MN-s/m)	Peak Acceptor Stack Left Surface Impulse (MN-s/m)	Impulse-Transfer Efficiency (-)
Massive Trapezoidal at 3.048-m Standoff	0.9016	0.3725	0.4132
Massive Trapezoidal at 2.75-m Standoff	0.9337	0.4044	0.4331
Massive Trapezoidal at 2.50-m Standoff	0.9381	0.4195	0.4472
Massive Trapezoidal at 2.25-m Standoff	0.9502	0.4279	0.4503
Massive Trapezoidal at 2.00-m Standoff	0.9630	0.4945	0.5135
Thick Rectangular at 3.048-m Standoff	1.241	1.063	0.8566
Thick Rectangular at 2.50-m Standoff	1.308	1.098	0.8395
Thick Rectangular at 2.00-m Standoff	1.396	1.144	0.8195
Thin Rectangular at 3.048-m Standoff	1.185	1.138	0.9603
Thin Rectangular at 2.50-m Standoff	1.283	1.154	0.8995
Thin Rectangular at 2.00-m Standoff	1.360	1.248	0.9177

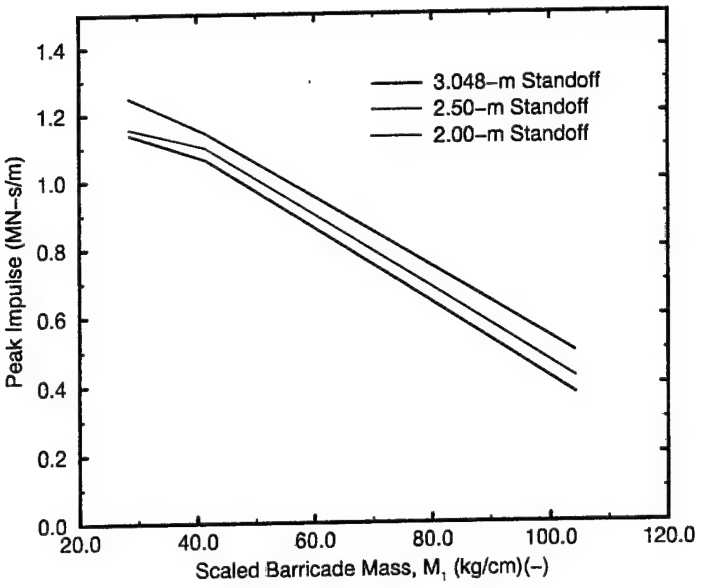

Figure 44. Acceptor Stack Peak X-Direction Total Impulse per Meter Depth Versus Barricade Mass, All Water Barricade Computations, Scaling Method 1.

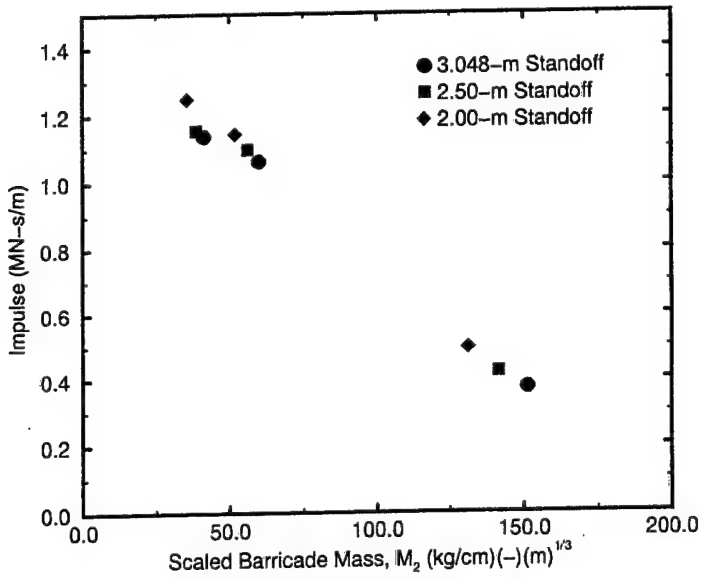

Figure 45. Acceptor Stack Peak X-Direction Total Impulse per Meter Depth Versus Barricade Mass, All Water Barricade Computations, Scaling Method 2.

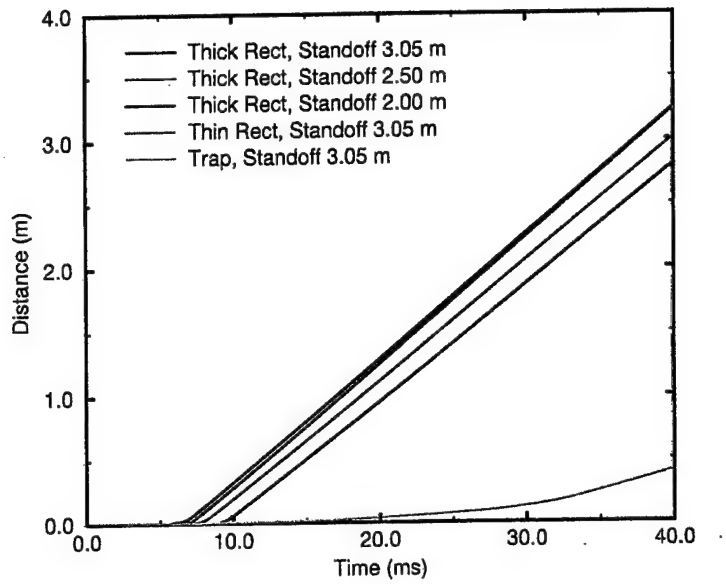

Figure 46. Acceptor Stack X-Direction Distance Moved, Computations 980918 Through 980924 (Thick Rectangular), Plus 980825 (Thin Rectangular) and 980505 (Trapezoidal).

data plotted against the inverse normalized standoff, with that normalization done in the same way as for Figure 39, including a forced scaling of the ordinate and abscissa to have each cover the same range of normalized data over the same axis length to facilitate comparison with Figure 39. Like the barricade, the normalized acceptor stack ordinate parameters are all relatively weak direct functions of inverse standoff ratio.

The simple standoff distance, measured from the stack base to the barricade base, may not be the only meaningful distance to consider when examining these parameters for the acceptor stack. The total distance between the right face of the donor stack and the left face of the acceptor stack, equal to twice the standoff plus the base width of the barricade, may be an informative parameter to use. For convenience, this distance is hereinafter referred to as "face separation." Figure 49 shows the ordinate values from Figures 47 and 48 plotted against an abscissa showing the face separation. Figure 50 shows the same ordinate data plotted against the inverse normalized face separation. The normalizing value in the numerator was the face separation for the 3.05 m standoff. One-to-one scaling for the normalized abscissa and ordinate was forced in this figure. All parameters show a weak correlation with the inverse normalized face separation.

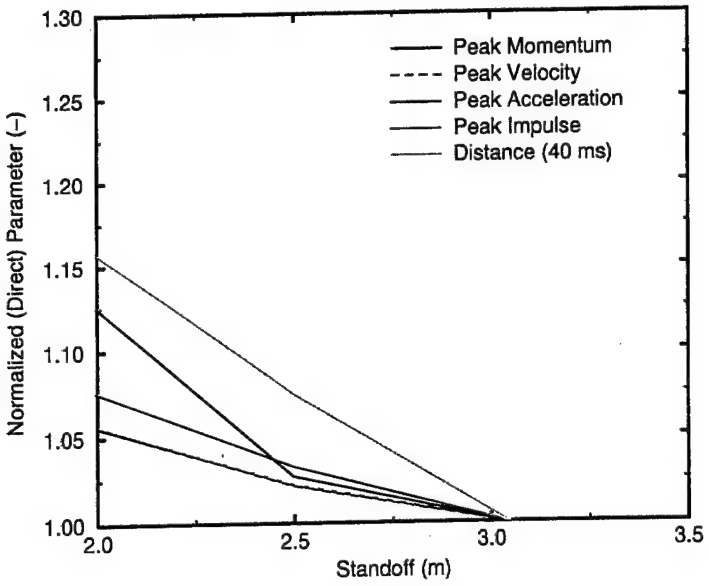

Figure 47. Normalized (Direct Ratio) Acceptor Stack Parameters Versus Standoff Distance, Computations 980918 Through 980924 (Thick Rectangular Barricade).

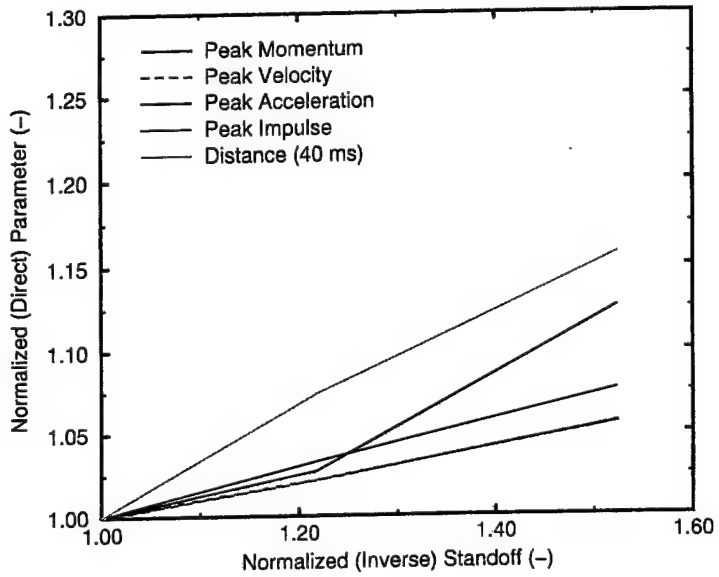

Figure 48. Normalized (Direct Ratio) Acceptor Stack Parameters Versus Normalized (Inverse Ratio) Standoff Distance, Computations 980918 Through 980924.

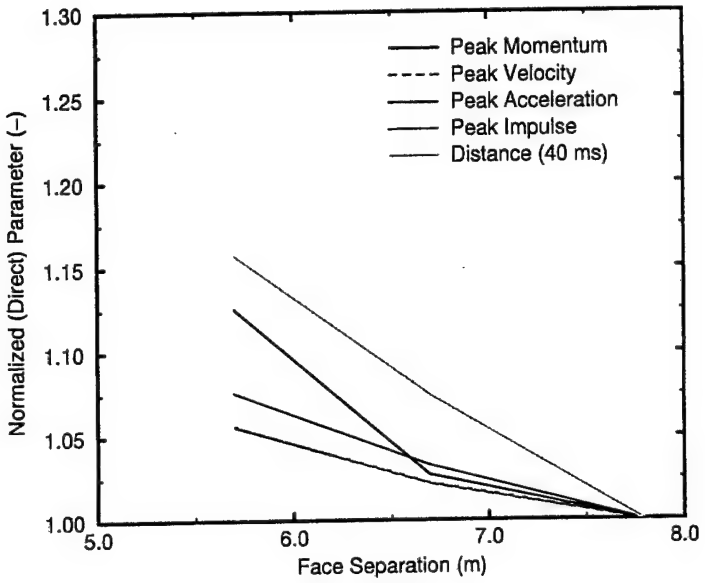

Figure 49. Normalized (Direct Ratio) Acceptor Stack Parameters Versus Face Separation, Computations 980918 Through 980924.

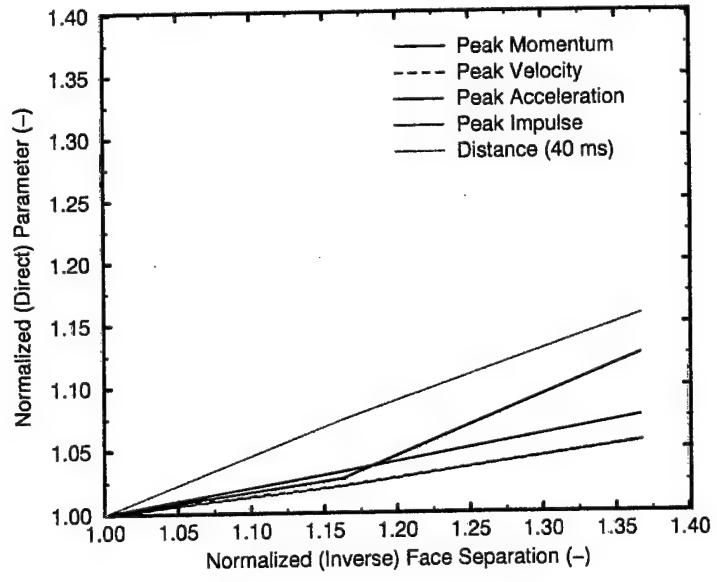

Figure 50. Normalized (Direct Ratio) Acceptor Stack Parameters Versus Normalized (Inverse Ratio) Face Separation, Computations 980918 Through 980924.

3.4. Acceptor Stack Left Surface Pressures

The pressures on the surface of the acceptor stack during this type of event are of great interest. Data from the 30 tracers that were placed uniformly along the left surface of the acceptor stack were processed to present a comprehensive summary of the overpressure history on that surface for each computation. An area-weighted average overpressure was computed using all of the 30 individual tracer pressures at each point in time. The maximum overpressure for any of the tracers at a given time was identified, as was the minimum. The results from the three computations for the thick rectangular barricade are presented here for each standoff distance. Figure 51 shows the average, maximum, and minimum overpressures versus time on the left surface of the acceptor stack for a standoff of 3.05 m for Computation 980918. It shows a peak average overpressure of 0.524 GPa at 9.49 ms and a peak overpressure for an individual point of 2.49 GPa, also at 9.49 ms. Similarly, Figure 52 shows the average, maximum, and minimum overpressures versus time on the left surface of the acceptor stack for a standoff of 2.50 m for Computation 980923. It shows a peak average overpressure of 0.536 GPa at 8.02 ms and a peak overpressure for an individual point of 2.00 GPa at 7.75 ms. Figure 53 shows the average, maximum, and minimum overpressures versus time on the left surface of the acceptor stack for a standoff of 2.00 m for Computation 980924. It shows a peak average overpressure of 0.580 GPa at 6.84 ms and a peak overpressure for an individual point of 1.76 GPa at 6.71 ms. There is an interesting, somewhat contradictory trend of increasing average overpressure on the acceptor stack left surface with decreasing standoff distance coincident with a trend of decreasing peak overpressure for an individual point with decreasing standoff distance. It appears to be caused by a trade-off in the system dynamics in the bulk acceleration of the barricade and in the time and distance required to accelerate it before it strikes the acceptor stack.

The figures that follow each show the average overpressure and the peak overpressure for an individual point for all water barricade computations reported to date for the massive trapezoidal water barricade[1] and the thin rectangular water barricade[2] at matching standoff distances to the values from Computations 980918 through 980924 just shown in Figures 51, 52, and 53. Figure 54 shows the average and individual peak overpressures versus time on the left surface of the acceptor stack for a standoff of 3.05 m for Computations 980918, 980825, and 980505 that are for the thick rectangular, thin rectangular, and trapezoidal water barricades, respectively. The order, from highest to lowest, of the peak individual overpressure is thick rectangular, thin rectangular, and then trapezoidal. The order for the average overpressure is thin rectangular (greatest), thick rectangular, and trapezoidal. Figure 55 shows the average and individual peak overpressures versus time on the left surface of the acceptor stack for a standoff of 2.50 m for Computations 980923, 980826, and 980521 that are for the thick rectangular, thin rectangular, and trapezoidal water barricades, respectively. The order, from highest to lowest, of the peak individual overpressure is thick rectangular (by a small margin), thin rectangular, and then trapezoidal. The order for the average overpressure is thin rectangular (greatest), thick rectangular, and trapezoidal. Figure 56 shows the average and individual peak overpressures versus time on the left surface

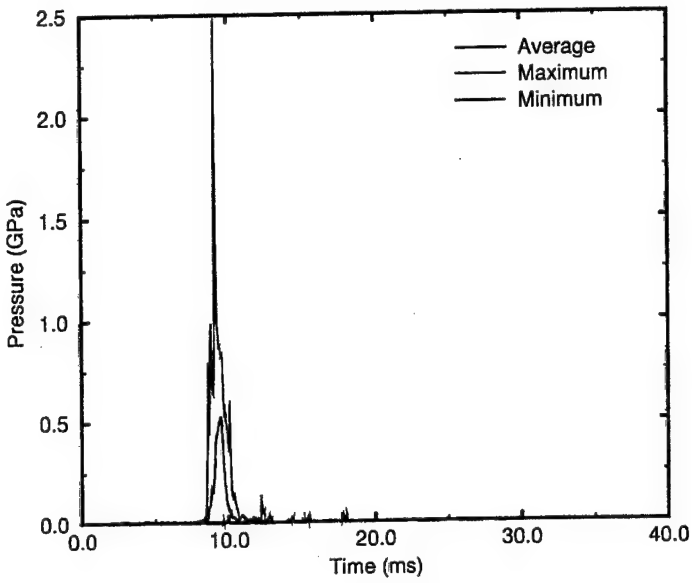

Figure 51. Acceptor Stack Left Surface Overpressure, 3.05-m Standoff, Computation 980918.

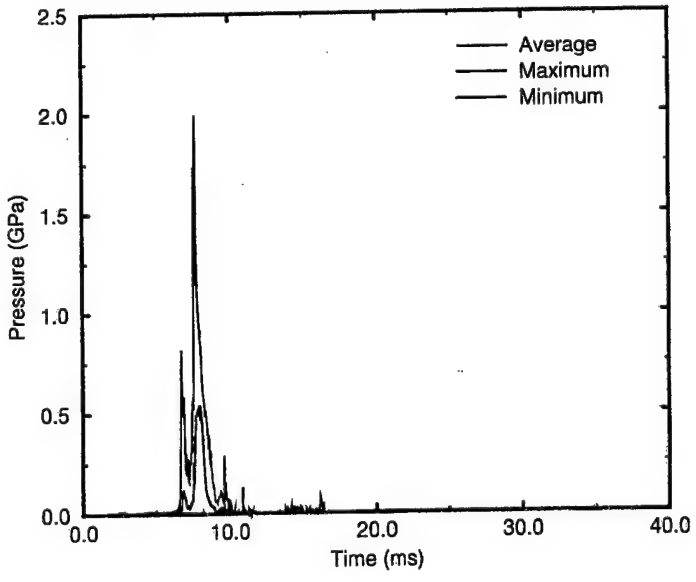

Figure 52. Acceptor Stack Left Surface Overpressure, 2.50-m Standoff, Computation 980923.

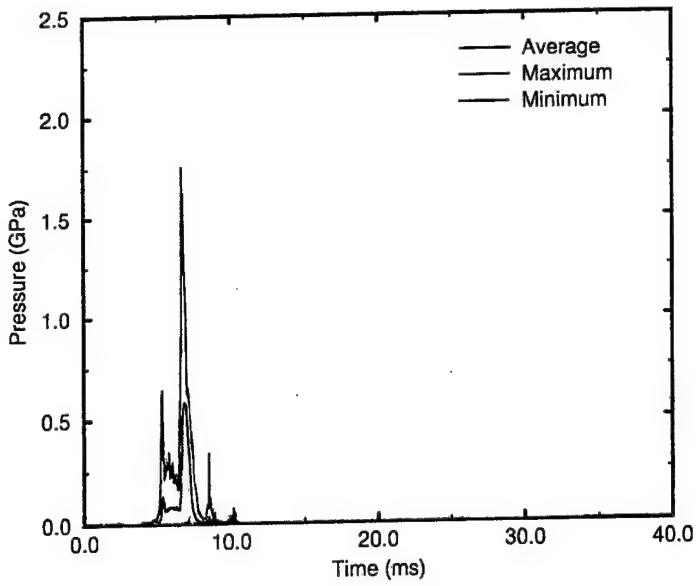

Figure 53. Acceptor Stack Left Surface Overpressure, 2.00-m Standoff, Computation 980924.

of the acceptor stack for a standoff of 2.50 m for Computations 980924, 980827, and 980610 that are for the thick rectangular, thin rectangular, and trapezoidal water barricades, respectively. The order, from highest to lowest, of the peak individual overpressure is thin rectangular, thick rectangular, and then trapezoidal. The order for the average overpressure is thin rectangular (greatest), thick rectangular, and trapezoidal. For all plots, the massive trapezoidal barricade always showed the smallest values by far of both peak individual overpressure and average overpressure on the acceptor stack left face. All plots showed an essentially negligible loading from the air shock at early time. All computations for both the thin and the thick rectangular water barricades show peak values of overpressure on the left surface of the acceptor stack in the range of 1.75 GPa (17.5 kbar) or higher. These are high enough pressures to represent a threat of inducing a chemical reaction in the acceptor stack if they are efficiently transmitted through packaging and/or casings to the energetic loads of the munitions. The report by Liddiard and Forbes[19] stated, for example, that the underwater sensitivity test (UST) showed that "...compression by a 3 or 4 kbar shock is, of itself, a sufficient external stimulus to start chemical reaction in a heterogeneous solid explosive such as pentolite..." and "...UST burning occurs at peak stresses of 4 to 12 kbar in the explosives..." A cautionary note: a simple shock stimulus is not the only initiating mechanism for an explosive.

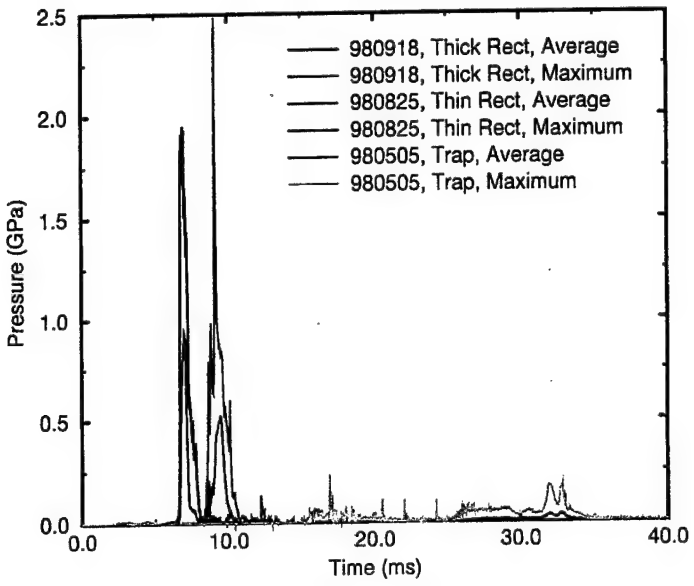

Figure 54. Acceptor Stack Left Surface Overpressure, 3.05-m Standoff, Computations 980918 (Thick Rectangular), 980825 (Thin Rectangular) and 980505 (Trapezoidal).

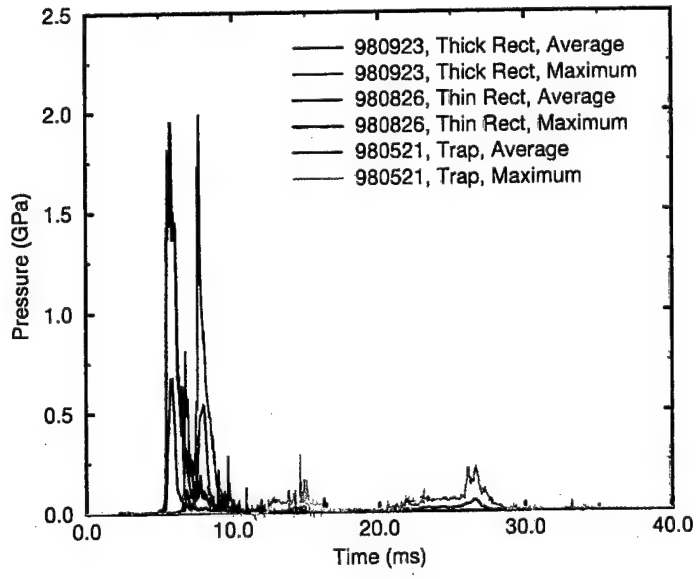

Figure 55. Acceptor Stack Left Surface Overpressure, 2.50-m Standoff, Computations 980923 (Thick Rectangular), 980826 (Thin Rectangular) and 980521 (Trapezoidal).

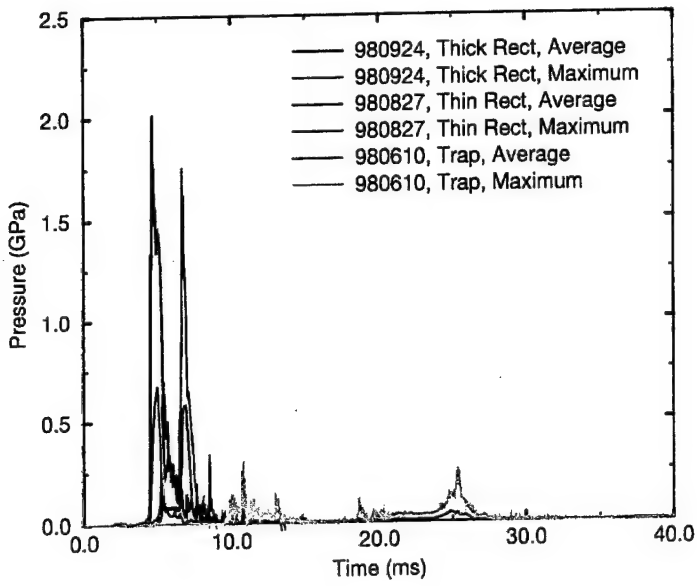

Figure 56. Acceptor Stack Left Surface Overpressure, 2.00-m Standoff, Computations 980924 (Thick Rectangular), 980827 (Thin Rectangular) and 980610 (Trapezoidal).

4. CONCLUSION

The coupled computations discussed herein modeled a simplified, uncased, rectangular explosive charge representing a nominal munitions stack containing 4,000 kg of Comp-B undergoing a complete, high-order detonation with the initiation point at its center. No munitions casings or packing materials (and their resulting fragments) were included. The only barricade design that was used was a solid, water-only 1.70-m-thick rectangle. These computations were compared with computations for a thin, 1.17-m rectangular water barricade and a massive trapezoidal water barricade at the same standoff distances. Those computations were reported previously. A geometrically simplified 2-D Cartesian coordinates system with the same finite-difference grid was used throughout the computations. This eliminated three-dimensional divergence effects that could reduce loadings considerably. The only parameter that was varied was the standoff distance.

The computations for the thick rectangular water barricade demonstrate a relatively weak inverse functional relationship between normalized values of the standoff distance and the loading on and whole-body response of the barricade. Similar results for both standoff and face separation were found for the loading on and whole-body response for the acceptor stack. The impact loading on the acceptor stack by the thick rectangular water barricade is much more severe than that reported earlier[1] for the massive trapezoidal water barricade, but somewhat less severe than for the thin rectangular water barricade. Peak individual

overpressures on the acceptor stack for the two different rectangular water barricades are high enough, 1.75 GPa or greater, to represent a threat of initiating a chemical reaction in munitions within the acceptor stack. Also, neither rectangular barricade was effective in keeping explosive products from the donor stack away from the acceptor stack. The trapezoidal barricade was effective in that regard. A relatively simple scaling of barricade mass with geometric parameters resulted in developing a single functional relationship with peak impulse for all water barricade shapes and standoff distances considered in the complete set of computations. Because the donor stack was represented by a simple, bare explosive charge, the synergistic effects of the impact of large numbers of high-speed fragments along with the barricade impact loading were not addressed. Additional computational studies of sand-filled barricades were in progress as of the expiration of this customer project. The possibility of extending the project to perform the sand barricade computations and computations simulating the impact of water or sand on individual munitions is being explored.

INTENTIONALLY LEFT BLANK

REFERENCES

1. R.E. Lottero, "Standoff Variation Study I: Detonation of a Donor Munitions Stack and Responses of a Trapezoidal Water Barricade and an Acceptor Stack," ARL-TR-1943, U.S. Army Research Laboratory, Aberdeen Proving Ground, MD, May 1999.

2. R.E. Lottero, "Standoff Variation Study II: Detonation of a Donor Munitions Stack and Responses of a Thin Rectangular Water Barricade and an Acceptor Stack," ARL-TR-1948, U.S. Army Research Laboratory, Aberdeen Proving Ground, MD, May 1999.

3. R.E. Lottero, "Responses of a Water Barricade and an Acceptor Stack to the Detonation of a Donor Munitions Stack," ARL-TR-1600, U.S. Army Research Laboratory, Aberdeen Proving Ground, MD, March 1998.

4. J.M. McGlaun, S.L. Thompson, L.N. Kmetck, and M.G. Elrick, "A Brief Description of the Three-Dimensional Shock Wave Physics Code CTH," SAND89-0607, Sandia National Laboratories, Albuquerque, NM, July 1990.

5. R.L. Bell, M.R. Baer, R.M. Brannon, M.G. Elrick, E.S. Hertel Jr., S.A. Silling, and P.A. Taylor, "CTHGEN User's Manual and Input Instructions, Version 4.00," CTH Development Project, Sandia National Laboratories, Albuquerque, NM, 10 March 1998.

6. R.L. Bell, M.R. Baer, R.M. Brannon, M.G. Elrick, E.S. Hertel Jr., S.A. Silling, and P.A. Taylor, "CTH User's Manual and Input Instructions, Version 4.00," CTH Development Project, Sandia National Laboratories, Albuquerque, NM, 13 March 1998.

7. J. Starkenberg, K.J. Benjamin, and R.B. Frey, "Predicting Fragmentation Propagation Probabilities for Ammunition Stacks," ARL-TR-949, U.S. Army Research Laboratory, Aberdeen Proving Ground, MD, January 1996.

8. Headquarters, Department of the Army, "Technical Manual. Army Ammunition Data Sheets. Artillery Ammunition. Guns, Howitzers, Mortars, Recoilless Rifles, Grenade Launchers, and Artillery Fuzes." TM-43-0001-28, April 1977.

9. Department of the Army, "Ammunition and Explosives Safety Standards," AR 385-64, 22 May 1987.

10. G.I. Kerley and T.L.C. Frear, "Composition B-3 Detonation Products," SAND93-2131, Sandia National Laboratories, Albuquerque, NM, 1993.

11. G.I. Kerley, "CTH Reference Manual: The Equation of State Package," SAND91-0344, Sandia National Laboratories, Albuquerque, NM, 24 May 1991.

12. B.M. Dobratz and P.C. Crawford, "LLNL Explosives Handbook, Properties of Chemical Explosives and Explosive Simulants," UCRL-52997, Change 2, Lawrence Livermore National Laboratory, Livermore, CA, 31 January 1985.

13. J. Starkenberg, Private communication, U.S. Army Research Laboratory, Aberdeen Proving Ground, MD, July 1998.

14. R.D. Cregar, Private communication, U.S. Army Research Laboratory, Aberdeen Proving Ground, MD, July 1998.

15. Hesco Bastion Limited, Unit 37, Knowsthorpe Gate, Cross Green Industrial Estate, Leeds LS9 ONP, West Yorkshire, England.

16. F.H. Ree, "Equation of State for Water," UCRL-52190, Lawrence Livermore National Laboratory, Livermore, CA, December 1976.

17. G.I. Kerley, "Multiphase Equation of State for Iron," SAND93-0227, Sandia National Laboratories, Albuquerque, NM, 1993.

18. H.C. Graboske, Data for dry air, UCID-16901, December 1981 (modified March 1992).

19. T.P. Liddiard and J.W. Forbes, "A Summary Report of the Modified Gap Test and the Underwater Sensitivity Test," NSWC TR 86-350, Naval Surface Warfare Center, Silver Spring, MD, 12 March 1987.

NO. OF COPIES ORGANIZATION

2 DEFENSE TECHNICAL INFORMATION CENTER
DTIC DDA
8725 JOHN J KINGMAN RD
STE 0944
FT BELVOIR VA 22060-6218

1 HQDA
DAMO FDQ
D SCHMIDT
400 ARMY PENTAGON
WASHINGTON DC 20310-0460

1 OSD
OUSD(A&T)/ODDDR&E(R)
R J TREW
THE PENTAGON
WASHINGTON DC 20301-7100

1 DPTY CG FOR RDE HQ
US ARMY MATERIEL CMD
AMCRD
MG CALDWELL
5001 EISENHOWER AVE
ALEXANDRIA VA 22333-0001

1 INST FOR ADVNCD TCHNLGY
THE UNIV OF TEXAS AT AUSTIN
PO BOX 202797
AUSTIN TX 78720-2797

1 DARPA
B KASPAR
3701 N FAIRFAX DR
ARLINGTON VA 22203-1714

1 NAVAL SURFACE WARFARE CTR
CODE B07 J PENNELLA
17320 DAHLGREN RD
BLDG 1470 RM 1101
DAHLGREN VA 22448-5100

1 US MILITARY ACADEMY
MATH SCI CTR OF EXCELLENCE
DEPT OF MATHEMATICAL SCI
MAJ M D PHILLIPS
THAYER HALL
WEST POINT NY 10996-1786

NO. OF COPIES ORGANIZATION

1 DIRECTOR
US ARMY RESEARCH LAB
AMSRL DD
J J ROCCHIO
2800 POWDER MILL RD
ADELPHI MD 20783-1145

1 DIRECTOR
US ARMY RESEARCH LAB
AMSRL CS AS (RECORDS MGMT)
2800 POWDER MILL RD
ADELPHI MD 20783-1145

3 DIRECTOR
US ARMY RESEARCH LAB
AMSRL CI LL
2800 POWDER MILL RD
ADELPHI MD 20783-1145

ABERDEEN PROVING GROUND

4 DIR USARL
AMSRL CI LP (305)

NO. OF COPIES	ORGANIZATION
1	DIRECTOR DEFENSE RSCH AND ENGNRNG DD TWP WASHINGTON DC 20301
1	COMMANDER FIELD COMMAND DSWA FCTTS E MARTINEZ KIRTLAND AFB NM 87115
1	DIRECTOR ADV RSCH PROJECTS AGNCY TECH LIB 3701 N FAIRFAX DR ARLINGTON VA 22203-1714
1	COMMANDER USA ARDEC AMSTA FSM W BARBER BLDG 94 PICATINNY ARSENAL NJ 07806-5000
1	COMMANDER USA ENGINEER DIVISION HNDED FD PO BOX 1500 HUNTSVILLE AL 35807
1	COMMANDER USA CORPS OF ENGNRS FT WORTH DSTRCT CESWF PM J PO BOX 17300 FT WORTH TX 76102-0300
1	COMMANDER USA RSCH OFFICE SLCRO D PO BOX 12211 RESEARCH TRIANGLE PARK NC 27709-2211
1	COMMANDER DAVID TAYLOR RSCH CTR TECH INFO CTR CODE 522 BETHESDA MD 20084-5000

NO. OF COPIES	ORGANIZATION
1	OFFICER IN CHARGE CIVIL ENGNRNG LAB NAVAL CONST BATTALION CTR TECH LIB CODE L31 PORT HUENEME CA 93041
1	COMMANDER NAVAL WEAPONS CTR TECH LIB CODE 533 CHINA LAKE CA 93555-6001
1	COMMANDER NSWC DAHLGREN DIVISION LIB CODE E23 DAHLGREN VA 22448-5000
1	COMMANDER NAVAL RSCH LAB TECH LIB CODE 2027 WASHINGTON DC 20375
1	COMMANDER NAVAL WEAPOONS EVAL FAC DOCUMENT CONTROL KIRTLAND AFB NM 87117
2	AIR FORCE ARMAMENT LAB AFATL DOIL AFATL DLYV EGLIN AFB FL 32542-5000
1	DIRECTOR LAWRENENC LIVERMORE NATL LAB TECH INFO DEPT L 3 PO BOX 808 LIVERMORE CA 94550
1	NAIC DXLA TECH LIB 4180 WATSON WAY WRIGHT PATTERSON AFB OH 45433-5648
1	KAMAN SCIENCES CORPORATION LIBRARY PO BOX 7463 COLORADO SPRINGS CO 80933-7463

NO. OF COPIES	ORGANIZATION
1	DIRECTOR SANDIA NATL LAB DOC CONTROL 3141 PO BOX 5800 ALBUQUERQUE NM 87185-5800
2	LOS ALAMOS NATL LAB RPT COLCTN CIC 14 MS P364 CID 14 MS P364 PO BOX 1663 LOS ALAMOS NM 87545
1	REPORT COLLECTION AGENCY RSCH LAB MS P362 PO BOX 7113 LOS ALAMOS NM 87544-7113
1	DIRECTOR SANDIA NATL LAB LIVERMORE LAB DOC CONTROL FOR THE LIB PO BOX 969 LIVERMORE CA 94550
1	DIRECTOR NASA LANGLEY RSCH CTR TECH LIB HAMPTON VA 23665
1	SUNBURST RECOVERY INC C YOUNG PO BOX 2129 STEAMBOAT SPRINGS CO 80477
2	SRI INTERNATIONAL J GRAN B HOLMES 333 RAVEWOOD AVE MENLO PARK CA 94025
2	DENVER RSCH INSTITUTE J WISOTSKI TECH LIB PO BOX 10758 DENVER CO 80210

NO. OF COPIES	ORGANIZATION
3	SOUTHWEST RSCH INSTITUTE C ANDERSON S MULLIN A B WENZEL PO DRAWER 28255 SAN ANTONIO TX 78228-0255
1	UNIVERSITY OF TEXAS ARL ELCTROMAG GROUP A TUCKER CAMPUS MAIL CODE F0250 AUSTIN TX 78712
1	UNIV OF MARYLAND R DICK RM 2168 ENGRG CLASSROOM BLDG COLLEGE PARK MD 20742-5121
1	US NAVAL ACADEMY TECH LIB 572 HOLLOWAY RD ANNAPOLIS MD 21402-5002
1	OLIN ORDNANCE RECH LIB J KIBIGER PRODUCT MATERIAL CONTROL 10101 9TH ST N ST PETERSBURG FL 33716
1	COMMANDER INDIAN HEAD DIV NSWC CODE 950T M SWISDAK 101 STRAUSS AVE INDIAN HEAD MD 20640-5035
1	COMMANDING OFFICER NFESC J TANCRETO ESC62 1100 23RD AVE BLDG 1100 PORT HUENEME CA 93043-4370
1	CHAIRMAN DOD EXPOSIVES SAFETY BOARD J WARD HOFFMAN BLDG 1 ROOM 856C 2461 EISENHOWER AVE ALEXANDRIA VA 22331-0600

NO. OF COPIES	ORGANIZATION
1	DEFENSE AMMOLOG ACTIVITY AMSTA AR AL D SCARBOROUGH PICATINNY ARSENAL NJ 07806-5000
1	US ARMY SOLDIER SYSTEMS CMD SSCNS WSO D LEMOINE KANSAS ST NATICK MA 01760-5018
5	USAE WATERWAYS EXP STN CEWES SD R P KINNEBREW B CARNES CEWES TL TECH LIB CEWES SD K DAVIS CEWES SS J WEATHERSBY 3909 HALLS FERRY RD VICKSBURG MS 39180-6199
1	DIR SNL ES HERTEL JR MS 0819 PO BOX 5800 ALBUQUERQUE NM 87185-0307
1	KERLEY PUB SUC G I KERLEY PO BOX 13835 ALBUQUERQUE NM 87192-3835
1	CENTRAL INTELLIGENCE AGENCY OFFICE OF TRANSNATIONAL ISSUES WEAPONS & TECHNOLOGY GROUP J D WALTON WASHINGTON DC 20505

NO. OF COPIES	ORGANIZATION
	ABERDEEN PROVING GROUND
1	COMMANDER US ARMY TECOM AMSTE TE F L TELETSKI
1	COMMANDER USATC STEC LI
30	DIR USARL AMSRL WM MA W CHIN T MULKERN C PERGANTIS AMSRL WM PB B GUIDOS H EDGE P PLOSTINS P WEINACHT AMSRL WM T B P BURNS AMSRL WM TB V BOYLE P BAKER T DORSEY R FREY W HILLSTROM W LAWRENCE R LOTTERO (5 CPS) E MCDOUGAL J STARKENBERG J WATSON AMSRL WM TC K KIMSEY D SCHEFFLER S SCHRAML AMSRL WM TD A M DIETRICH P KINGMAN M RAFTENBERG S SCHOENFELD P SIMMERS

REPORT DOCUMENTATION PAGE

Form Approved
OMB No. 0704-0188

1. AGENCY USE ONLY *(Leave blank)*	2. REPORT DATE	3. REPORT TYPE AND DATES COVERED
	August 1999	Final, 1 Oct 98 - 31 May 99

4. TITLE AND SUBTITLE
Standoff Variation Study III: Detonation of a Donor Munitions Stack and Responses of a Thick Rectangular Water Barricade and an Acceptor Stack

5. FUNDING NUMBERS
JONO: 9810F1

6. AUTHOR(S)
Richard E. Lottero

7. PERFORMING ORGANIZATION NAME(S) AND ADDRESS(ES)
U.S. Army Research Laboratory
ATTN: AMSRL-WM-TB
Aberdeen Proving Ground, MD 21005-5066

8. PERFORMING ORGANIZATION REPORT NUMBER
ARL-TR-2035

9. SPONSORING/MONITORING AGENCY NAMES(S) AND ADDRESS(ES)

10.SPONSORING/MONITORING AGENCY REPORT NUMBER

11. SUPPLEMENTARY NOTES

12a. DISTRIBUTION/AVAILABILITY STATEMENT
Approved for public release; distribution is unlimited.

12b. DISTRIBUTION CODE

13. ABSTRACT *(Maximum 200 words)*

This report documents the third stage of the continuation of the fully coupled numerical modeling of the detonation of a simplified munitions stack in a temporary storage area and the subsequent effects on the immediate surroundings of the stack. Three plausible configurations of this munitions stack, referred to as the "donor" stack, an intervening water barricade, and an "acceptor" munitions stack, are modeled in two-dimensional (2-D) Cartesian hydrocode computations using the CTH hydrodynamics computer code. The distance between each munitions stack and the barricade, referred to here as the "standoff" distance, is varied from one computation to the next, with the physical characteristics of the munitions stacks and barricade themselves remaining unchanged. The donor stack is modeled as an uncased, condensed high-explosive charge with a rectangular cross section. The water barricade has a relatively thick rectangular cross section, and the acceptor stack is modeled as a solid iron rectangle. The loadings on both the barricade and the acceptor stack are computed, as are their fully coupled responses to those loadings. Only a relatively weak inverse functional relationship with standoff distance was found in the barricade response. Weak correlations with both standoff distance and face separation were also found for all parameters that were evaluated for the acceptor stack response. The results are also compared with those of the first two parts of this study on the coupled blast loading and response computations for a massive water barricade with a trapezoidal cross section and computations for a thin rectangular water barricade.

14. SUBJECT TERMS	15. NUMBER OF PAGES
munitions, survivability, detonation, barricade, hydrocode	83
	16. PRICE CODE

17. SECURITY CLASSIFICATION OF REPORT	18. SECURITY CLASSIFICATION OF THIS PAGE	19. SECURITY CLASSIFICATION OF ABSTRACT	20. LIMITATION OF ABSTRACT
UNCLASSIFIED	UNCLASSIFIED	UNCLASSIFIED	UL

INTENTIONALLY LEFT BLANK

USER EVALUATION SHEET/CHANGE OF ADDRESS

This Laboratory undertakes a continuing effort to improve the quality of the reports it publishes. Your comments/answers to the items/questions below will aid us in our efforts.

1. ARL Report Number/Author ARL-TR-2035 (Lottero) Date of Report August 1999

2. Date Report Received _____

3. Does this report satisfy a need? (Comment on purpose, related project, or other area of interest for which the report will be used.) _____

4. Specifically, how is the report being used? (Information source, design data, procedure, source of ideas, etc.) _____

5. Has the information in this report led to any quantitative savings as far as man-hours or dollars saved, operating costs avoided, or efficiencies achieved, etc? If so, please elaborate. _____

6. General Comments. What do you think should be changed to improve future reports? (Indicate changes to organization, technical content, format, etc.) _____

CURRENT ADDRESS

_____
Organization

_____
Name E-mail Name

_____
Street or P.O. Box No.

_____
City, State, Zip Code

7. If indicating a Change of Address or Address Correction, please provide the Current or Correct address above and the Old or Incorrect address below.

OLD ADDRESS

_____
Organization

_____
Name

_____
Street or P.O. Box No.

_____
City, State, Zip Code

(Remove this sheet, fold as indicated, tape closed, and mail.)
(DO NOT STAPLE)